甲548

Study of Quasi One-Dimensional Organic Alloy $Co_xNi_{1-x}Pc(AsF_6)_{0.5}$

Yuqin Ding

Doctor of Philosophy

Department of Structural Molecular Science
School of Mathematical and Physical Science
The Graduate University for Advanced Studies

2001

Acknowledgements

I would like to express my heartful appreciation to my supervisor, Prof. Kyuya Yakushi for his continuous interest, constant encouragement, enlightening guidance and discussions through the whole period of my doctoral courses. What I have learnt through these three years will also play an important role in my future work.

I am deeply thankful to Dr. Mkhital Simonyan for assisting and teaching me in sample preparation, ESR and SQUID experiment, and for his cooperation and encouragement. I am indebted to Prof. Jianhua Lin of the College of Chemistry and Molecular Engineering, Peking University for his enthusiastic help and constant encouragement.

I would like to express my sincere gratitude to Dr. Mikio Uruichi for teaching and assisting me in Raman and reflection spectra measurement. I would like to express my hearty gratitude to Dr. Kaoru Yamamoto for assisting and teaching me in doing experiments. I would like to express my gratitude to Dr. Chikako Nakano for teaching and assisting me how to use the PPMS instrument. I would like to thank Dr. Mikhail Maksimuk for teaching and assisting me in far infrared spectra measurement. I should thank Dr. Yukako Yonehara for teaching me in the EPMA experiment. I wish to thank Dr. Jiangyong Ouyang for his help and also the other members at Prof. Yakushi's group: Prof. Jacek Ulanski, Dr. Olga Drozdova and Mr. Kenji Suzuki.

Thanks go to all members of the Institute for Molecular Science for various contribution and kindness.

Contents

Chapter 1

General Introduction

1.1 Organic conductors

Organic compounds were regarded as excellent insulator for a long time because their covalent bond characteristic and Van der Waals force interaction in the intermolecularly. However, recognition about organic compounds was remarkably changed since the found of charge-transfer complex between perylene and halogen, which shows high conductivity about 10^{-1} $\Omega^{-1}cm^{-1}$.[1]

Organic conductors are charge-transfer compounds typically consisting of organic donor molecules such as TTF, TSF, TMTTF, TMTSF, and acceptors which may be organic (TCNQ) or inorganic (AsF_6^-, PF_6^-, ClO_4^-, and ReO_4^-). The great progress has been made in this field of the organic conductor after the obtained TTF-TCNQ in 1973.[2] TCNQ was synthesized in 1960 and later on TTF was obtained, respectively.[3,4] TCNQ and TTF are very good acceptor and donor to form charge-transfer salts, which are still used today. After the appearance of TCNQ and TTF, many charge-transfer organic conductors were synthesized by good acceptors or donors. The organic charge-transfer salt of TTF-TCNQ, which exhibits high conductivity with 10^3 Scm^{-1} even at room temperature, showed metallic conductivity down to 58 *K*.[2,5] The metallic behavior also was demonstrated by the polarized reflectance spectra.[6,7] Ever since then, a new research field in the organic conductor has been created.

Organic superconductivity was first discovered in 1980, that compound of $(TMTSF)_2PF_6$ showed the superconductive behavior below 0.9 *K* under a pressure of 12 Kbar.[8] Subsequently, a series of compounds were obtained by replacing PF_6^- with other anions such as AsF_6^-, SbF_6^-, ReO_4^-, and ClO_4^-. It was found that these analogous compounds were different from each other in their symmetry and in the electronegativity

of the central atom.[9-12] However, these compounds present the analogous transition at high pressure.[13] Since $(TMTSF)_2ClO_4$ was obtained with the superconductivity characteristic below 1.3 *K* at ambient pressure in 1981,[14] the organic conductors developed to organic superconductor stage.

About the structure characteristic of charge-transfer organic conductors, TTF-TCNQ is the typical example, which the almost-planar TTF radical cation and the TCNQ radical anions form segregated columnar stacks in the *b*-direction, and the conduction band is formed by the overlap along the stacks of the highly directional π-molecular orbital. Since the donor and acceptor molecules separately stack as segregated columns, the conductivity shows a strong anisotropy. Many organic conductors are such materials whose electrical conductivity is high only along one direction. It is regarded as quasi one-dimensional conductor. Such materials are of interest because nearly one-dimensional metals are expected to exhibit unusual collective behavior. Experimental studies of one-dimensional electronic systems only started at the beginning of 1970, i.e. at the same time when it became possible to synthesize one-dimensional conductor. During the course of these investigations, many characteristics of one-dimensional electronic systems have been revealed. Organic conductors exhibit a large variety of electronic behaviors and transport properties. Depending on the compound, on the temperature, on the pressure, they can be found as metals, semi-metals, semi-conductors, superconductors and very often, they reach these peculiar electronic ground state through phase transition some of which are strongly related to the quasi one-dimensional character of the electron gas.

The Peierls instability is well-known a characteristic of electronic systems in one-dimensional system for a potential having the wave number $2k_F$ given by phonons to electrons. This instability gives rise to a collective state of electrons called a charge-density wave (CDW) which tends to occur in low-dimensional electronic system and causes a metal-insulator transition regarded as Peierls transition. Therefore, the Peierls transition is caused by the electron-phonon interaction. It is worth noticed that the Peierls transition is based on the one-electron model without the consideration of the Coulomb interaction between conduction electrons. The electron-electron correlation sometime plays a very important role in the low-dimensional organic conductors, when the presence of a Coulomb repulsion U cannot be negligible compared to kinetic energy of the electrons. The kinetic energy to be compared with U is represented by the bandwidth $4t_{//}$. In the half-filled energy band case, the conductive properties are revealed due to the contest of U and t. When with the $U<<t$, the Coulomb repulsive interaction will lead only to some small corrections to band, i.e. the electrons are regarded as free particles without electron-electron correlation. However, on the other hand, when $U>>t$, the ground state changes radically and each electron is localized on its site. Clearly, this state will be nonconducting. Moreover, the metallic state in the one-dimensional case turns out to be unstable for an arbitrary U. Somewhere at $U\approx t$ a metal-nonmetal transition should occur. The instability of metallic state of organic conductors is due to the one-dimensional characteristic. To stabilitate the metallic state, one method is certain that to expand the systematic dimensionality.

1.2 The technique of study on organic conductors

Such kind of compound so-called organic metal presents a series of characteristic of metallic conductance, for instance, a high conductivity above $10^2\ \Omega^{-1}cm^{-1}$ at room temperature; the negative temperature coefficient of conductivity ($\partial\sigma/\partial T<0$); the polarized reflection spectrum appears Drude-model plasma edge and the thermoelectric power is direct proportion to temperature (K). However, the organic metal does not have all the behaviors of the element metal, such as the conductivity in most of the organic metal shows high anisotropy and exists metal-insulator phase transition. These characteristic of organic metal are caused by the charge carries which comes from the itinerant π-electron of plane-coordination molecule, however, the relationship of conductivity dependence temperature is changed with the different systems. Therefore, it is necessary to study the nature of the band structure of organic conductors. Since the discovery of the organic metal TTF-TCNQ, reflection spectroscopy has been a powerful method to extract the information of the transfer integral, which is the most basic quantity to describe the band structure. The transfer integrals can be roughly estimated from the analysis of the reflectivity curve in the mid-infrared and near-infrared regions.

Let us discuss the one-electron band model to describe the weakly interacting system. The bandwidth of an organic conductor is typically less than 1 eV and this narrow bandwidth comes from the charge-transfer interaction. Due to the weakly overlapped frontier orbital, the tight-binding approximation is usually taken to describe the band structure. In the tight-binding approximation, the kinetic energy term of the Hamiltonian is expressed by the following equation:

$$H = -\sum_{l,l'} \sum_{m,m'} t_{lml'm'} a^{+}_{lm} a_{l'm'}, \qquad (1)$$

where a_{lm}^{+} and $a_{l'm'}$ are the creation and annihilation operators at l-th and l'-th unit cells and m-th and m'-th sites in the unit cell, $t_{lml'm'}$ is the transfer integral between m-th site in the l-th unit cell and m'-th site in the l'-th unit cell. Since the distance between the molecules is far, the transfer integrals of nearest neighbor molecules are taken into account and other ones are neglected. The estimation of the transfer integral is conducted using the Mulliken approximation as $t_{lml'm'} \propto S_{lml'm'}$, where $S_{lml'm'}$ is the overlap integral of the frontier orbital between the neighbor molecules. If the unit cell involves one molecule, the eigen value of Eq. 1, $E(k)$, has one branch. In this case only the intra-band transition is allowed near the Fermi energy, if the band is partially filled and thus the system is in metallic state. The intra-band transition is formulated based on the Boltzmann equation, and the complex optical conductivity $\sigma(\omega)$ is expressed by the Drude model. The integrated intensity of this optical transition is given by the square of the plasma frequency ω_p. When the unit cell contains two molecules, the energy band $E(k)$ split into two branches. In this case another type of optical transition is allowed. This inter-band transition occurs vertically, in other words, the hole and electron is produced at the same wave vector k.

When the electron-electron interaction is strong (strong correlation), which is more general in organic conductors, the Hubbard model is adopted to described the correlated system. The correlation effect gets more obvious in the half-filled band system. The Hubbard Hamiltonian is given by the following equation,

$$H = \sum_{lml'm'} t_{lml'm'} a_{lm}^{+} a_{l'm'} + U \sum_{lm} a_{lm\uparrow}^{+} a_{lm} a_{lm\downarrow}^{+} a_{lm\downarrow}, \qquad (2)$$

where U is the on-site Coulomb energy. The on-site Coulomb energy describes the repulsive Coulomb energy between the electrons. In this model, the repulsive force is taken into account within the same molecule, and the inter-molecular Coulomb force is neglected. The introduction of the nearest neighbor Coulomb force to the Hamiltonian (2) leads to an extended Hubbard model. The Hubbard model for a one-dimensional system with a half-filled band is exactly solved, and a finite U opens a gap at the Fermi-level. In this model, the excitation energy to create an electron-hole pair is given by the following equation,[15]

$$\begin{aligned} E(k_+,k_-)/4t &= u - \frac{1}{2} + \int_0^\infty \frac{J_1(\omega)}{\omega(1+\exp(2u\omega))}d\omega + \frac{\cos(k_+)+\cos(k_-)}{4} \\ &+ \int_0^\infty \frac{J_1(\omega)\{\cos(\omega\sin(k_+)+\cos(\omega\sin(k_-))\}}{\omega(1+\exp(2u\omega))}d\omega \end{aligned} \tag{3}$$

where k_+ and k_- are the quasi-moments of electron and hole, $u=U/4t$, and $J_i(\omega)$ is the Bessel function of the first kind with order i. As displayed in Fig. 2, $E(k_+,k_-)$ takes a minimum at $k_+=k_-=\pi$, which corresponds to the absorption edge. The vertical transition ($k_+=k_-$) spans from $E(\pi,\pi)$ to $E(\pi,\pi)+4t$. The plasma frequency is given by the following equation,

$$\frac{\varepsilon_0}{Ne^2d^2}\frac{\hbar^2\omega_p^2}{4t} = \int_0^\infty \left(\frac{1}{\omega(1+\exp(2u\omega))}+\frac{u}{1+\cosh(2u\omega)}\right)J_0(\omega)J_1(\omega)d\omega \tag{4}$$

where N is the density of charge, ε_0 the vacuum dielectric constant, d the inter-molecular spacing between molecules along the chain direction and ω_p the plasma frequency. Combining Eq. 3 with Eq. 4, we can estimate the Hubbard parameter t and U from the analysis of the optical transition.

The reflectivity of an organic conductor provides us with a wealth of information on the electronic structure. Raman spectroscopy is a complementary method to reflection spectroscopy for investigating molecular vibrations.

Except introduced above methods, the magnetic susceptibility and electron spin resonance (ESR) measurements also became extremely important technique to research organic metal conductors. If the organic compound was a simple metal, a Pauli paramagnetism would be expected in the metallic phase and a paramagnetism due to thermally excited electrons would appear in the insulating phase when metal-insulator transition happened. Real phenomena, however, are found to be more complicated.

1.3 The study of the phthalocyanine salts

Phthalocyanine (Pc) compounds have attracted a great deal of attention for a longtime because of their unique properties such as semiconductivity, photoconductivity, and chemical activity.[17] Besides their excellent photoconductivity properties, phthalocyanines have the advantage of being very stable against thermal and chemical decomposition and present very intense optical absorption in the visible. Also they were expected to serve as active materials for molecular electronic devices.[18,19] Furthermore, interest in phthalocyanine compounds has been renewed due to the discovery that they form "molecular metals" after partial oxidation.[20] The crystal structure of *M*Pc (*M*=Co^{2+}, Ni^{2+}, Cu^{2+}, and Zn^{2+}) has different type crystal modifications in which the β-form crystal of *M*Pc belongs to monoclinic system with the space group of $P2_1/a$ as shown in Fig. 3.[21] The crystal is needle-like along the *b*-axis and develops the (001) and (201) faces.

Contrary to the typical coordination compounds, the electronic spectrum of transition-metal phthalocyanine (*M*Pc) is dominated by the conjugated π-electron system like the polycyclic aromatic compounds such as anthracence or tetracence. When it is used as an electron donor molecule, the role of the molecule resembles again the conjugated π-electron system such as TTF and BEDT-TTF, in contrast to the conducting coordination compound KCP. These properties come from the nature of the frontier orbital: HOMO and LUMO of phthalocyanine are regarded to have a pure π character. There is so-called *Q*-band in the reflection spectra of phthalocyanine in the visible region. The *Q*-band is assigned to a π-π^* transition from HOMO (a_{1u}) to degenerate LUMO (e_g). The degeneracy of the *Q*-band is removed in the solid state and strong dependence upon the central metal. As shown in Fig. 4, each polarized spectrum of *M*Pc at room temperature exhibits two peaks, and the position and intensities of these two peaks strongly depend upon the light polarization. The spectral feature is qualitatively reproduced by the conventional exciton theory, which was developed to explain the solid spectrum of polycyclic aromatic hydrocarbons.[22,23] The spectrum involves information on the transition density of the molecule, which plays an important role in the theory of Litte's excitonic superconductivity.[24] In the case of *Q*-band, HOMO and LUMO of phthalocyanine primarily contribute to the transition density. It is interesting to note that the remarkable difference is found in the way of splitting of the *Q*-band between Pcs with empty $3d_{x^2-y^2}$ orbitals (CoPc and NiPc) and those with singly and doubly occupied $3d_{x^2-y^2}$ orbitals (CuPc and ZnPc).

The transition metal phthalocyanine makes a stable one-dimensional conductor when the molecule is oxidized with a stable counter anion such as AsF_6^-.

Phthalocyanine conductors take a characteristic molecular arrangement, in which metal (*M*) chain and ligand (Pc) chain coexist in the same molecular stack. This kind of composition structure resembles the model compounds of an excitonic superconductor.[24,25] When we oxidize metallophthalocyanine, the electron is usually extracted from the HOMO of the ligand, so the optical absorption in the *Q*-band region systematically changes and yields new inter-band transition depending upon the oxidation. Some phthalocyanine molecules contain unpaired *d*-electrons in the conjugated π-electron system such as $CoPc(AsF_6)_{0.5}$. The unpaired *d*-electron in $CoPc(AsF_6)_{0.5}$ is spacially separated from the highest occupied molecular orbital (HOMO). Due to this nature in $CoPc(AsF_6)_{0.5}$, the itinerant π-electrons coexist with the unpaired *d*-electrons. It has not been investigated in the charge-transfer salt if the unpaired *d*-electron occupies the $3d_{z^2}$ orbital like in neutral CoPc. To elucidate the electronic structure of this possible two-band system, we prepared the charge-transfer salts of NiPc, CoPc and their mixed crystals, and characterized them by means of elementary analysis, crystal structural analysis, ESR, Raman spectroscopy, reflection spectroscopy, and magnetic susceptibility. Based on the analysis of the well-resolved hyperfine structure in the very dilute alloy such as $Co_{0.01}Ni_{0.99}Pc(AsF_6)_{0.5}$, the unpaired *d*-electron in Co was confirmed to occupy the $3d_{z^2}$ orbital, which is extended perpendicular to the molecular plane. As the $3d_{z^2}$ orbital is doubly occupied in NiPc and singly occupied in CoPc, therefore the $3d_{z^2}$ orbital forms a half-filled one-dimensional band ($3d_{z^2}$ band) along the Co chain. Almost all of the experiment carried out on $NiPc(AsF_6)_{0.5}$ indicated that the π-band is responsible for the electrical conduction. On the other hand, the unpaired *d*-electron in $CoPc(AsF_6)_{0.5}$ directly appears in the magnetic

property of this compound. The optical transition related to $3d_{z^2}$ orbital directly observed in the reflection spectrum of $CoPc(AsF_6)_{0.5}$ in the mid-infrared region. A resonance effect is found in the Raman spectra of the mixed crystals $Co_xNi_{1-x}Pc(AsF_6)_{0.5}$ which suggests that a new excited state is formed in the mixed crystal along the stack direction to which the 3*d* orbital contributes. Therefore, the study on the alloy system $Co_xNi_{1-x}Pc(AsF_6)_{0.5}$ to investigate the role of 3*d*-electron in phthalocyanine charge-transfer salts is the main domain of this thesis.

1.4 Intention and arrangement of this thesis

The quasi one-dimensional phthalocyanine charge-transfer salts of $MPc(X)_y$ (M=H_2^{2+}, Ni^{2+}, Co^{2+}, Cu^{2+}, Pt^{2+}; X=I_3^-, BF_4^-, ClO_4^-, AsF_6^-, SbF_6^-; y=0.33-1.0) consist of metal and macrocycle (Pc) two chains in which the one-dimensional metal chain is surrounded by the macrocycle chain. The *M*Pc is stacked near the metal-over-metal overlapping fashion. Among those salts, the π-band is oxidized playing as a conducting band except CoPcI which the central metal of Co is oxidized. Thus charge-transport in CoPcI proceeds along a one-dimensional chain of metal centers, and the band filling is 1/3 for this case. This molecular complex represents the first metal-spine conductor.[26,27] According to the orbital symmetry, the π-electrons are not only delocalized within the macrocycle but also extended to the neighboring molecules, whereas 3*d*-electrons are localized near the central metal. Because of the structural characteristics, phthalocyanine conductors show π- and *d*-characters in the solid state properties. The effect of 3*d* orbital becomes obvious, particularly when the 3*d* orbital of the central metal is singly occupied such as CuPc and CoPc.

The comparative study based on the phthalocyanine conductor in order to elucidate the effect of $3d$ orbital has been performed on MPcI (M=Cu^{2+}, Co^{2+} and Ni^{2+}) and their alloy system with the paramagnetic and diamagnetic ions.[28-32] As mentioned above, CoPcI is a metal-spine conductor with the electrons in a less than half-filled band because the oxidation site is on the central metal. On the other hand, the charge carriers of CuPcI and NiPcI are associated with the HOMO of Pc ring. In both alloy system, the paramagnetic d band (Cu^{2+}: d^9, Co^{2+}: d^7) is diluted by the introduction of diamagnetic ions. In our study for $NiPc(AsF_6)_{0.5}$ and $CoPc(AsF_6)_{0.5}$, the π-chain is oxidized with ¾ filled band as the conducting band in both salts by the AsF_6^- anion. Although the crystal structure of both compounds is nearly isostructural to each other, their properties are different. The localized d-electron might be responsible for the different properties. We considered that the $3d_{z^2}$ orbital may play some roles in $CoPc(AsF_6)_{0.5}$. Elucidation of the effect of $3d_{z^2}$ orbital in $CoPc(AsF_6)_{0.5}$ was carried out by the study on the alloy system of $Co_xNi_{1-x}Pc(AsF_6)_{0.5}$.

The format of this thesis is arranged as follows. Chapter 2 comprehends all the experimental processes for this study. Chapter 3 presents the formation of this alloy system $Co_xNi_{1-x}Pc(AsF_6)_{0.5}$, in which a series of evidences are contained to support the formation of mixed crystals. For instant, the boundary of crystal structure with orthorhombic and tetragonal system is located between x=0.25 and x=0.45 in this alloy system, and the parameter c decreases systematically with the increase of the cobalt concentration x; the obtained hyperfine structure in the alloy system in the range of $0<x<0.09$ below 30 K and the angle dependence of g value at 3.2 K; the appearance of the characteristic Raman band with its second harmonic band in the mixed crystals even

in the very diluted alloy of $Co_{0.01}Ni_{0.99}Pc(AsF_6)_{0.5}$; the systematically changed reflection spectra with the increasing cobalt concentration of x. Such experimental results demonstrate that the mixed crystals are formed on a molecular level. The electronic structure of the organic alloy $Co_xNi_{1-x}Pc(AsF_6)_{0.5}$ is presented and discussed in Chapter 4 based on the optical spectroscopy combined with the magnetic properties. The well-observed hyperfine structure in the very dilute alloy is discussed and the unpaired *d*-electron in Co was confirmed to locate the $3d_{z^2}$ orbital. The appearance of the characteristic Raman bands in the alloy system is discussed and assigned to the a_{1g} breathing mode of mycrocycle around the central metal and its second harmonic band because the new bands are observed only in the (c,c) polarization. To assign these new Raman peaks, a factor group analysis was performed on $CoPc(AsF_6)_{0.5}$, which provides the information on the symmetry of molecular vibration due to its high symmetry, D_{4h}. We proposed that a new excited state is formed in the alloy system according to the analysis of the Raman spectra of the alloy system. The Co-concentration dependence of the Raman intensity of the new peaks is analyzed according to its asymmetrical tendency with respect to the concentration of Co. In this chapter, the different reflection spectra of $NiPc(AsF_6)_{0.5}$ and $CoPc(AsF_6)_{0.5}$ are analyzed by the Drude-Lorentz models. Since the $3d_{z^2}$ orbital forms a half-filled one-dimensional band along the Co chain in $CoPc(AsF_6)_{0.5}$, it is well-known that a half-filled one-dimensional band is split into upper and lower Hubbard bands if we take the on-site Coulomb interaction into account. Therefore, in order to obtain the bandwidth of *d*- and π-bands for $CoPc(AsF_6)_{0.5}$, one-dimensional Hubbard band model was employed for *d*-band and one-dimensional tight-binding model was used for π-band. According to the analysis of the reflection spectra,

the additional optical transition for $CoPc(AsF_6)_{0.5}$ in the mid-infrared region is assigned to the inter-band transition between the two Hubbard bands. And the very surprising small excitation energy (about 0.5 eV) also is discussed. The x dependence of reflectivity along the c-axis is consistent with the interpretation about the assignment of the optical transition in the mid-infrared region, and an energy diagram with the $3d$-electron near the Fermi level is presented. In chapter 5, the magnetic properties of all alloys are presented. In this chapter, the results of ESR and static spin susceptibility of organic conductors $Co_xNi_{1-x}Pc(AsF_6)_{0.5}$ are discussed. We analyzed the temperature dependence of the g value and linewidth in the high temperature regime based on Hasegawa's phenomenological theory for the dilute magnetic alloys. The density of state at the Fermi level and the exchange energy between the local d- and itinerant π-spins were estimated as D_F=3.8±0.2 eV^{-1} and $|J_{\pi d}|$=0.013±0.002 eV by the numerical simulation of the ESR line shape. The magnetic susceptibility of the entire alloy is analyzed by the Curie and Weiss law.

Abbreviations of donors and acceptors

Donor

TTF	Tetrathiafulvalene
TSF	Tetraselenafulvalene
TMTTF	Tetramethyltetrathiafulvalene
TMTSF	Tetramethyltetraselenafulvalene
MPc	Metal Phthalocyanine
BEDT-TTF	Bis(ethylenedithio)tetrathiafulvalene
BEDO-TTF	Bis(ethylenedioxy)tetrathiafulvalene

Acceptor

TCNQ	Tetracyanoquinodimethane

References

[1] H. Akamatsu, H. Inokuchi and Y. Matsunaga, *Nature*, **173**, 168 (1954).

[2] J. Ferraris, D. O. Cowan, V. Walatka, Jr. Perlstein, and J. H. Perlstein, *J. Am. Chem. Soc.*, **95**, 948 (1973).

[3] D. S. Acker, R. J. Harder, W. R. Hertler, W. Mahler, L. R. Melby, R. E. Benson, and W. E. Mochel, *J. Chem. Soc.*, **82**, 6408 (1960).

[4] F. Wudl, G. M. Smith, E. J. Hufnagel, *J. Chem. Soc., Chem. Commun.*, 1453 (1970).

[5] S. Etemad, *Phys. Rev. B*, **13**, 2254 (1976).

[6] A. A. Bright, A. F. Garito, and A. J. Heeger, *Solid state Commun.*, **13**, 943 (1973).

[7] D. B. Tanner, C. S. Jacobsen, A. F. Garito, and A. J. Heeger, *Phys. Rev.* B, **13**, 3381 (1976).

[8] D. Jerome, A. Mazaud, M. Ribault, and K. Bechgaard, *J. Phys. Lett.*, Paris, **41**, L95 (1980).

[9] R. Brusett, M. Ribault, D. Jerome, and K. Bechgaard, *J. Phys.*, Paris, **43**, 801 (1982).

[10] S. S. P. Parkin, D. Jerome, and K. bechgaard, *Mol. Cryst. Liq. Cryst.*, **79**, 213 (1982).

[11] S. S. P. Parkin, M. Ribault, D. Jerome, and K. Bechgaard, *J. Phys.* C, **14**, L445 (1981).

[12] S. S. P. Parkin, M. Ribault, D. Jerome, and K. Bechgaard, *J. Phys.* C, **14**, 5305 (1981).

[13] K. Bechgaard, K. Carneiro, M. Olsen, F. B. Rasmusen, and C. S. Jacolsen, *phys. Rev. Lett.*, **46**, 852 (1981).

[14] K. Bechgaard, K. Carneiro, M. Olsen, F. B. Rasmusen, and M. Olsen, *phys. J. Amer. Chem.,Soc.*, **103**, 2440 (1981).

[15] I. A. Musurkin and A. A. Ovchinnikov, *Soviet Physics Solid State,* **12**, 2031 (1971).

[16] W. P. Dumke, *Phys. Rev.* **124**, 1813 (1961).

[17] J. Simon, and J.-J. Andre, *Molecular Semiconductors,* Chap. III.

[18] B.P. Lever, M. R. Hempstead, C. C. Leznoff, W. Lin, M. Melnik, W. A. Nevin, and R. Seymour, *Pure. Appl. Chem.* **58**, 1467 (1986).

[19] R. A. Collins and K. A. Mohammed, *J. Phys.*, D **21**, 154 (1988).

[20] T. J. Markas, *Science,* **227**, 881 (1985).

[21] P. A. Reynolds, B. N. Fggis, and E. S. Kucharski, *Acta. Crystallogr.* B, **47**, 899 (1991).

[22] D. P. Craig and S. H. Walmsey, *Physics and Chemistry of the Organic Solid State,* vol. 1, ed. by D. Fox, M. M. Labes, A. Weissenberger. Interscience: New York, 585 (1963).

[23] S. A. Rice and J. Jortner, *Physics and Chemistry of the Organic Solid State,* vol. 3, ed. by D. Fox, M. M. Labes, and A. Weissenberger, Interscience, New York, 199 (1967).

[24] D. Davis, H. Gutfreund and W. A. Little, *Phys. Rev.*, B **13**, 4766 (1976).

[25] W. A. Little, *Phys. Rev.*, **134**, A1416 (1964).

[26] J. L. Petersen, C. S. Schramm, D. R. Stojakovic, B. M. Hoffman, and T. J. J. Marks, *J. Am. Chem. Soc.*, **99**, 286 (1977).

[27] J. Martinsen, R. L. Greene, S. M. Palmer, and B. M. Hoffman, *J. Am. Chem. Soc.*, **105**, 677 (1983).

[28] M. Y. Ogawa, J. Martinsen, S. M. Palmer, J. L. Stanton, J. Tanaka, R. L. Greene, B. M. Hoffman, and J. A. Ibers, *J. Am. Chem. Soc.*, **109**, 1115 (1987).

[29] Soonchil Lee, M. Yudkowsky, W. P. halperin, M. Y. Ogawa, and B. M. Hoffman,

Phys. Rev., B, **35**, 5003 (1987).

[30] M. Y. Ogawa, S. M. Palmer, K. Liou, G. Quirion, J. A. Thompson, M. Poirier, and B. M. Hoffman, *Phys. Rev.*, B **39**, 10682 (1989).

[31] J. Martinsen, J. L. Stanton, R. L. greene, J. Tanaka, and B. M. Hoffman, *J. Am. Chem. Soc.*, **107**, 6915 (1985).

[32] J. Thompson, K. Murata, R. Durcharne, M. poirier, and B. M. Hoffman, *Phys. Rev.*, B **60**, 523 (1999).

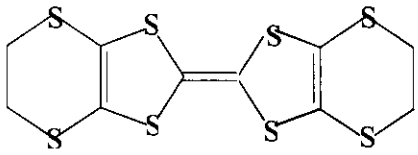

BEDT-TTF

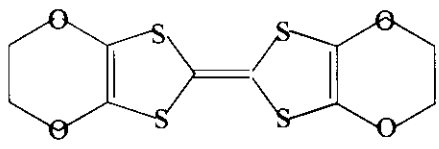

BEDO-TTF

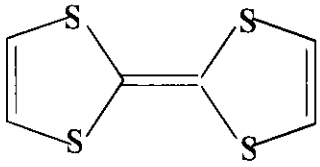

TTF

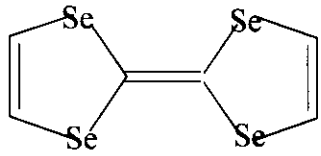

TSF

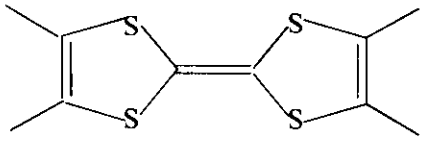

TMTTF

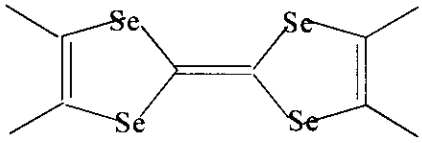

TMTSF

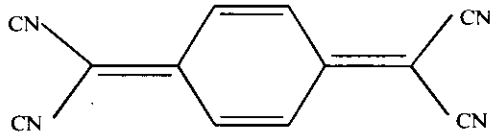

TCNQ

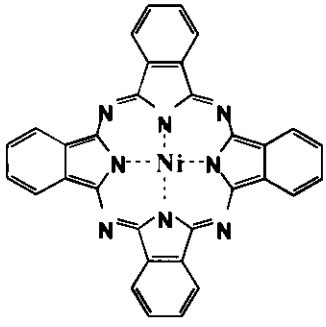

NiPc

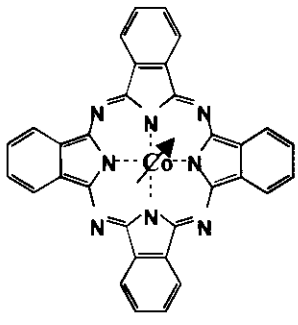

CoPc

Fig.1 Molecular structure of some organic donors and acceptors

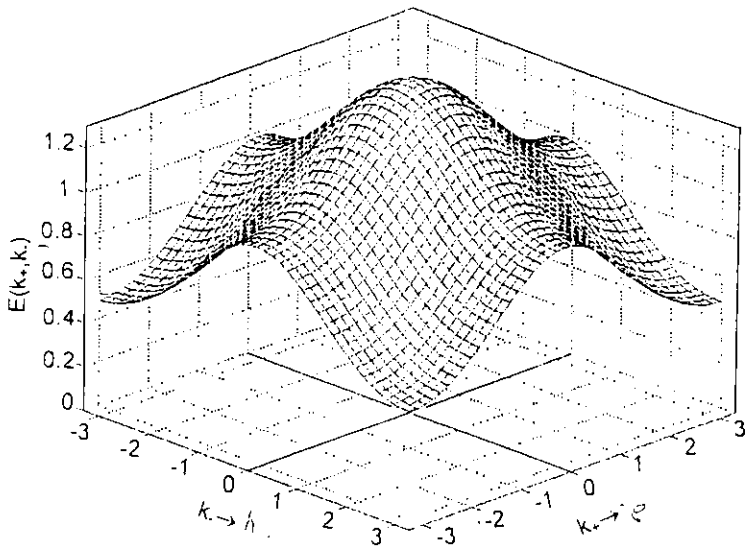

Fig. 2 Excitation energy to produce an electron-hole pair
in one-dimensional half-filled Hubbard model

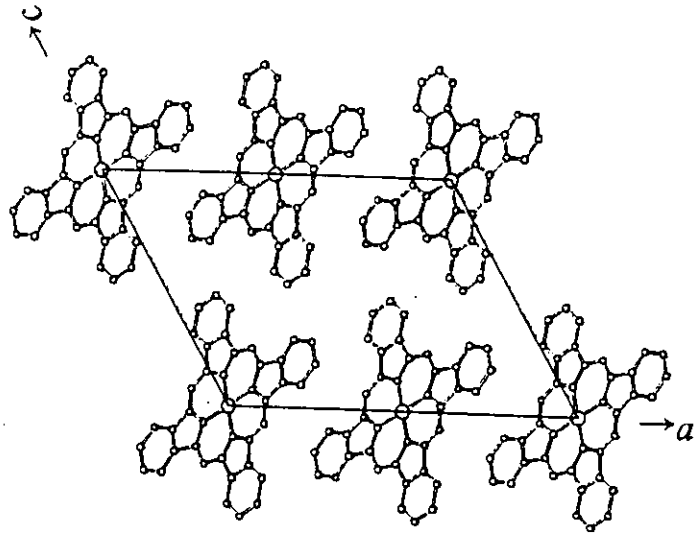

Fig. 3 Crystal structure of β-form CoPc viewed along b-axis

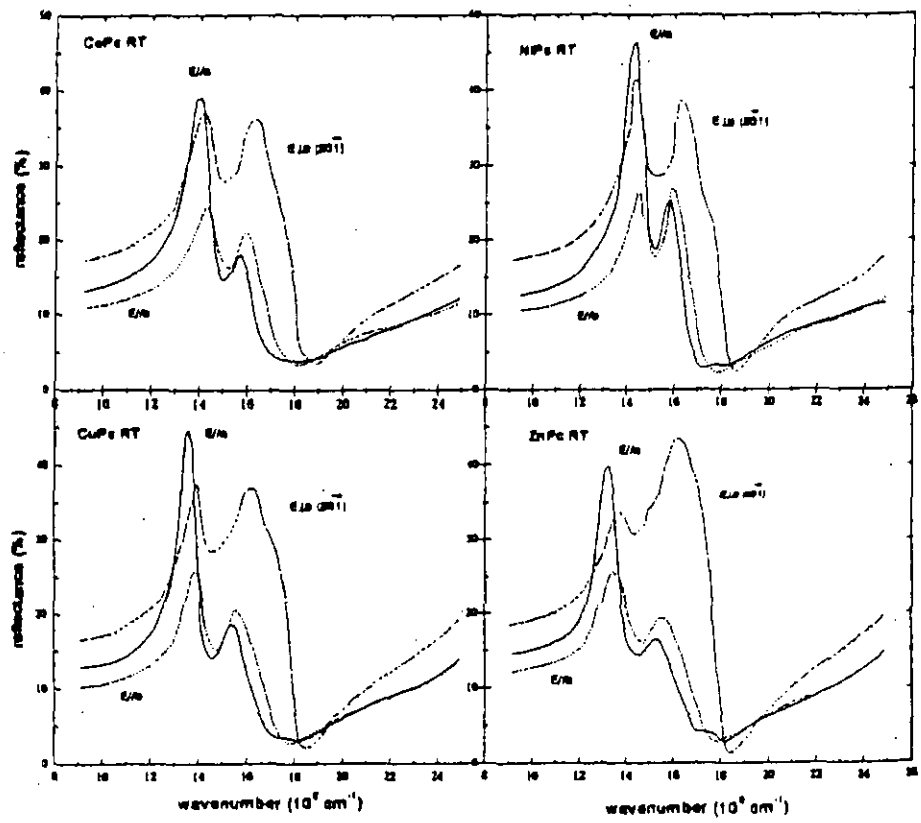

Fig. 4 Room temperature polarized reflection spectra of CoPc, NiPc, CuPc and ZnPc. The spectra are classified into two groups (CoPc, NiPc and CuPc, ZnPc).

Chapter 2

Experimental

2.1 Synthesis and EPMA analysis

The single crystals of $Co_xNi_{1-x}Pc(AsF_6)_{0.5}$ were grown electrochemically in 1-chloronaphthalene solution.[1] For the preparation of $Co_xNi_{1-x}Pc(AsF_6)_{0.5}$, crystals of crude CoPc and NiPc were carefully weighted and ground together with corresponding weighting factor (NiPc:CoPc=100:1, 50:1, 20:1, *etc.*). The resulting mixtures were sublimed four times under high vacuum (about 10^{-5} Pa) to ensure intimate mixing of $Co_xNi_{1-x}Pc$. The salts of $Co_xNi_{1-x}Pc$ and $(n\text{-}C_4H_9)_4NAsF_6$ were solubilized in an electrochemical cell which is separated into two compartments by a glass filter. The concentration of the electrolytes, $(n\text{-}C_4H_9)_4NAsF_6$, and $Co_xNi_{1-x}Pc$ in 1-chloronapthalence used as the solvent of electrochemical crystallization were 2.5×10^{-3} and 3×10^{-4} mol/l, respectively. The solvent was refluxed with CaH_2 and purified by vacuum distillation. After allowing the electrochemical reaction to proceed for three weeks with a galvanostatic mode of 2~4 μA at 120°C under Ar atmosphere, all the starting materials were transformed into the AsF_6 salts near the glass filter in the anode compartment.

The atomic ratio between Ni and Co in the $Co_xNi_{1-x}Pc(AsF_6)_{0.5}$ single crystals was determined by means of EPMA (Hitachi *S*-450) using JEOL superprobe 733. The alloy Kovar (Nilaco), $CoPc(AsF_6)_{0.5}$, and $NiPc(AsF_6)_{0.5}$ were used as the standard materials of the analysis of cobalt and nickel concentrations for the alloy system. Several points on each single crystal were examined by use of the electron beam of 1μm.

2.2 Raman spectrum measurement

The resonance Raman scattering spectra were measured On a micro-Raman spectrometer (Renishaw Ramanscope System-1000) with a back-scattering geometry excited by He-Ne and Ar^+ laser with the wavelength of 633 nm and 515 nm, which were performed at room temperature on the mixed crystals of $Co_xNi_{1-x}Pc(AsF_6)_{0.5}$ (X=0, 0.01, 0.02, 0.05, 0.09, 0.25, 0.45, 0.55, 0.87, 0.92 and 1). The numerical aperture of the objective lens of the microscope was 0.42, in which the maximum incident angle was 25°. The scattered light was analyzed using a polarization filter with an extinction ratio of 10^{-4}. For example, the (c,a) spectrum denotes an experimental condition in which the laser is polarized along the c-axis, the analyzer is polarized along the a-axis. A He-Ne laser and Ar^+ laser were employed as an excitation light. The laser power was reduced by a neutral filter down to 0.2 mW and was focused on the 2 μm ϕ area of the single crystal.

2.3 Reflection spectrum measurement

The polarized reflection spectrum in the Far-infrared region, 50-700 cm^{-1}, was measured on a Bruker IFS-113v FT-IR spectrometer attaching the home-made reflection optics and sample holder. The IFS-113v optical layout of the reflectance module is shown in Fig. 1. The spectra in the region from 50 to 700 cm^{-1} were collected using a Hg lamp, a silicon #1936 bolometer as a highly sensitive helium-cooled detector, different five beam splitters which are able to select by a beamsplitter changer, and wire-grid polarizer. The absolute value of reflectivity was determined by comparing the reflected light from a gold mirror. Because in the case of the small dimension, specular surface of single crystal it is impossible to match perfectly the sizes of the sample and

reference, so that the reflectance cannot be measured directly. One such technique is to assemble mosaics composed of many small crystals to refrain the diffraction from the small sample. This method was adopted for the measurement of $NiPc(AsF_6)_{0.5}$ in far infrared region. The several single crystals of $NiPc(AsF_6)_{0.5}$ were carefully aligned on the area of 1 mm diameter hole as mosaic sample using silicon grease or Sanvac compound. The gold mirror as a reference was fixed in the same area of diameter with sample. It is worthy noted that the sample and a reference mirror are mounted on nonreflecting hole. For the measurement, the gold mirror and sample were inserted in a sample holder. The position of the sample and gold mirror are interchanged by a 360° rotation using a goniometer. The beam was adjusted so as to be the best incident light pass through the sample. At the focus an aperture should be selected to fit the diameter for both the sample and reference by using the aperture changer. The optical components used in the experiments are listed in Table 1. After the normal measurement, the sample was covered by gold as the reference to avoid the scattering from the mosaic sample. To verify the reliability of this instrument, we measured a large crystal of LiV_2O_5 using 2 mm diameter hole. The measurement result for LiV_2O_5 is found to be in good agreement with the spectra made on this material measured by Jian Dong *et al.* The result comparing with the known spectra shown in Fig.2 indicates that the spectrum in far infrared region measured by this instrument is reliable.

The polarized reflectance spectrum in the infrared and visible region was observed using two spectrometers combined with a microscope: FT-IR spectrometer, Nicolet Magna 760, for 600-12000 cm^{-1} region and multi-channel detection system, Atago Macs 320, for 11000-30000 cm^{-1} region. The spectra in the region from 600 to 7000

cm^{-1} were collected using a globar light, MCT detector, KBr beam splitter, and wire-grid polarizer; the 4000-10000 cm^{-1} region was obtained using a halogen lamp, MCT detector, Quartz beam splitter, and Glan-Tompson polarizer; the 8500-12000 cm^{-1} region data were measured using a halogen lamp, Si photodiode detector, quartz beam splitter, and Glan-Tompson polarizer; the 11000-30000 cm^{-1} region was collected using a xenon lamp, photodiode array system, and Glan-Tompson polarizer. The absolute reflectivity was determined by comparing the reflected light from a gold mirror (600-12000 cm^{-1}) and silicon single crystal (11000-30000 cm^{-1}). The dimensions of the crystals used for the measurement of optical reflectivity were 0.2×0.2×2 mm^3 for $NiPc(AsF_6)_{0.5}$, 0.1×0.1×2 mm^3 for $CoPc(AsF_6)_{0.5}$, 0.2×0.2×2 mm^3 for mixed crystals. The single crystal was fixed on a copper sample holder by silicon grease, and the crystal face was adjusted so as to be normal to the incident light by use of a goniometer head.

2.4 ESR and Magnetic susceptibility measurement

ESR measurements were carried out with a Bruker ESP-300E spectrometer equipped with an *x*-band cavity. The temperature was controlled within ±0.1 *K* using a helium-gas flow-type cryostat of Oxford instrument ESR-900 combined with the temperature controller ITC-4. The measurements were performed at temperature between 3.2-300 *K*. The samples Co:Ni=1:10, 1:20, 1:50, 1:70, 1:100, and 1:200 were used. For the angular dependent ESR experiment, aligned single crystals were mounted on a quartz rod by a small amount of silicon vacuum grease. The orientational study was accomplished by using a goniometer, which enable to rotate the sample 360° around a

single axis. One kind of sample alignment was adopted with the *c*-axis as the rotating axis.

The static magnetic susceptibility measurements were carried out on the Quantum Design MPMS 7000 SQUID magnetometer. The measurements were conducted at temperatures between 2-300 *K*. All sorts of diluted crystals were used for static susceptibility measurement. The temperature dependencies of ESR and SQUID measurements for single crystals were carried out in both directions of the magnetic field: parallel or perpendicular to the crystallographic *c*-axis. About 1 mg of single crystals was aligned on a quartz plate to detect the anisotropy.

2.5 Thermopower measurement

The thermoelectric power of $NiPc(AsF_6)_{0.5}$ and $CoPc(AsF_6)_{0.5}$ single crystals was measured by the method of Chaikin and Kwak[2] with a temperature gradient of 0.5 *K* across the sample along the conducting axis. The crystal was bounded on the thick of 1 μm gold foils by silver or carbon paint at the both edges of crystal as a bridge mounted over the sample puck of PPMS. The gold foils were bonded by the silver paint on a copper plate, which was put on the arms of two sides of the sample puck. One of the arms was heated by manganin wire to make the temperature different, which was measured by a thermocouple. A Keithley 2001 multimeter measured the voltage between the electrodes. The sample puck was installed carefully into the sample chamber of Quantum Design PPMS, and the software program for controlling the heater current and for sampling the voltage was combined with the temperature control system of PPMS.

References

[1] T. Hiejima and K. Yakushi, *J. Chem. Phys.*, **103**, 3950 (1995).

[2] P. M. Chaikin and J. F. Kwak, *Rev. Sci. Instrum.* **46**, 218 (1975).

Table 1.Optical elements used in each frequency range

	1	2	3	4	5
Detector		Silicon Bolometer			
Range (cm^{-1})	10-100	20-100	35-200	50-400	100-700
Source	Hg lamp	Hg lamp	Hg lamp	Hg or Globar	Hg or Globar
Beam splitter (Mylar*)	50 (50micron)	23 (23micron)	12 (12micron)	6 (6micron)	3. 5 (3.5micron)
Electronic filter:					
Low pass	7(137Hz)	7(137Hz)	7(137Hz)	6(275)	5(550Hz)
High pass	open-	7(17Hz)	7(17Hz)	7(17Hz)	7(17Hz)
Region (cm^{-1})	205-0	205-25	205-25	413-25	826-25
Bolometer filter (cm^{-1})	2; <100	2; <100	1; <600	1; <600	1; <600
Gain	1000	1000	200	200	200

*Mylar--- Trademark of E.I. du Pont de Nemours. Inc.

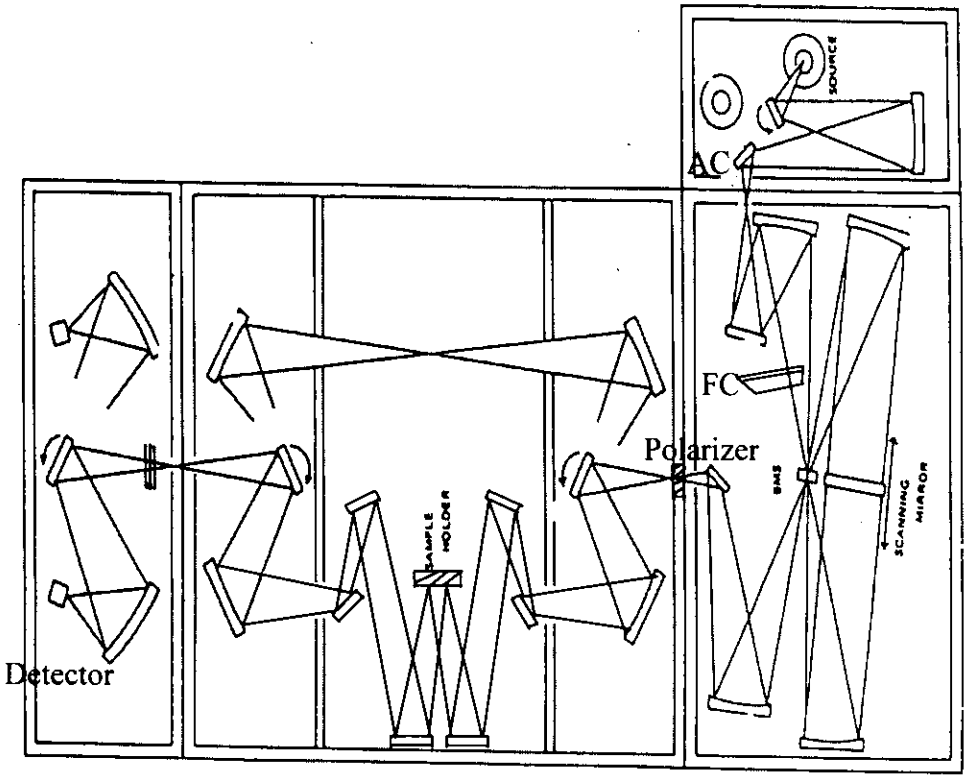

Fig. 1 Optical layout of module for FIR measurement

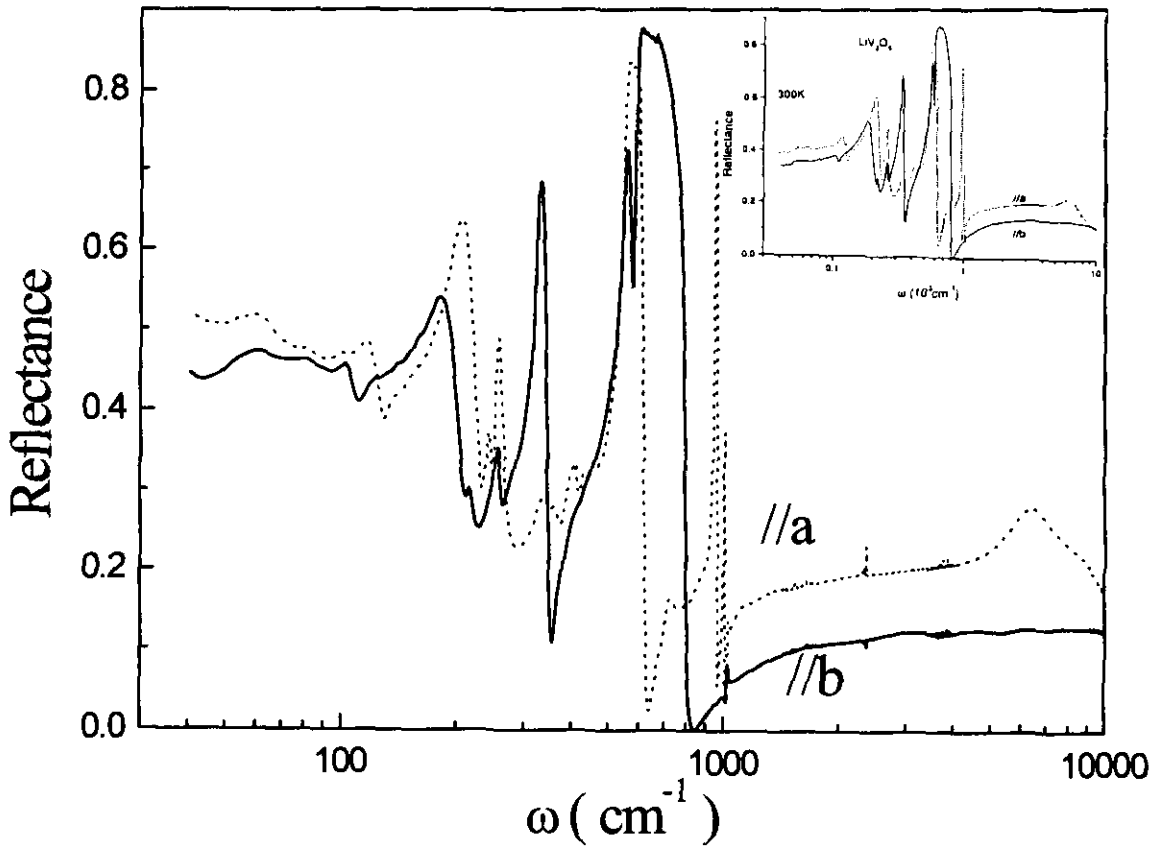

Fig. 2 The far-infrared reflectivity of LiV_2O_5 for proving the instrument which was used for the far-infrared region measurement of $NiPc(AsF_6)_{0.5}$. Inset figure shows the measurement result by using another instrument.

Chapter 3

Formation and characterization of mixed crystal system

$Co_xNi_{1-x}Pc(AsF_6)_{0.5}$ ($0 \leq x \leq 1$)

Yuqin Ding, Mkhital Simonyan, Yukako Yonehare, Mikio Uruichi, and Kyuya Yakushi

Formation of mixed crystal system $Co_xNi_{1-x}Pc(AsF_6)_{0.5}$

Mol. Cryst. Liq. Cryst., in press

Kyuya Yakushi, Mkhital Simonyan, and Yuqin Ding

Spectroscopic studies of solid phthalocyanines and their charge-transfer salts

J. Porphyrins & phthalocyanines, **5** (2001) 13-24

3.1 Introduction

The quasi one-dimensional phthalocyanine conductors $M\text{Pc}(X)_y$ (M=H_2^{2+}, Co^{2+}, Ni^{2+}, Cu^{2+}; Pc=$(C_{32}N_8H_{16})^{2-}$; y=0.5 for X=AsF_6^-, y=0.33 for I_3^-) constitute a unique system that involves magnetic ions near the conducting pathway. Both the paramagnetic (M=Co^{2+}, Cu^{2+}) and diamagnetic(M=H_2^{2+}, Ni^{2+}) phthalocyanine yield isostructural conductive crystals. Comparative study of the phthalocyanine-based conductors with paramagnetic and diamagnetic molecules and their alloy system has been conducted in order to elucidate the influence of the localized spins on the conduction electrons. Ogawa *et al.* suggested a strong coupling between the localized spin of Cu^{2+} (S=1/2) and the conduction electron of the Pc chain in $CuPc(I_3)_{0.33}$.[1,2] The influence of the localized spin of Cu^{2+} on the conductivity was studied by Quirion *et al.* on $CuPc(I_3)_{0.33}$ and analogous compounds, in which in the microwave resistivity experiment they found a huge negative magnetoresistance and proposed a spin-flip scattering process produced by Cu^{2+} local spin.[3,4] They studied the alloys, $Cu_xNi_{1-x}Pc(I_3)_{0.33}$[5,6] and $Cu_xH_{2(1-x)}Pc(I_3)_{0.33}$.[7]

Martinsen *et al.* reported the phthalocyanine conductor of another paramagnetic ion, Co^{2+} (S=1/2), on $CoPc(I_3)_{0.33}$, in which the central metal spine was responsible for the conductivity.[8] A similar Co-containing phthalocyanine conductor $CoPc(AsF_6)_{0.5}$ was reported by this group previously.[9-10] In contrast to $CoPc(I_3)_{0.33}$, the Pc chain played a part in the electrical conductivity, and thus the Co^{2+} ions were anticipated to play the same role as Cu^{2+} in $CuPc(I_3)_{0.33}$. To elucidate the role of the Co^{2+} spin in $CoPc(AsF_6)_{0.5}$, we prepared the alloy system $Co_xNi_{1-x}Pc(AsF_6)_{0.5}$. The mixed crystal system $Co_xNi_{1-x}Pc(AsF_6)_{0.5}$ was characterized by elementary analysis of EPMA, X-ray

diffraction, ESR, Raman and Reflection spectra. It is shown that the mixed crystal system is formed in a wide range of x, although the $CoPc(AsF_6)_{0.5}$ is not exactly isomorphous to $NiPc(AsF_6)_{0.5}$. The ESR, Raman and reflection spectra established the formation of mixed crystal in a whole range of x. In this chapter, we present some of the experimental results of these alloys measured using in above-mentioned methods to demonstrate the formation of the alloy system.

3.2 Results and discussion

3.2.1 Elementary analysis and crystals structure

The analysis of several points on each single crystal by means of EPMA indicated that the distribution of Co and Ni atoms in the samples was homogeneous as shown in Fig.1. In all cases, the Co to Ni ratio agreed with the ratio of the initial mixture within 10%.

The crystal structure of $Co_xNi_{1-x}Pc(AsF_6)_{0.5}$ with x=0.25 and 0.45 are isostructural to orthorhombic $NiPc(AsF_6)_{0.5}$ (x=0)[11] and tetragonal $CoPc(AsF_6)_{0.5}$ (x=1),[12] respectively. The lattice parameters were listed in Table 1 along with those of $NiPc(AsF_6)_{0.5}$ and $CoPc(AsF_6)_{0.5}$. The boundary of the tetragonal and orthorhombic systems is located between x=0.25 and 0.45 in this alloy system. The unit cell of $NiPc(AsF_6)_{0.5}$ involves two conducting columns with a metal-over-metal stack, half of the unit cell being almost same as the unit cell of $CoPc(AsF_6)_{0.5}$. Therefore the structure of $CoPc(AsF_6)_{0.5}$ is nearly isostructural to $NiPc(AsF_6)_{0.5}$, which is the reason for the formation of the mixed crystal system in a wide range of x. The most important evidence is that the intermolecular distance of all alloys shortened accompanying the Co

concentration increase, in other words, the higher the Co concentration, the shorter the intermolecular distance will be. As shown in Table 1, the intermolecular distance of both mixed crystals of $Co_{0.25}Ni_{0.75}Pc(AsF_6)_{0.5}$ and $Co_{0.45}Ni_{0.55}Pc(AsF_6)_{0.5}$ are 3.218 and 3.207 *Å* in comparing with 3.233 *Å* of $NiPc(AsF_6)_{0.5}$ and 3.148 *Å* of $CoPc(AsF_6)_{0.5}$, respectively. Among of them the intermolecular distance of $CoPc(AsF_6)_{0.5}$ is the shortest and $NiPc(AsF_6)_{0.5}$ is the longest, while the intermolecular distance of both mixed crystals of $Co_{0.25}Ni_{0.75}Pc(AsF_6)_{0.5}$ and $Co_{0.45}Ni_{0.55}Pc(AsF_6)_{0.5}$ is just between pure compounds. The electron structure of the central ion is responsible for the difference of the intermolecular distance. The Ni^{2+} ion does not have an unpaired electron, however, the Co^{2+} ion has an unpaired electron occupied the $3d_{z^2}$ orbital, which is extended to the neighboring molecules and forms a one-dimensional band. The result of the parameter *c*, which decreases systematically with the increase of *x*, shows that CoPc is mixed in the $NiPc(AsF_6)_{0.5}$ crystal lattice on a molecular level when x=0.25 and 0.45. As mentioned above, the intermolecular distance of these mixed crystals is a quite reasonable result to support the formation of the mixed crystals.

3.2.2 ESR properties

Figure 2 shows well-resolved anisotropic hyperfine structures of $Co_{0.01}Ni_{0.99}Pc(AsF_6)_{0.5}$ at 3.5 *K* ($H//c$) and 3.2 *K* ($H\perp c$). The *g* value was determined at the mid-field between M_I=±1/2 lines. The NiPc molecules are stacked along the *c*-axis making their molecular planes exactly parallel to the *ab* plane. Therefore the *c*-axis of the crystal is parallel to the fourfold rotation axis of the NiPc molecule, and the *a* and *b* axes are nearly equivalent with each other. Based on the characteristic crystal structure,

the angular dependence of g value is expected to conform to the following equation, if CoPc is relevantly substituted in the crystal lattice of $NiPc(AsF_6)_{0.5}$,

$$g(\theta) = (g_{//}^2 \cos^2\theta + g_{\perp}^2 \sin^2\theta)^{1/2}, \quad (1)$$

where θ is the angle between the c-axis and magnetic field, $g_{//}$ and $g_{\perp}$ the principal g values parallel and perpendicular to the c-axis, respectively. As shown in Fig. 3, the experimentally obtained angular dependence (squares) g value of $Co_{0.01}Ni_{0.99}Pc(AsF_6)_{0.5}$ at 3.2 K agrees perfectly with the theoretical curve (solid line) calculated by eq. (1). This result clearly shows that the doped CoPc is relevantly substituted in the alloy.

Hyperfine structure is interpreted according to the Hamiltonian involving the electron and nuclear spins in the field of axial symmetry,[13] which is used to analyze the ESR signal of the magnetically diluted CoPc.[14] The anisotropic g values and hyperfine constants A and B of $Co_{0.01}Ni_{0.99}Pc(AsF_6)_{0.5}$ are $g_{//}$=2.056, $g_{\perp}$ = 3.045, A=0.019 cm^{-1} and B=0.029 cm^{-1}. In comparison with those of CoPc diluted in the insulating β-NiPc and α-ZnPc crystals, the hyperfine constants of the Co^{2+} ion in $Co_{0.01}Ni_{0.99}Pc(AsF_6)_{0.5}$ resemble those in β-$Co_{0.01}Ni_{0.99}Pc$ (A=0.015 cm^{-1} and B=0.028 cm^{-1}) rather than α-$Ni_{0.01}Zn_{0.99}Pc$ (A=0.0116 cm^{-1} and B=0.0066 cm^{-1}). The resemblance of the anisotropic g values as well as the anisotropic hyperfine constants to the magnetically diluted CoPc in β-NiPc indicates that the ESR signal of this compound is coming from the $CoPc^0$ substituted in the molecular column of $NiPc^{0.5+}$. The very similar hyperfine signals were observed in the mixed crystals with x=0.005, 0.014, 0.02, and 0.05. The signal of $Co_{0.09}Ni_{0.91}Pc(AsF_6)_{0.5}$ is nearly a single peak with the linewidth of *ca.* 500 G. No ESR signal was observed in the alloy with x>0.09. We examined the angle dependence of the g values in all these alloys as displayed in Fig. 4. Every signal with $x \leq 0.09$ follows

equation (1). This means that CoPc is microscopically substituted in $NiPc(AsF_6)_{0.5}$ at least in the range of $0.005 \leq x \leq 0.009$.

3.2.3 Raman spectrum

The Raman spectra of these compounds provide another experimental evidence for the formation of the mixed crystals in a whole range of x. The Raman spectrum of $Co_xNi_{1-x}Pc(AsF_6)_{0.5}$ excited by He-Ne laser (633 nm) polarized perpendicular to c-axis looks like to be simply a superposition of those of $CoPc(AsF_6)_{0.5}$ and $NiPc(AsF_6)_{0.5}$ as shown in Fig. 5 and Fig. 6. There is not characteristic band found in the mixed crystal system in this direction. However, the new Raman peaks at 368 cm^{-1} and 736 cm^{-1} appear in the Raman spectra of polarized parallel to c-direction excited by He-Ne laser as shown in Fig. 7 and Fig. 8, which were observed neither in $CoPc(AsF_6)_{0.5}$ nor $NiPc(AsF_6)_{0.5}$ but found in all mixed crystal system. It is surprising that these Raman bands are observable even in a dilute alloy $Co_{0.01}Ni_{0.99}Pc(AsF_6)_{0.5}$. The band at 736 cm^{-1} is the overtone mode of 368 cm^{-1} band. As shown in Fig. 9 and 10, these Raman bands were strongly suppressed when an Ar^+ laser (515 nm) was employed as the excitation light. The resonance effect can explain the appearance of the second harmonic band at 736 cm^{-1}, strong excitation-energy dependence, and high sensitivity to the introduction of CoPc in $NiPc(AsF_6)_{0.5}$. Since the 368 cm^{-1} band appears only in the mixed crystal and the polarized parallel to c-axis Raman spectra, we consider that the excited state was formed in the mixed crystals. The new excited state is proposed to associate with the charge-transfer transition between the neighboring CoPc and NiPc molecules, because this excited state can be formed only in the mixed crystals and the transition

moment to this excited state is parallel to c-axis. The 368 cm^{-1} band tentatively assigned to the a_{1g} breathing mode of NiPc.[15,16] We can know from Fig. 7 and 8, the intensity of the new Raman band, which appears only in the mixed crystals, apparently depends on the Co concentration x. This result of appearance of new Raman bands in mixed crystals strongly indicates the formation of the mixed crystal in a wide range of x.

3.2.4 Reflection spectrum

In all the salts, the c-axis is the stacking axis and they are quasi one-dimensional conductors. As described above, the crystal structure of $CoPc(AsF_6)_{0.5}$ is nearly isostructural to $NiPc(AsF_6)_{0.5}$. The $3d_{z^2}$ orbital of Co^{2+} in $CoPc(AsF_6)_{0.5}$ is singly occupied but the $3d_{z^2}$ orbital of Ni^{2+} is fully occupied in $NiPc(AsF_6)_{0.5}$, and Pc HOMO in both $NiPc(AsF_6)_{0.5}$ and $CoPc(AsF_6)_{0.5}$ are oxidized sustaining the $3d_{z^2}$ electron as it is. This is concluded both by appearing inter-band transition in visible region, diagnostic phonons, and positive thermoelectric power in whole temperature range.[9,12] Although the crystal structure of $CoPc(AsF_6)_{0.5}$ and $NiPc(AsF_6)_{0.5}$ is nearly same with each other, the reflectivity is quite different as presented in Fig. 11 along with the conductivity spectra of both compounds. The plasma edge of $CoPc(AsF_6)_{0.5}$ appears at much higher energy than $NiPc(AsF_6)_{0.5}$. The spectral weight of $NiPc(AsF_6)_{0.5}$ is mostly concentrated below 1500 cm^{-1}, whereas the optical conductivity of $CoPc(AsF_6)_{0.5}$ shows a broad tail up to 6000 cm^{-1} in the infrared region. One of the possible reasons is the enhancement of the bandwidth due to the shortening of the c-axis, since the c-axis of $CoPc(AsF_6)_{0.5}$ is 3% shorter than that of $NiPc(AsF_6)_{0.5}$. The relation between the plasma frequency and lattice constant of $NiPc(AsF_6)_{0.5}$ has been investigated by the high-pressure

experiment.[17] According to the high-pressure experiment, the contraction of *c*-axis by 3% enlarges the plasma frequency only by 4%, which is much smaller than the observed enhancement in $CoPc(AsF_6)_{0.5}$. We therefore consider that the 3*d* orbital also contributes to the optical transition of $CoPc(AsF_6)_{0.5}$ in the mid-infrared region, since the singly occupied $3d_{z^2}$ orbital of Co^{2+} in $CoPc(AsF_6)_{0.5}$ is extended to the neighbor molecules. This idea is confirmed by the systematically changed reflection spectra of mixed crystal polarized parallel to *c*-axis as shown in the Fig. 16 of Chapter 4, which exhibits very similar spectra to $NiPc(AsF_6)_{0.5}$ when the cobalt contents are lower than 0.45. The characteristic line shape of $CoPc(AsF_6)_{0.5}$ is observed in the region of $0.87 \leq x \leq 1$, which is close to $x=1$.

Figure 12 shows a systematic change of the *x* dependent reflection spectra of all mixed crystals polarized perpendicular to *c*-axis in the visible region. Figure 13 presents the conductivity spectra of all alloys polarized perpendicular to *c*-axis, which were calculated by the Kramers-Kronig transformation of the perpendicular to *c*-axis reflectance spectra. In this region as the spectra presented, there appear two intermolecular excitations around 15800 cm^{-1} and 18000 cm^{-1}, both of which are polarized parallel to the molecular plane. As mentioned in the Chapter 1, these two bands appear in the *Q*-band region, which strongly depend upon the central metal and the oxidation.

Before discussing the palorized perpendicular spectra of all alloys, first let us study the spectrum of pure compound $NiPc(AsF_6)_{0.5}$, which was comparatively studied with the solution spectrum of $LuPc_2$,[18] because the same degree of oxidation. The comparison with the spectrum of $LuPc_2$ is useful to assign these two electronic

transitions. In the polarized perpendicular spectrum of crystal $NiPc(AsF_6)_{0.5}$ two electronic transitions are observed at 15800 cm^{-1} and 18000 cm^{-1}. The spectrum of $NiPc(AsF_6)_{0.5}$ in this region has been interpreted in Ref. 18. The band at 15800 cm^{-1} is assigned to the Q-band: the optical transition from the bottom of the conduction band formed by the a_{1u} MO[19,20] to the vacant band formed by the e_g MO. The other band at 18000 cm^{-1} is a new electronic transition to be assigned to the optical transition from the lower fully occupied e_g band to the conduction (HOMO) a_{1u} band. This assignment leads to the important conclusion that this band in the solid spectrum becomes characteristic band of the ligand-centered oxidation, since this transition is not allowed when the central metal is oxidized and should disappear in the neutral molecule. The both two bands were obtained also in the polarized perpendicular spectrum of $CoPc(AsF_6)_{0.5}$ at 15700 cm^{-1} and 19000 cm^{-1}, which can be unanimously assigned to the way as having done the assignment for $NiPc(AsF_6)_{0.5}$. One thing should be noted is that the intensity of the two bands comparing with both compounds of $NiPc(AsF_6)_{0.5}$ and $CoPc(AsF_6)_{0.5}$ is different due to the strong dependence upon the central metal.

In all the alloys, these two bands show a systematic change with the increase of Co concentration x, such as the little shift of these peaks, the spectra appear very similar to $NiPc(AsF_6)_{0.5}$ in the range $0 \leq x < 0.45$ but very close to $CoPc(AsF_6)_{0.5}$ in the range $0.45 \leq x < 1$.

The results of the systematically changed reflectivity polarized parallel to c-axis in the infrared region and perpendicular to c-axis in the visible region forcefully demonstrated the formation of the mixed crystal in a wide range of x.

3.3 Summary

The elementary analysis by means of EPMA suggests that organic alloys $Co_xNi_{1-x}Pc(AsF_6)_{0.5}$ were prepared in a wide range of x. According to the analysis of crystal structure, the boundary of the tetragonal and orthorhombic systems is located between x=0.25 and x=0.45 in this alloy system and the parameter c decreases systematically with the increase of x. In particular, in the range of $0<x\leq0.09$, the very similar hyperfine signals were observed in the ESR experiment. The appearance of new vibrational Raman bands only in the mixed crystals was proposed to associate with the charge-transfer excited state between CoPc and NiPc molecules. This means that the new excited state is formed in the mixed crystal system. The reflectivity shows the systematically changed with the increase of x in both parallel and perpendicular to c direction. All of the observations indicate that the organic alloys $Co_xNi_{1-x}Pc(AsF_6)_{0.5}$ were mixed on a molecular level in a wide range.

References

[1] M. Y. Ogawa, B. M. Hoffman, S. Lee, M. Yudkowski, and W. P. Halperin, *Phys.Rev. Lett.*, **57**,1177 (1986).

[2] M. Y. Ogawa, J. Martinsen, S. M. Palmer, J. L. Stanton, J. Tanaka, R. L. Green, B. M. Hoffman, and J. A. Ibers, *J. Amer. Chem. Soc.*, **109**, 1115 (1987).

[3] G. Quirion, M. poirier, K. K. Liou, M. Y. Ogawa, and B. M. Hoffman, *Phys. Rev.* B, **37**, 4272 (1988-I).

[4] G. Quirion, M. Poirier, C. Ayache, K. K. Liou, and B. M. Hoffman, *J. Phys. I France* **2**, 741 (1992).

[5] M. Y. Ogawa, S. M. Palmer, K. K. Liou, G. Quirion, J. A. Thompson, M. poirier, and B. M. Hoffman, *Pfys. Rev.* B, **39**, 10682 (1989-1).

[6] J. Martinsen, J. L. Stanton, R. L. Green, J. Tanaka, B. M. Hoffman, and J. A. Ibers, *J. Amer. Chem. Soc.*, **107**, 6915 (1985).

[7] J. Thompson, K. Murata, R. Durcharne, m. Poirier, and B. M. Hoffman, *Phys. Rev.* B, **60**, 523 (1999-1).

[8] J. Martinsen, J. L. Stanton, R. L. Green, J. Tanaka, B. M. Hoffman, and J. A. Ibers, *J.Amer. Chem. Soc.*, **107**, 6915 (1985).

[9] K. Yakushi, H. Yamakado, T. Ida, and A. Ugawa, *Solod State Commun.*, **78**, 919 (1991).

[10] H. Yamakado, A. Ugawa, T. Ida, and K. Yakushi, *The physics and chemistry of organic superconductors*, p.**311**, Ed. By G. Saito and S. Kagoshima, Springer-Verlag Berlin, Heidelberg (1999).

[11] G. M. Sheldrick, *Acta Crystallogr.*, Sect. A, **46**, 467 (1990).

[12] H. Yamakado, T. Ida, A. Ugawa, K. Yakushi, K. Agawa, Y. Maruyama, K. Imaeda, and H. Inokuchi, *Synth. Met.*, **62**, 169 (1994).

[13] B. Bleany, *Philos. Mag.*, **42**, 441 (1951).

[14] J. M. Assour and W. K. kahn, *J. Amer. Chem. Soc.*, **87**, 207 (1965).

[15] X.-Y. Li, R. S. Czernuszewicz, J. R. Kincaid, Y. O. So, and T. G. Spiro, *J. Phys. Chem.*, **94**, 31 (1990).

[16] X.-Y. Li, R. S. Czernuszewicz, J. R. Kincaid, P. Stein, and T. G. Spiro, *J. Phys. Chem.*, **94**, 47, (1990).

[17] Hiejima T, Yakushi k, Adachi T, Shimomura O, Takeda K, Shirotani I, Imaeda K, Inokuchi H. *Mol. Cryst. Liq. Cryst.* **296,** 255 (1997).

[18] K. Yakushi, T. Ida, A. Ugawa, H. Yamakado, H. Ishii, and H. Kuroda, *J. Phys. Chem.* **95**, 7636 (1991).

[19] The e_g obital is located 0.57 eV below the a_{1u} HOMO on the calculation by the DV-X_α method [20].

[20] Kutzler FW, Ellis DE. *J. Chem. Phys.* **84**, 1033 (1986).

Table 1. Lattice parameters of $Co_xNi_{1-x}Pc(AsF_6)_{0.5}$

	$NiPc(AsF_6)_{0.5}$	$Co_{0.25}Ni_{0.75}Pc(AsF_6)_{0.5}$	$Co_{0.45}Ni_{0.55}Pc(AsF_6)_{0.5}$	$CoPc(AsF_6)_{0.5}$
Formula	$C_{32}H_{16}N_8NiAs_{0.5}F_3$	$C_{32}H_{16}N_8Co_{0.25}Ni_{0.75}As_{0.5}F_3$	$C_{32}H_{16}N_8Co_{0.45}Ni_{0.55}As_{0.5}F_3$	$C_{32}H_{16}N_8CoAs_{0.5}F_3$
Formula weight	665.7	665.8	665.8	665.9
crystal class	orthorhombic	orthorhombic	tetragonal	tetragonal
space group	*Pnc2*	*Pnc2*	*P4/mcc*	*P4/mcc*
a/Å	14.015(1)	14.033(4)	14.226(2)	14.234(2)
b/Å	28.485(2)	28.54(1)	14.226(2)	14.234(2)
c/Å	6.466(3)	6.435(2)	6.414(1)	6.296(2)
Z	4	4	2	2
R-factor	6.5%	6.8%	7.0%	7.3%

*Cite from Y. Yonehara's thesis.

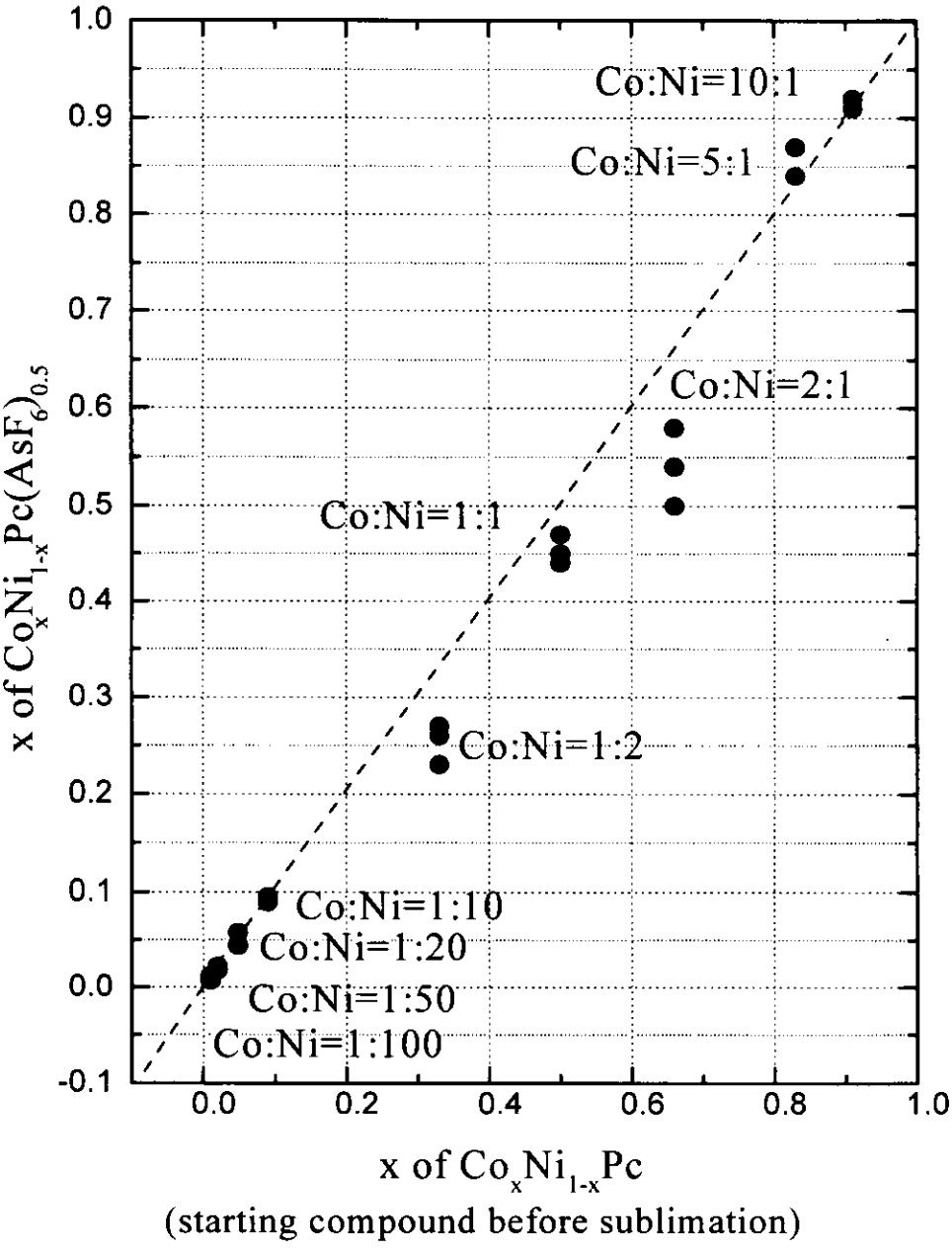

Fig.1 Compositions of mixed crystals $Co_xNi_{1-x}Pc(AsF_6)_{0.5}$

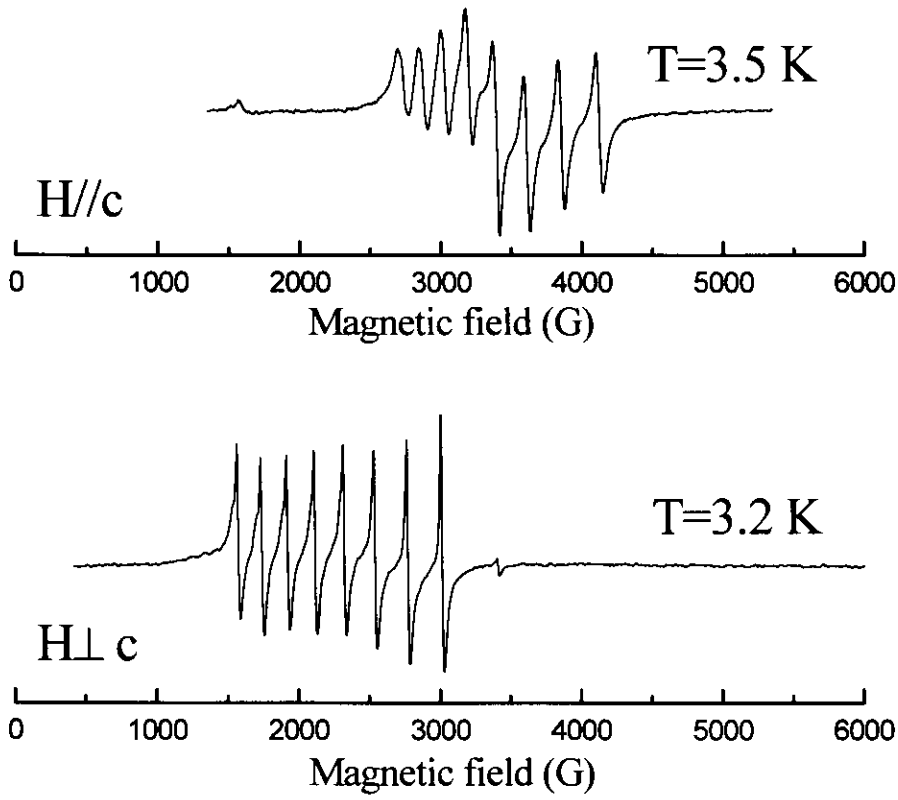

Fig.2 Hyperfine structure of $Co_{0.01}Ni_{0.99}Pc(AsF_6)_{0.5}$

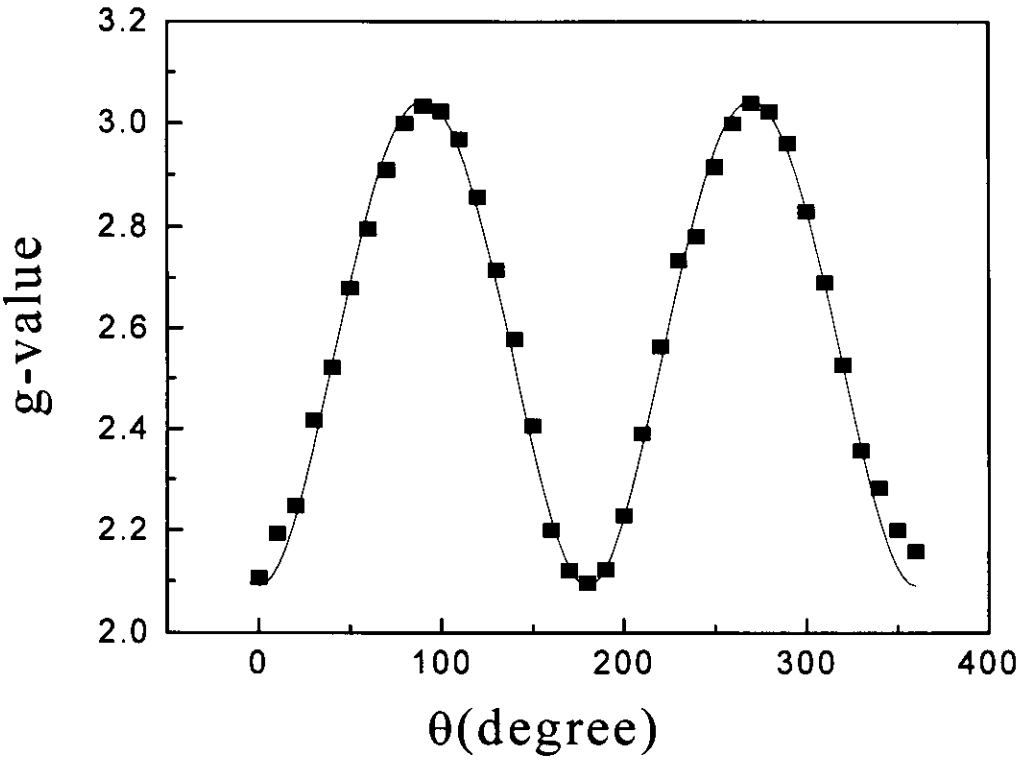

Fig.3 Angle dependence of *g*-value of $Co_{0.01}Ni_{0.99}Pc(AsF_6)_{0.5}$ at 3.2 *K*

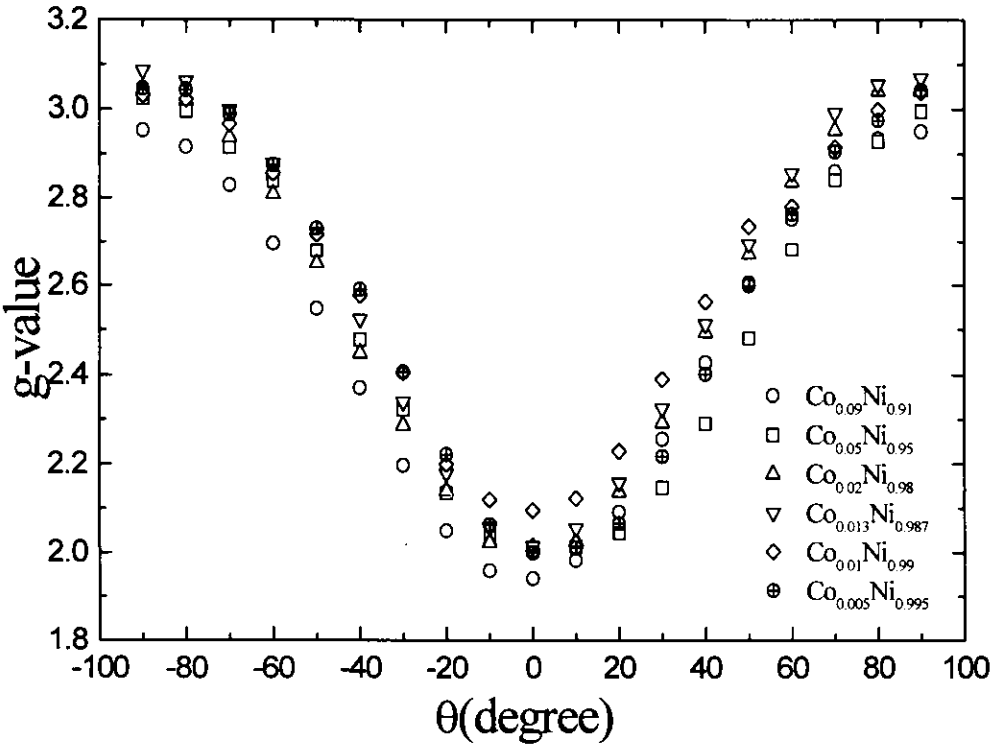

Fig. 4 Angle dependence of g-value of $Co_xNi_{1-x}Pc(AsF_6)_{0.5}$ at 3.5 K

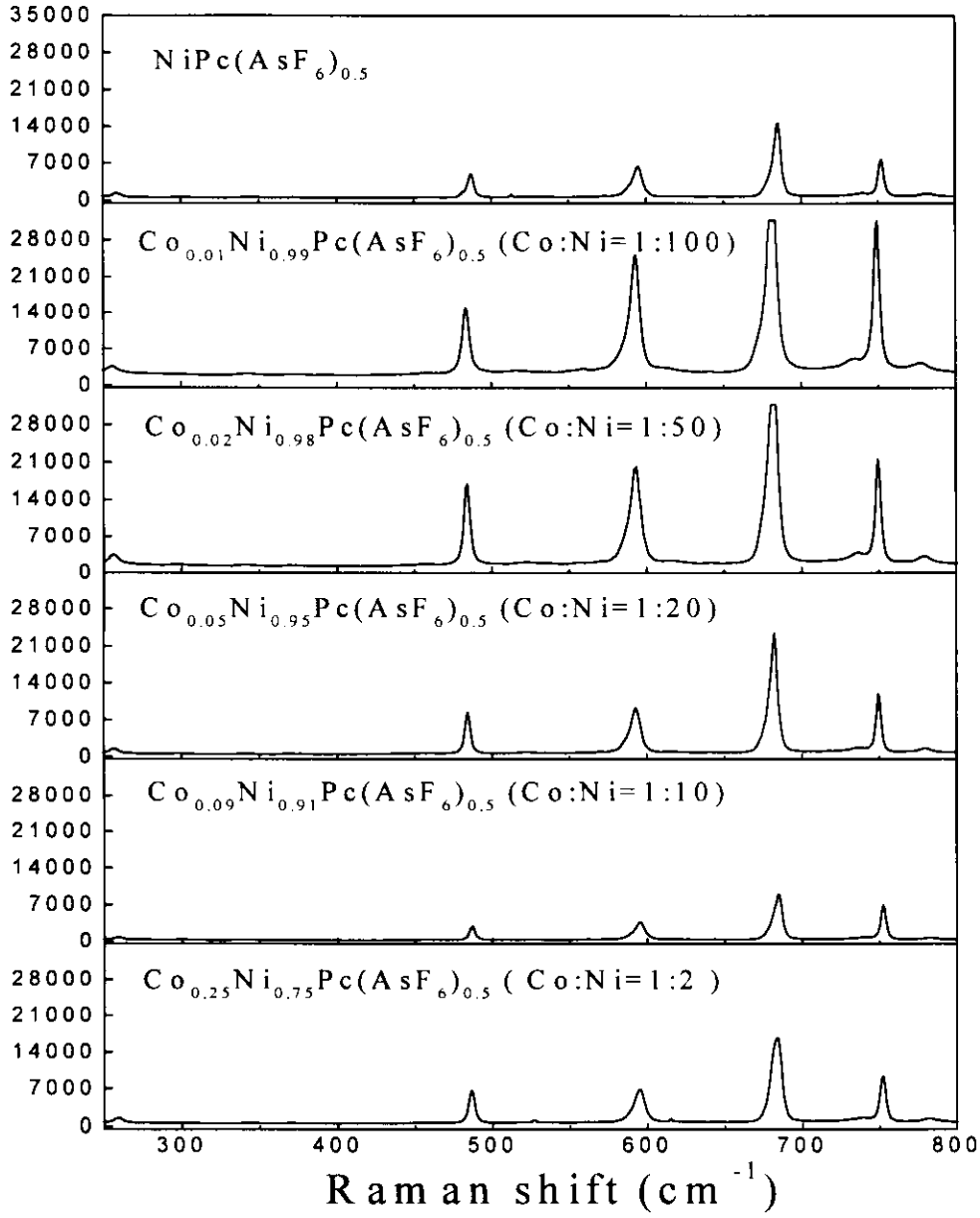

Fig.5 Raman spectra of $Co_xNi_{1-x}Pc(AsF_6)_{0.5}(0\leq x\leq 0.25)$ excited by He-Ne laser polarized perpendicular to *c*-axis

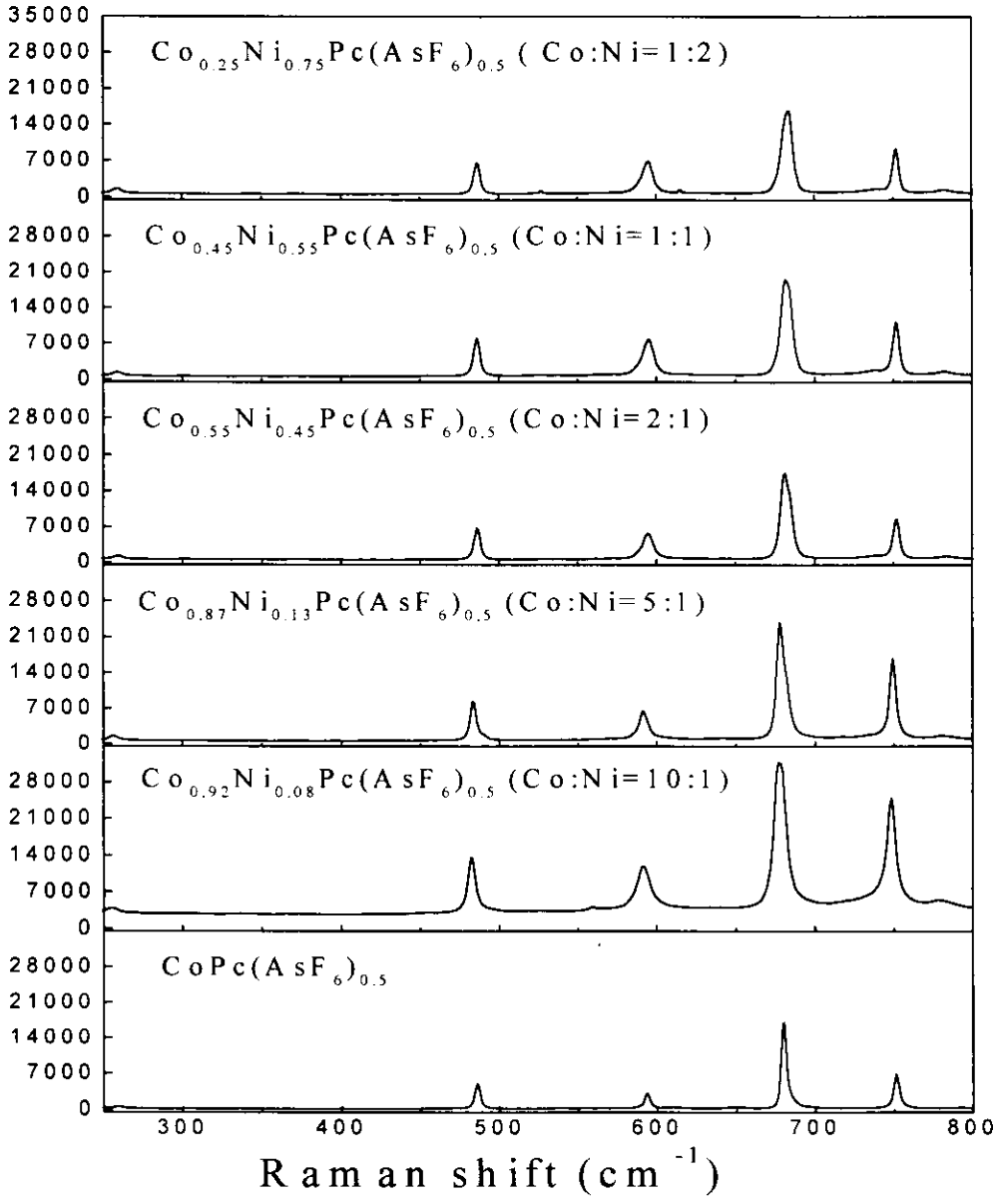

Fig.6 Raman spectra of $Co_xNi_{1-x}Pc(AsF_6)_{0.5}(0.25 \leq x \leq 1)$ excited by He-Ne laser polarized perpendicular to *c*-axis

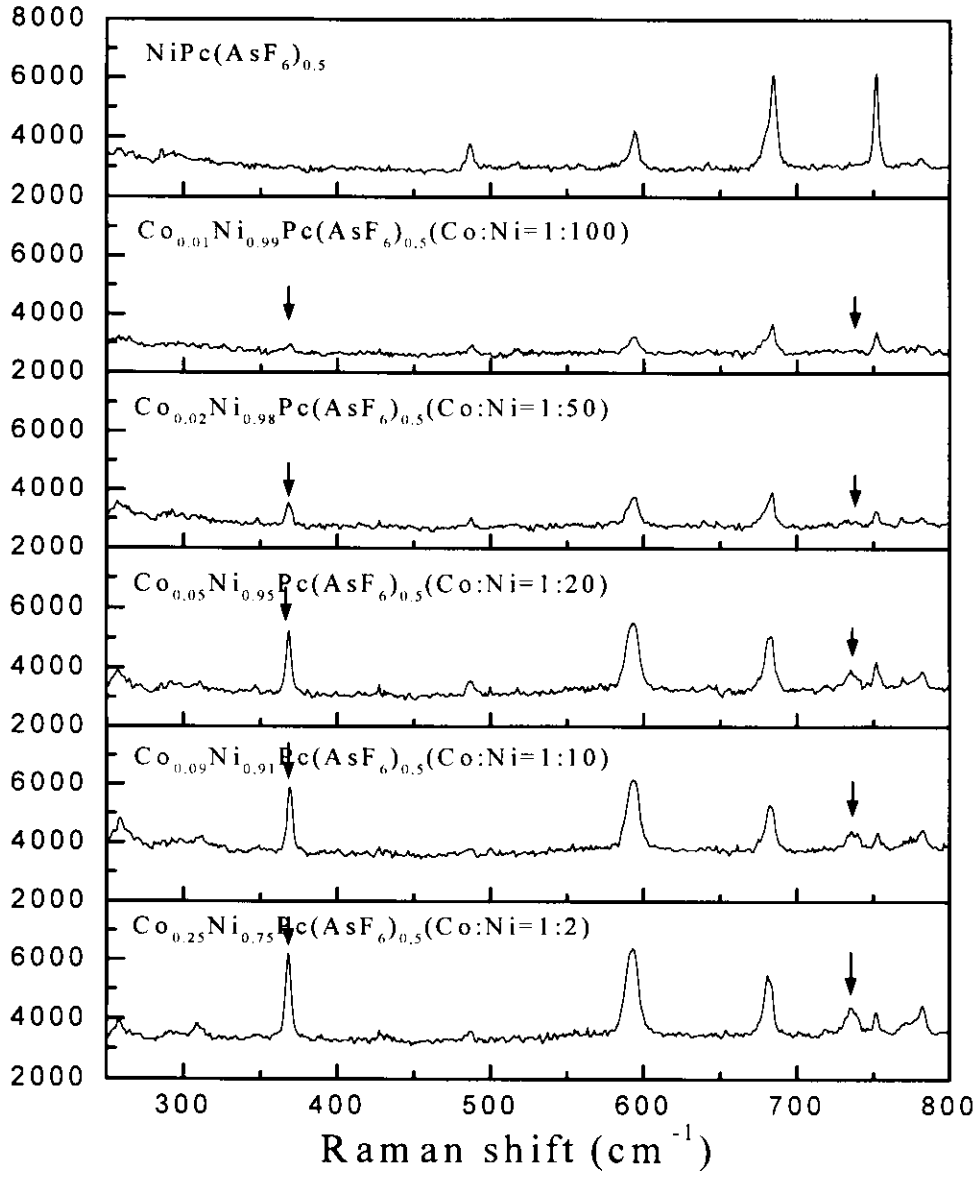

Fig.7 Raman spectra of $Co_xNi_{1-x}Pc(AsF_6)_{0.5}(0\leq x\leq 0.25)$ excited by He-Ne laser polarized parallel to *c*-axis

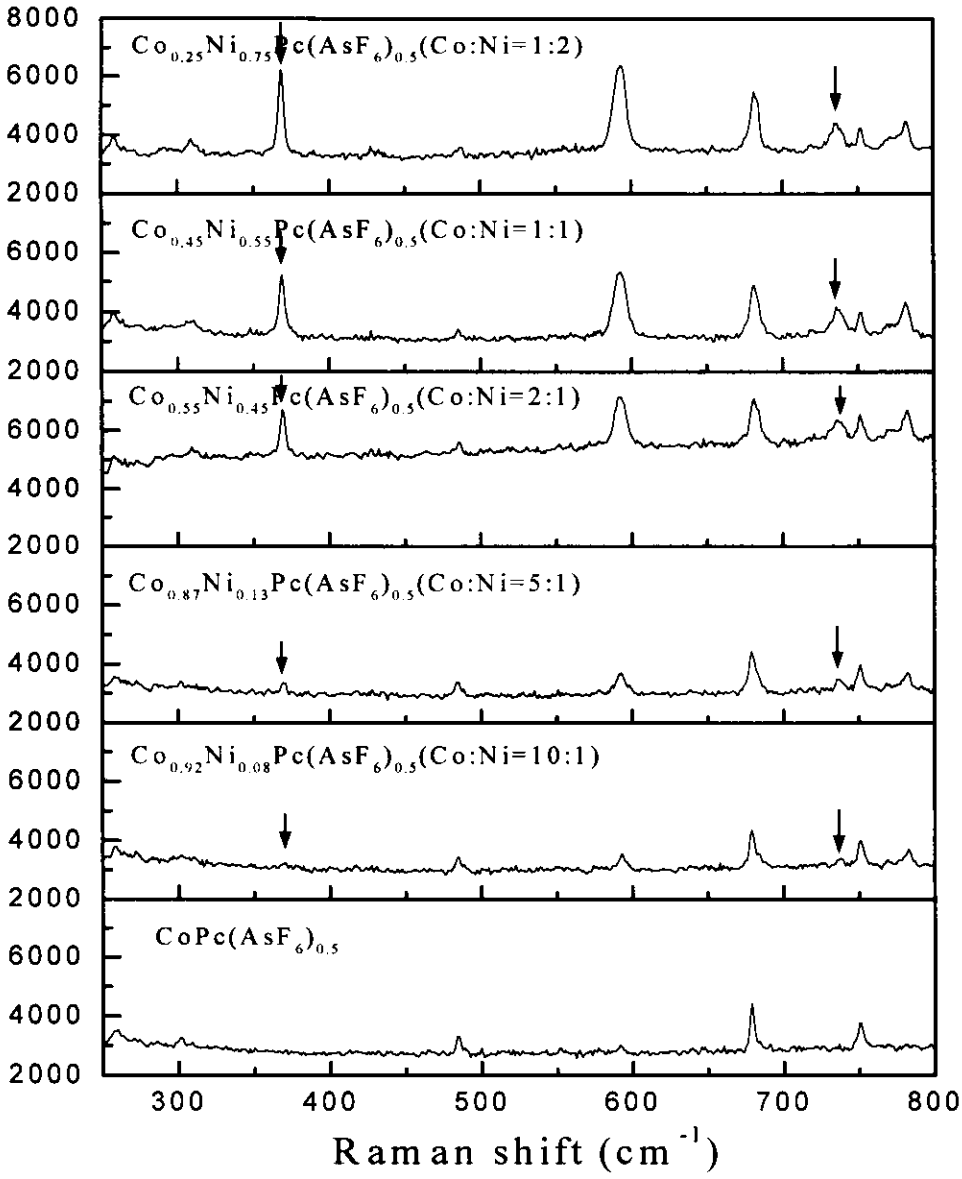

Fig.8 Raman spectra of $Co_xNi_{1-x}Pc(AsF_6)_{0.5}(0.25\leq x\leq 1)$ excited by He-Ne laser polarized parallel to *c*-axis

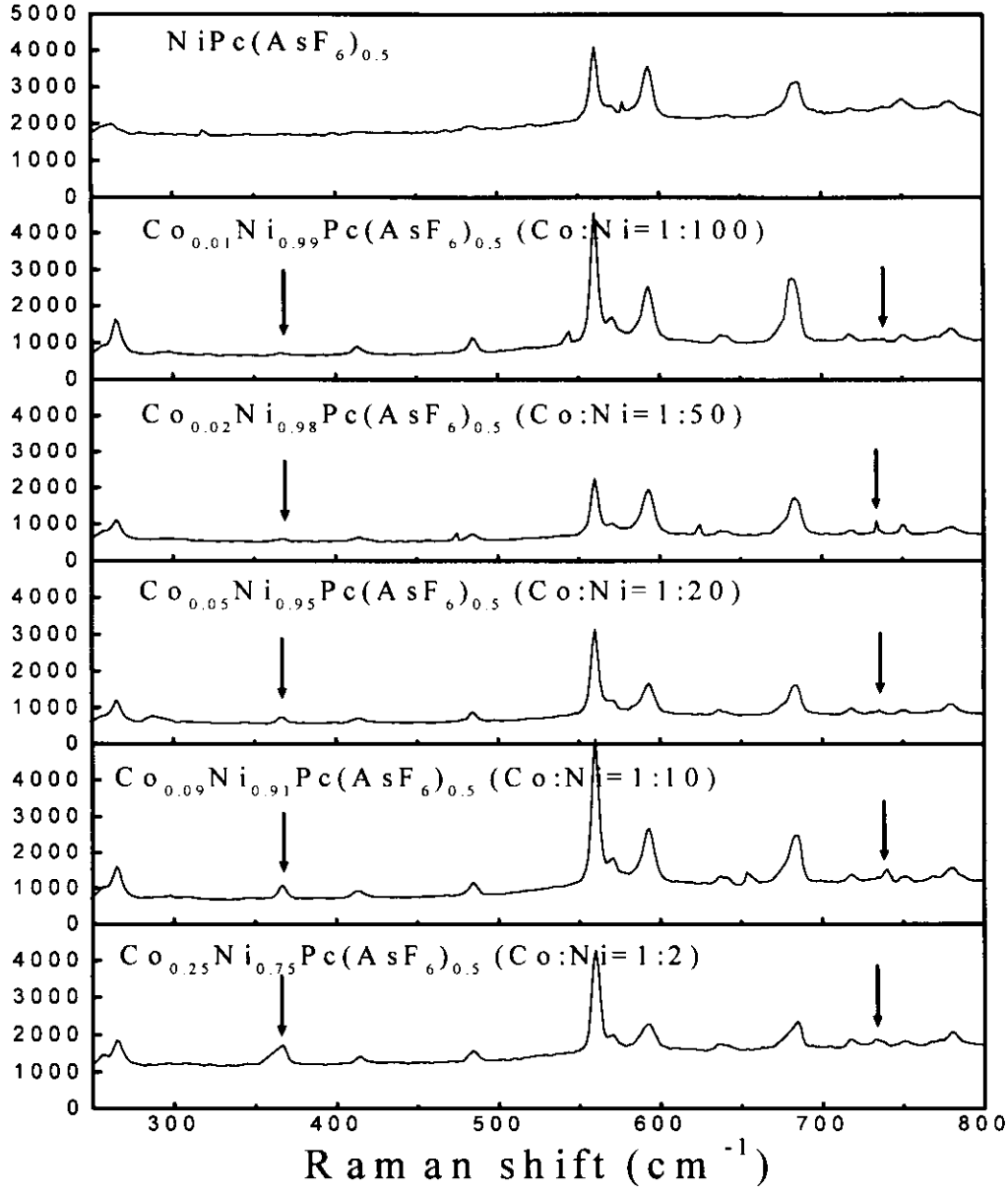

Fig.9 Raman spectra of $Co_xNi_{1-x}Pc(AsF_6)_{0.5}(0\leq x\leq 0.25)$ excited by Ar^+ laser polarized parallel to *c*-axis

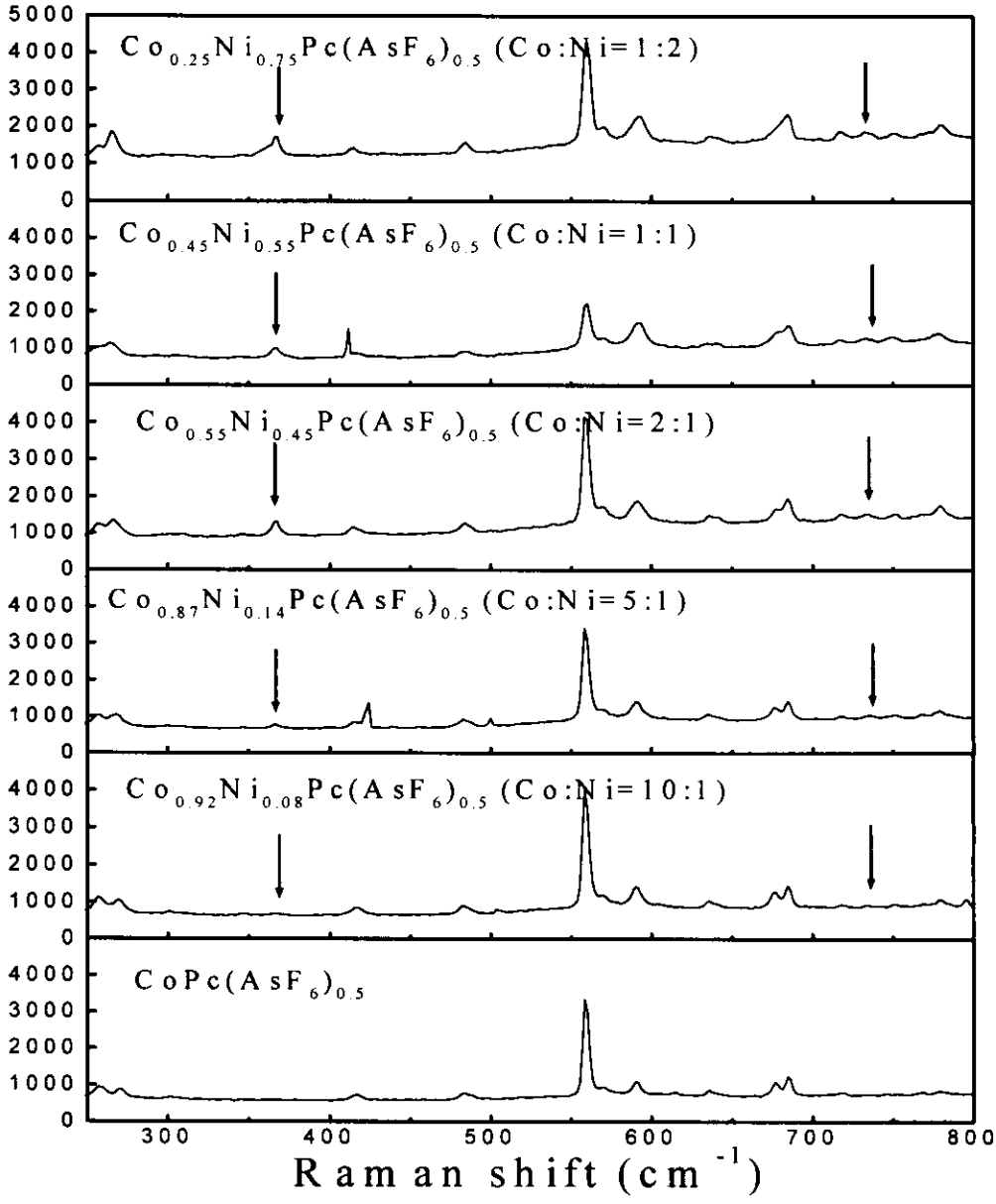

Fig.10 Raman spectra of $Co_xNi_{1-x}Pc(AsF_6)_{0.5}(0.25\leq x\leq 1)$ excited by Ar^+ laser polarized parallel to *c*-axis

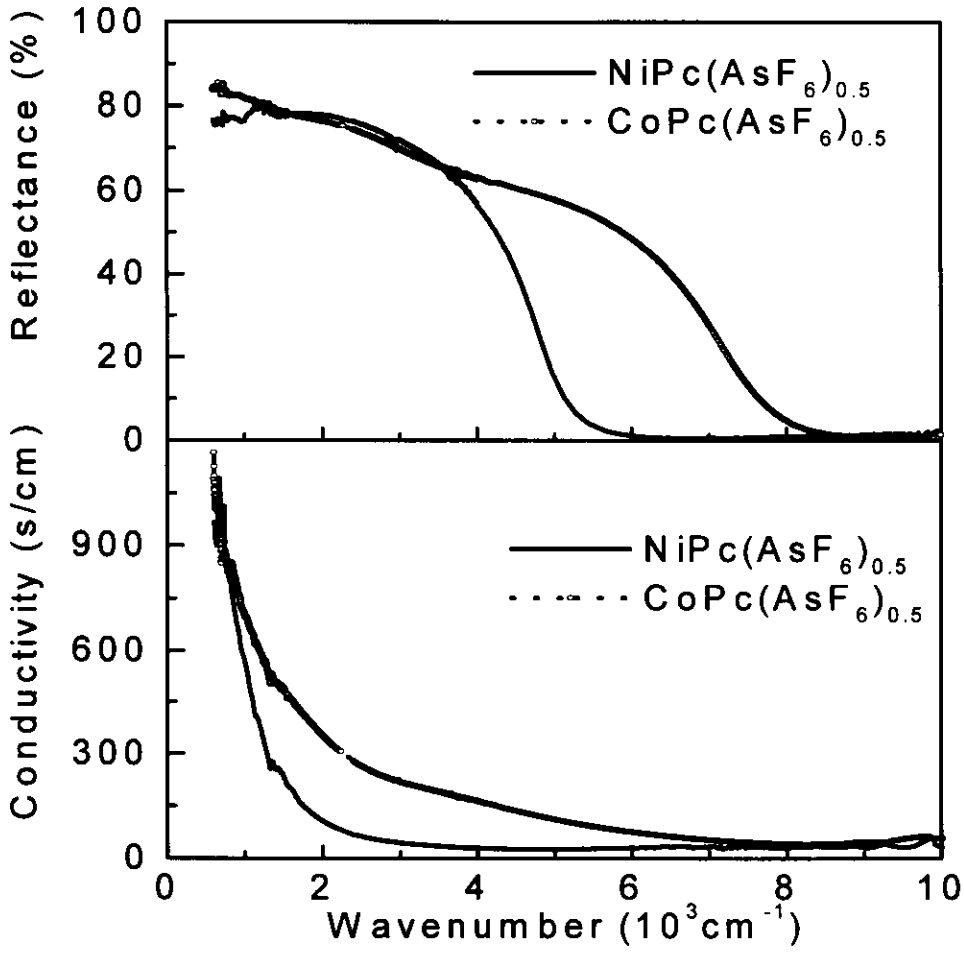

Fig. 11 Reflectivity and conductivity of $NiPc(AsF_6)_{0.5}$ and $CoPc(AsF_6)_{0.5}$ polarized parallel to *c*-axis in infrared region

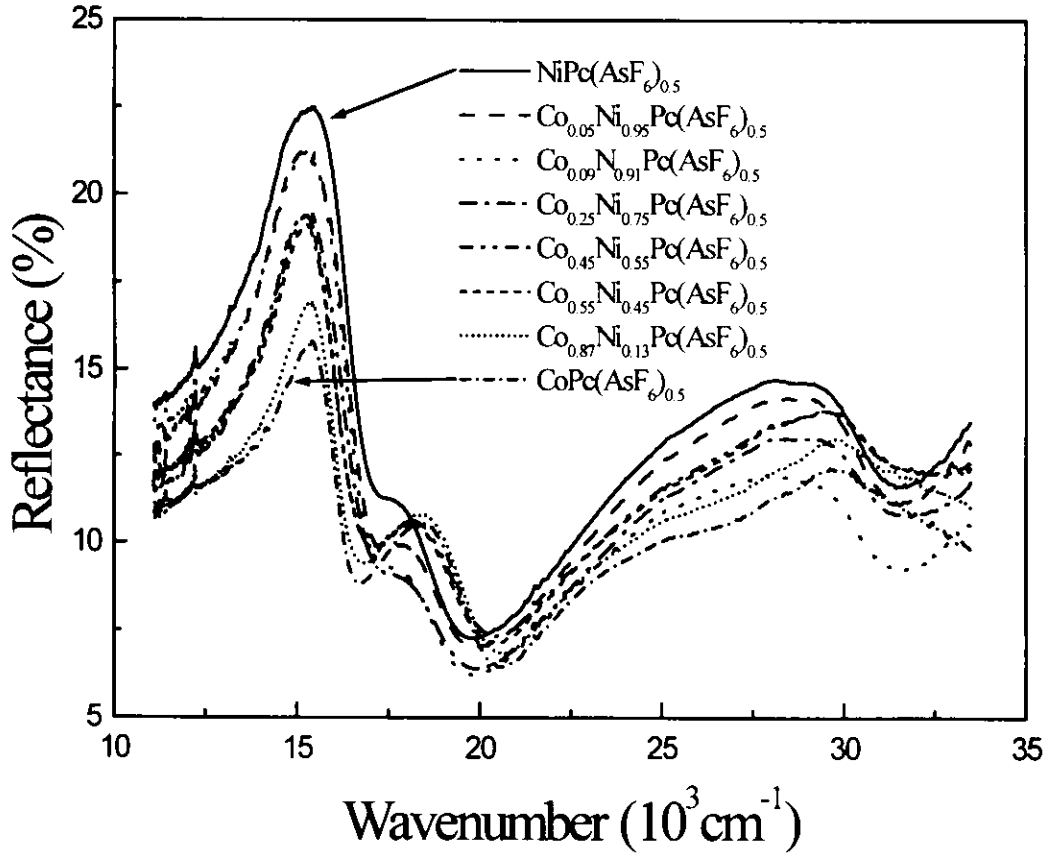

Fig.12 Reflection spectra of $Co_xNi_{1-x}Pc(AsF_6)_{0.5}$ perpendicular to *c*-axis in visible region

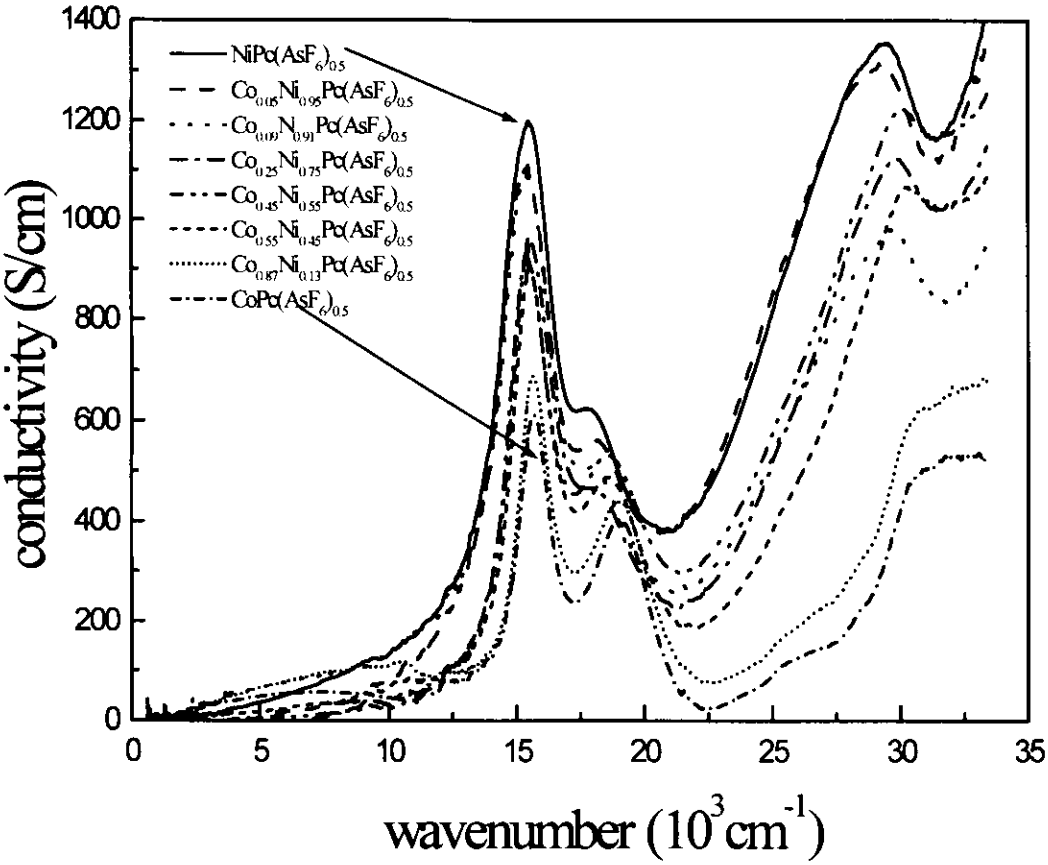

Fig.13 Conductivity spectra of $Co_xNi_{1-x}Pc(AsF_6)_{0.5}$ perpendicular to *c*-axis in visible region

Chapter 4

Electronic structure of organic alloy $Co_xNi_{1-x}Pc(AsF_6)_{0.5}$ ($0 \leq x \leq 1$)

Y. Ding, M. Simonyan, Y. Yonehara, M. Uruichi, and K. Yakushi

Preparation and characterization of phthalocyanine-based organic alloy

$Co_xNi_{1-x}Pc(AsF_6)_{0.5}$ ($0 \leq x \leq 1$)

J. Mater. Chem., **11** (2001) 1469-1475

4.1 Introduction

The metallo-phthalocyanine (*M*Pcs) make up a family of quasi one-dimensional phthalocyanine conductors such as $MPc(X)_y$ (M=H_2^{2+}, Co^{2+}, Ni^{2+}, Cu^{2+}, Pc=$(C_{32}N_8H_{16})^{2-}$; y=0.5 for X=AsF_6^-, y=0.33 for I_3^-). These charge transfer salts are unique two-chain and two-band system, in which the metal and macrocycle (Pc) chains run parallel to each other, and form a one-dimensional (1D) *d*- and π-bands, respectively. Since the molecules are stacked on a metal-over-metal fashion, the 1D metal chain is surrounded with the 1D macrocycle chain. Owing to the orbital symmetry, the 3*d* orbitals except for $3d_{xy}$ and $3d_{yz}$ are not hybridized with the $2p_z$ orbital of Pc, and thus preserve independent *d*-character. The π-electrons are not only delocalized within the macrocycle but also extended to the neighboring molecules, whereas 3*d*-electrons are localized near the central metal. Because of the structural characteristics, phthalocyanine conductors show π- and *d*-characters in the solid state properties. The effect of 3*d* orbital becomes obvious, particularly when the 3*d* orbital of the central metal is singly occupied such as in paramagnetic CuPc and CoPc. The comparative study of the phthalocyanine-based conductors with paramagnetic (M=Co^{2+}, Cu^{2+}) and diamagnetic (M=H_2^{2+}, Ni^{2+}) molecules and their alloys has been conducted in order to elucidate the role of the singly occupied 3*d* electrons.[1-8] In the case of $CoPc(AsF_6)_{0.5}$, 3*d* orbital of Co has an unpaired electron in comparison with the fully occupied 3*d* orbital of Ni in $NiPc(AsF_6)_{0.5}$. In contrast to $CuPc(I_3)_{0.33}$, the Pc chain played a part in the electrical conductivity, and thus the Co^{2+} ions were anticipated to play the same role as Cu^{2+} in $CuPc(I_3)_{0.33}$. However, the singly occupied molecular orbital (SOMO) of Co^{2+} is very suppressed in $CoPc(AsF_6)_{0.5}$,[9] whereas, the Cu^{2+} spin of

$CuPc(I_3)_{0.33}$ is nearly free from the antiferromagnetic interaction.[2] The plasma edge of $CoPc(AsF_6)_{0.5}$ appears at significantly higher energy than that of $CuPc(I_3)_{0.33}$.[2,9] To elucidate the role of the $3d$ orbital of Co^{2+} in $CoPc(AsF_6)_{0.5}$, we investigated the alloys with $NiPc(AsF_6)_{0.5}$.

In this chapter, we present and analyze the experimental results. The appearance of new Raman bands was interpreted as a resonance effect, because first the second harmonic band appears, second they show a strong excitation dependence, and third they are highly sensitive to the introduction of CoPc. To obtain the bandwidth of the $CoPc(AsF_6)_{0.5}$, we analyzed the reflection and conductivity spectra using Drude and Lorentz models. Finally we propose a model for the energy band near the Fermi level including the $3d$ bands. This band model explains the difference in the magnetic and optical properties between $CoPc(AsF_6)_{0.5}$ and $NiPc(AsF_6)_{0.5}$.

4.2 Results and discussion

4.2.1 Crystal structure

We have determined the crystal structures of $Co_xNi_{1-x}Pc(AsF_6)_{0.5}$ with x=0.25 and x=0.45 as shown in Fig. 1 viewed along the stacking axis. The structure was solved using the occupancy factor of Ni and Co determined by EPMA. Owing to the high symmetry of the $CoPc(AsF_6)_{0.5}$ crystal, AsF_6^- is orientationally disordered. The lattice parameters are listed in Table 1 of Chapter 3 along with those of $NiPc(AsF_6)_{0.5}$ (x=0)[10] and $CoPc(AsF_6)_{0.5}$ (x=1)[9]. There is a significant difference in the c-axes between $NiPc(AsF_6)_{0.5}$ and $CoPc(AsF_6)_{0.5}$. This difference is explained by the doubly occupied $3d_{z^2}$ orbital in NiPc and singly occupied $3d_{z^2}$ orbital in CoPc.[9] Owing to the metal-over-

metal stacking fashion, a repulsive force works between the neighboring Ni atoms in $NiPc(AsF_6)_{0.5}$, whereas an attractive force works between the Co atoms in $CoPc(AsF_6)_{0.5}$. Probably from this reason, NiPc is stacked in a slightly zigzag fashion, and thus the symmetry of the molecular arrangement is lowered from the tetragonal symmetry. The parameter c decreases systematically with the increase of x. This result is due to the enhancement of the Co content, which makes the probability of close CoPc increase.

4.2.2 Magnetic properties

The ESR signals were found in the alloy with $x \leq 0.09$. Figure 2 shows the typical anisotropic hyperfine structure found in $Co_{0.01}Ni_{0.99}Pc(AsF_6)_{0.5}$ at 3.5 K ($H//c$) and 3.2 K ($H \perp c$). The separation between the hyperfine lines significantly increases toward higher field. This hyperfine structure is analyzed according to the Hamiltonian in the field of axial symmetry,[11] which is used for the analysis of the ESR signal of the magnetically diluted CoPc.[12] The hyperfine constants of the Co^{2+} ion in $Co_{0.01}Ni_{0.99}Pc(AsF_6)_{0.5}$ resemble those in β-$Co_{0.01}Ni_{0.99}Pc$ rather than α-$Co_{0.01}Zn_{0.99}Pc$. This is because the local environment of the Co^{2+} ion doped in $NiPc(AsF_6)_{0.5}$ resembles that in β-NiPc.[12] Resemblance of the anisotropic g value as well as the anisotropic hyperfine constants to the magnetically diluted CoPc in β-NiPc indicates that the hyperfine signal of this compound is coming from the $CoPc^0$ substituted in the molecular column of $NiPc^{0.5+}$. No super-hyperfine structure from the nearest four nitrogen atoms is observed in $Co_{0.01}Ni_{0.99}Pc(AsF_6)_{0.5}$ or in magnetically diluted CoPc in α-ZnPc and β-NiPc. This result indicates that the unpaired electron occupies the $3d_{z^2}$ orbital of Co^{2+}, and this

orbital is not extended to the nitrogen atoms.[13] The very anisotropic g value also supports the $3d_{z^2}$ orbital for the location of the unpaired electron in CoPc.[14]

As shown in Fig. 2, the *H//c* signal is well reproduced by the superposition of the sharp hyperfine signals and broad one with a linewidth of 420 *G*. The circles in *H//c* spectrum represent the experimental data, and the solid line is the least-squares-fit curve composed of 8 sharp and 1 broad Lorentzians. The each Lorentzian is drawn in the bottom of this figure. The integrated intensity of the sum of the sharp signals and broad signal is 15% and 85%, respectively. The sharp signals are ascribed to free CoPc isolated from other CoPc and the broad one to relatively close CoPc, the signal of which is broadened by the dipole-dipole interaction. The ESR signal ascribed to isolated $CoPc^+$ is not found in this alloy. This result is consistent with the fact that the oxidation potential of NiPc is lower than that of CoPc. When the CoPc content is increased, the contribution of the broad signal increases. As a result, the signal of $Co_{0.09}Ni_{0.91}Pc(AsF_6)_{0.5}$ (x=0.09) becomes nearly a single peak with the linewidth of *ca.* 500 *G* and no ESR signal was observed in the alloy with x>0.1. This tendency is reasonable, since the probability of close CoPc quickly increases when x increases.

4.2.3 Polarized Raman spectrum

We have compared the Raman spectra of CoPc and NiPc with those of the corresponding charge-transfer salts $CoPc(AsF_6)_{0.5}$ and $NiPc(AsF_6)_{0.5}$ in the region of 150-2000 cm^{-1} polarized parallel and perpendicular to the long axis excited by He-Ne laser. The frequency shift caused by partial oxidation is less than 6 cm^{-1} as shown in Fig. 3 and 4. It is much smaller than the oxidation shift found in organic conductors

such as (BEDO-TTF)$_2X$.[15] Since CoPc$(AsF_6)_{0.5}$ has a high symmetry D_{4h}, the polarized Raman spectrum of this compound provides the information on the symmetry of the molecular vibration. The normal modes of the free CoPc molecule are classified into the following representation:

$$\Gamma_{vib} = 14a_{1g} + 13a_{2g} + 14b_{1g} + 14b_{2g} + 13e_g + 6a_{1u} + 8a_{2u} + 7b_{1u} + 7b_{2u} + 28e_u$$

Among these intramolecular vibrations, these of a_{1g}(R; $\alpha_{xx}+\alpha_{yy}$, α_{zz}), a_{2g}(RR; $\alpha_{xy}=-\alpha_{yx}$), b_{1g}(R; $\alpha_{xx}-\alpha_{yy}$), b_{2g}(R; α_{xy}), and e_u(IR; T_x, T_y) modes are in-plane vibrations of CoPc molecule, and these of a_{1u}, a_{2u}(IR; T_z), b_{1u}, b_{2u}, and e_u(R; α_{xz}, α_{yz}) modes are out-of-plane intramolecular vibrations of CoPc molecule. The unit cell contains two molecules, in which one of the two molecules is related by glide plane $\{\sigma_{xz}|c/2\}$, $\{\sigma_{yz}|c/2\}$,$\{\sigma_{x+y}|c/2\}$, $\{\sigma_{x-y}|c/2\}$ and two-fold rotation, $\{C_2^x\}$, $\{C_2^y\}$, $\{C_2^{x+y}\}$, $\{C_2^{x-y}\}$, therefore, these symmetry operations produce nine correlated vibrations with A_{1g}, A_{2g}, B_{1g}, B_{2g}, E_g, A_{1u}, A_{2u}, B_{1u}, A_{2u} and E_u modes. In these vibrations, the A_{1g}, B_{1g}, B_{2g} and E_g modes are Raman active from first principles of vibrational theory and the A_{2g} mode can be become active in resonance Raman. The symmetry of the coupled vibrations in the unit cell, which is connected with that of the free molecule by means of factor group analysis, is shown in Table 1. The in-plane vibrations of a_{1g}, a_{2g} and b_{1g}, b_{2g} operations produce the in-phase and out-of-phase vibrations, respectively. In-phase vibration has A_{1g} and B_{1g} symmetry, and out-of-phase vibration has A_{2g} and B_{2g} symmetry. The symmetry of these vibrations is shown in Fig. 5.

The polarized Raman spectra of CoPc$(AsF_6)_{0.5}$ excited by He-Ne laser are shown in Fig. 6. Only the low frequency Raman spectra were concerned because the observed new Raman peaks in alloy are in this region. The four strong bands at 484, 592, 678 and

750 cm^{-1} in (a,a) polarization have been respectively assigned to a_{2g}, b_{2g}, a_{1g}, and b_{1g} modes by Bartholomew *et al.*[16] According to Table 1, A_{1g} and B_{1g} modes are Raman active in (a,a) polarization, and these modes are derived from a_{1g}, a_{2g}, b_{1g} and b_{2g} molecular vibrations.[17] Thus the result of the (a,a) spectrum is consistent with ref. 16. In (a,b) polarization, the Raman active modes are assigned to B_{2g} symmetry that are derived from the b_{1g} or b_{2g} molecular vibrations. Therefore, the a_{1g} and a_{2g} molecular vibrations should disappear in (a,b) polarization among the observed modes in (a,a) polarization. As shown in Fig. 6, the 592 and 678 cm^{-1} bands disappear in (a,b) polarization, and thus these two bands can be assigned to the a_{1g} or a_{2g} mode. From the same reason, the symmetry of the 484 and 750 cm^{-1} bands is assigned to b_{1g} or b_{2g}. As shown above, the polarization dependence indicates that the symmetry of the 484 and 592 cm^{-1} bands is different from the assignment of ref. 16. The symmetry of these bands should be corrected as b_{1g} or b_{2g} for 484 cm^{-1} and a_{1g} or a_{2g} for 592 cm^{-1}. No Raman active band was found in (c,a) polarization. This is reasonable because only the E_g mode, which is an out-of-plane vibration, is allowed in this polarization. The spectrum in (c,c) polarization is also very weak, since this polarization is associated with the Raman tensor of $d\alpha_{cc}/dQ$, which is the tensor component perpendicular to the molecular plane.

Before discussing the polarized Raman spectra of $NiPc(AsF_6)_{0.5}$, we first analyze the symmetry of molecular vibrations as the way as having done for $CoPc(AsF_6)_{0.5}$. In comparison with $CoPc(AsF_6)_{0.5}$, the molecular arrangement of $NiPc(AsF_6)_{0.5}$ is approximately the same as $CoPc(AsF_6)_{0.5}$. This means that the intramolecular vibration of NiPc is exactly same with CoPc. However, the crystal symmetry of $NiPc(AsF_6)_{0.5}$ is

lower than $CoPc(AsF_6)_{0.5}$, since the unit cell contains four molecules. These molecules in the unit cell are related by the glide planes $\{\sigma_{xz}|c/2\}$ and $\{\sigma_{yz}|(b+c)/2\}$, and two-fold rotation, $\{\sigma_2^y\}$. These symmetry operations produce four correlated vibrations with A_1, A_2, B_1, and B_2 symmetry. Table 2 shows the symmetry of the correlated vibrations in the unit cell connected with the free molecule according to the factor group analysis. The polarized Raman spectra of $NiPc(AsF_6)_{0.5}$ excited by He-Ne laser as shown in Fig. 7 are nearly the same as that of $CoPc(AsF_6)_{0.5}$ except the above four bands at 484, 592, 678 and 750 cm^{-1} weakly appear in (c,c) polarization spectrum due to the lower crystal symmetry than that of $CoPc(AsF_6)_{0.5}$.

The Raman spectra of $Co_xNi_{1-x}Pc(AsF_6)_{0.5}$ in (a,a) polarization consist of the superposition of the spectra of $CoPc(AsF_6)_{0.5}$ and $NiPc(AsF_6)_{0.5}$. However, in (c,c) polarization, new peaks were found at 368 cm^{-1} and 736 cm^{-1} in addition to the A_{1g} bands. For instance, the polarized Raman spectra of $Co_{0.25}Ni_{0.75}Pc(AsF_6)_{0.5}$ excited by He-Ne laser are shown in Fig. 8, in which the new Raman bands are indicated by arrows. These new bands were observed neither in $CoPc(AsF_6)_{0.5}$ nor $NiPc(AsF_6)_{0.5}$ but found in all alloys, and observed only in (c,c) polarization. This polarization dependence indicates that the 368 cm^{-1} and 736 cm^{-1} bands are the a_{1g} or a_{2g} in-plane molecular vibrations. It is surprising that these Raman bands were observed even in a very dilute alloy $Co_{0.01}Ni_{0.99}Pc(AsF_6)_{0.5}$. The 736 cm^{-1} band is regarded as the second harmonic band of 368 cm^{-1}. Furthermore, these new Raman bands were suppressed when an Ar^+ laser (515 nm) was used as an excitation source. We therefore consider that these two bands are enhanced by a resonance effect *via* the newly formed excited state in the alloy and thus belong to the a_{1g} symmetry. The optical transition to the new excited state at ~2

eV should be polarized along the conducting axis (c-axis). Accordingly, this optical transition can be ascribed to the inter-molecular charge-transfer transition between CoPc and NiPc. We measured the $E//c$ polarized reflectivity of $Co_xNi_{1-x}Pc(AsF_6)_{0.5}$ in the region of 1.3-4.1 eV. The $E//c$ reflectivity in this spectral region as shown in Fig. 9 is less than 3% and has almost no structure. More exactly, a very weak and broad hump is found at 1.8-2.3 eV in the crystals of x=0.25, 0.45, and 0.55. In this spectral region, there is an allowed optical transition (Q-band) from HOMO (a_{1u}) to LUMO (e_{1g}) polarized parallel to the a and b-axes. The vacant $3d_{x^2-y^2}$ orbital (b_{1g}) is located near LUMO (e_g) and occupied $3d_{z^2}$ orbital is near HOMO (a_{1u}), according to the molecular orbital calculation.[18] Thus, the energy difference between the $3d_{x^2-y^2}$ and $3d_{z^2}$ orbital is considered to be ~2 eV. We therefore propose that the new optical transition produced in the alloy system is associated with the inter-molecular charge-transfer transition between the $3d_{z^2}$ orbital (a_{1g}) and $3d_{x^2-y^2}$ orbital (b_{1g}). This charge-transfer transition is forbidden when the molecules are arranged in a tetragonal system. This property is consistent with the extremely weak dispersion in the reflectivity and the rather weak intensity for a resonantly enhanced Raman mode. According to the normal coordinate analysis of porphyrins,[19,20] the ~350 cm^{-1} band is assigned to the breathing mode (a_{1g}) of the macrocycle around the central metal. We therefore assign the 368 cm^{-1} and 736 cm^{-1} bands to the a_{1g} breathing mode and its second harmonic mode. These bands of the 368 cm^{-1} and 736 cm^{-1} appear more strongly in x<0.5 than in x>0.5 according to the x-dependence of the Raman intensities of these bands. The probability of finding NiPc and CoPc in the neighboring position in $Co_xNi_{1-x}Pc(AsF_6)_{0.5}$ is $x(1-x)$, which is a symmetrical function with respect to x=0.5. If we assign the 368 cm^{-1} band to the

breathing mode of NiPc, the intensity is proportional to $x(1-x)^2$, which qualitatively reproduces the x dependence of the Raman intensity as shown in Fig. 10.[21] Therefore plausible assignment for the optical transition is described by the following scheme,

$$Co(3d_{z^2})^1(3d_{x^2-y^2})^0Ni(3d_{z^2})^2(3d_{x^2-y^2})^0 \rightarrow Co(3d_{z^2})^0(3d_{x^2-y^2})^0Ni(3d_{z^2})^2(3d_{x^2-y^2})^1.$$

This means that the introduction of the electron into the $3d_{x^2-y^2}$ orbital induces the geometrical change to the inner macrocycle.

4.2.4 Reflection spectrum and band structure

The reflectivity data in the low-frequency region provide the information on the bandwidth and anisotropy of a conduction band. Figure 11 shows the reflection spectra of $NiPc(AsF_6)_{0.5}$ and $CoPc(AsF_6)_{0.5}$. It is obvious from the polarization of the reflectivity that both compounds have a quasi one-dimensional band along the c-axis. In both compounds, the macrocycles (Pc) are oxidized half, so Pc forms a ¾-filled quasi one-dimensional band (π-band). It is confirmed by the thermopower as displayed in the Fig. 12. The thermopower measured along the high conducting axis of $NiPc(AsF_6)_{0.5}$ and $CoPc(AsF_6)_{0.5}$ is positive throughout all temperature region from 5-300 K. The sign of the predominant charge carries is given by the sign of the thermopower, and the thermopower thus identifies holes as the predominant charge carriers in both $NiPc(AsF_6)_{0.5}$ and $CoPc(AsF_6)_{0.5}$. Therefore, it is consistent with the site of the macrocycle ring oxidation and the charge carries are associated with the highest occupied π orbital of the ring. The valence band formed from this orbital would be doubly occupied in a neutral MPc stack as shown in the inset of Fig. 12. Oxidation by ½ electrons per site, leads to a ¾-filled band, which corresponds to a band in which charge

transport is associated with a band ¼-filled with positive holes and a positive thermopower. In addition to the same band filling and same oxidation site, the crystal structure of $CoPc(AsF_6)_{0.5}$ is nearly the same as $NiPc(AsF_6)_{0.5}$, however the reflectivity of both compounds is very different. Before going to contrast the both spectra, we first describe the reflectivity of $NiPc(AsF_6)_{0.5}$ in the far infrared region.

The most popular method used to find the optical constants of material is the measurement of specular reflectance over a wide range of frequencies followed by a Kramers-Kronig analysis that yields the phase.[22] The optical constants can then be easily calculated. However, the most interesting sample are also small and frequently irregular in shape, being either polycrystalline with rough granular surface or single crystals with cleavage steps lacking large, planar faces. Even in the case of small, specular surface it is impossible to match perfectly the sizes of the sample and reference, so that the reflectance cannot be measured directly. If the surface is irregular, this problem is even more complicated. Therefore, the reflectance technique becomes particularly difficult in the far infrared region because of the weakness of mercury-arc lamps and the lack of photoconductive detectors. To compensate for the rough surface, a number of groups have coated the sample surface with a good metal (typically gold) and used the coated sample as reference in the reflectance measurement. If this procedure is performed carefully, much of the structure, because of the interference of rays that reach the detector by different paths and that appear when a flat mirror is used as a reference, is divided out. The reflectance is measured at near-normal incidence, and the entire sample area is used, thus permitting small samples to be examined. The scattering effects caused by the surface microstructure are corrected using the sample as its own reference

by evaporating onto it a material whose reflectance is known, such as gold.[23] It is assumed that the overcoating is thin enough that it does not change the microstructure of the sample. Yet thick enough that it is greater than the penetration depth, so that the ratio of the sample reflectance with respect to the overcoated sample yields a good approximation of the true reflectance of the sample, as it would in the case of specular reflectance. While this technique works particularly well with small samples with irregular surface, it is also an excellent way to measure the reflectance of a small sample with a flat surface. This technique permits the entire sample to be illuminated, and the ratios measured with a flat reference mirror can be used only to calculate the reflectance if the sample is overcoated and used as a final reference. A potential problem with the method is the implicit assumption that the diffraction effects for wavelengths comparable with the sample size and with the size of irregularities of the surface will cancel out in the overcoating process. Except this method, one such technique is to assemble mosaics composed of many small crystals, however a mosaic sample can also introduce a number of problems, such as the scattering from the individual crystals. We combined both methods to make the measurement for $NiPc(AsF_6)_{0.5}$ in far infrared region (50~700 cm^{-1}), which keep away from the diffraction of small crystal and scattering of mosaic sample. The spectrum of $NiPc(AsF_6)_{0.5}$ parallel to *c*-axis in far infrared region is shown in Fig. 13. The dashed curve shows the ratio of the sample with respect to a polished reference mirror such as gold and the solid curve is the reflectance of $NiPc(AsF_6)_{0.5}$ with respect to coated sample as reference mirror. Note that the reflectivity has been enhanced very much. The peak at ~400 cm^{-1} marked by arrow is assigned to the vibration t_{1u} mode of AsF_6, which also appears in the spectrum of

perpendicular direction and much stronger than that in parallel direction. Comparison of the reflectance of $NiPc(AsF_6)_{0.5}$ measured on this procedure, the structure introduced by surface scattering is seen to be removed when the overcoating method is used. Unfortunately, we could not measure the reflectivity of $CoPc(AsF_6)_{0.5}$ in the far infrared region even using this method, since the large size single crystals could not be obtained.

Now let us analyze the reflectivity of $NiPc(AsF_6)_{0.5}$ and $CoPc(AsF_6)_{0.5}$ as presented in Fig. 11. In $NiPc(AsF_6)_{0.5}$, the high-frequency part of the reflectivity can be fitted well by a Drude model. Owing to the broad dip at ~600 cm^{-1}, the optical conductivity exhibits a peak at this spectral region. Although the origin of the broad dip around 600 cm^{-1} is not clear at the moment, we consider that this is associated with the correlation gap which is found in highly correlated quasi one-dimensional organic metals such as $(TMTSF)_2X$.[24] On the other hand, the reflectivity of $CoPc(AsF_6)_{0.5}$ in the low-frequency region appears to be Drude-like down to 600 cm^{-1} but the reflectivity in the mid-infrared region cannot be reproduced by a Drude model. To reproduce the reflectivity curve, a Lorentz oscillator is necessary at ~4000 cm^{-1} in addition to the Drude term.

We analyzed the reflection spectra using the following Drude and Lorentz models,

$$\varepsilon(\omega) = \varepsilon_\infty - \frac{\omega_p^2}{\omega(\omega + i\gamma)} + \frac{\Omega_p^2}{\Omega_0^2 - \omega^2 - i\omega\Gamma},$$

where ε_∞ stands for the frequency-independence dielectric constant coming from the high-frequency polarization, ω_p and γ are the plasma frequency and the relaxation rate in a Drude model, respectively; Ω_p, Ω_0 and Γ are the plasma frequency, the damping constant, and resonant frequency in Lorentz model, respectively. The best fitting curves

for reflectivity of both compounds are shown in Fig. 11 by the dashed line, and the parameters are shown in Table 3. The total plasma frequency defined by $\Omega_p^T=(\omega_p^2+\Omega_p^2)^{1/2}$ is associated with the transition probability of the optical transition in this spectral region. The ratio of the square total plasma frequency $(\Omega_p^T(\mathrm{Co})/\Omega_p^T(\mathrm{Ni}))^2$ is calculated as 1.6 by using the fitting parameters of reflectivity. We have also done the Drude-Lorentz fitting for the conductivity of both compounds, which were obtained by the Kramers-Kronig transformation of the polarized parallel to *c*-axis reflectance spectra. The increase of the spectral weight in the mid-infrared region of the optical conductivity is clear. The best fitting curves for conductivity of both $NiPc(AsF_6)_{0.5}$ and $CoPc(AsF_6)_{0.5}$ are shown in the Fig. 14 and 15. The fitting parameters are tabulated in Table 4. The ratio of the square total plasma frequency $(\Omega_p^T(\mathrm{Co})/\Omega_p^T(\mathrm{Ni}))^2$ is obtained as 2.0 by using the fitting parameters from conductivity. Since the fitting conductivity also depends on the Kramers-Kronig transformation, the ratio of the square total plasma frequency $(\Omega_p^T(\mathrm{Co})/\Omega_p^T(\mathrm{Ni}))^2$ is considered to be in the range of 1.6~2.0. If the spectrum consists of a single component, the oscillator strength of this optical transition is determined by the overlap integral of the a_{1u} HOMOs of the macrocycle (Pc) between the nearest neighbor molecules. The ratio of the square total plasma frequency in the range of 1.6~2.0 is too large to be regarded as a single component. The large ratio strongly suggests that the 3*d* orbital also contributes to the optical transition of $CoPc(AsF_6)_{0.5}$ in the mid-infrared region. As shown in Fig. 14 and Fig. 15, we present the conductivity of $NiPc(AsF_6)_{0.5}$ and $CoPc(AsF_6)_{0.5}$ along with the Drude and Lorentz curves. It is assumed that the total plasma frequency contributes to the π-band of $NiPc(AsF_6)_{0.5}$, on the other hand, the Drude and Lorentz terms are respectively

associated with the ¾-filled π-band and a half-filled $3d$-band of $CoPc(AsF_6)_{0.5}$. Therefore, we estimated the bandwidth of π-band for $NiPc(AsF_6)_{0.5}$ and $CoPc(AsF_6)_{0.5}$ using 1D tight-binding model as shown by the following function:

$$4t = \left(\frac{\varepsilon_0}{e^2}\right)\left(\frac{V}{z}\right)\frac{\hbar^2 \pi \rho \omega_p^2}{d^2 \sin(\pi\rho/2)},$$

where ε_0 is the dielectric constant of vacuum, e is the electron charge, the V is the volume of the unit cell, the d is the interplanar distance between the adjacent phthalocyanine, ρ is the band-filling factor, ω_p is the plasma frequency, z is the number of the CoPc molecules in the unit cell. The bandwidth of π-band is in the range of 1.4~1.5 eV for $NiPc(AsF_6)_{0.5}$ but in the range of 1.8~2.1 eV for $CoPc(AsF_6)_{0.5}$. Since the singly occupied $3d_{z^2}$ orbital is extended to the neighbor molecules, the $3d_{z^2}$ orbital forms a half-filled 1D band ($3d_{z^2}$ band) along the Co chain. It is well-known that a half-filled 1D band is split into upper and lower Hubbard bands, if we take the on-site Coulomb interaction into account. Accordingly, 1D Hubbard band model was employed to estimate bandwidth of d-band. From the exact solution of this model, the optical excitation energy and the oscillation strength (f)[25] are given by

$$E_{opt}/4t = u - 1 + 2\int_0^\infty \frac{J_1(\omega)}{\omega(1+\exp(2u\omega)}d\omega$$

$$\left(\frac{f}{4t}\right)\left(\frac{\hbar^2}{m_e d^2}\right) = \int J_0(\omega)J_1(\omega)\{\frac{1}{\omega[1+\exp(2u\omega)]} + \frac{u}{1+\cos\hbar(2u\omega)}\}d\omega$$

where u is $U/4t$ (U the on-site Coulomb energy), m_e is the electron mass, d is the inter-molecular distance, and $J_0(\omega)$ and $J_1(\omega)$ are the Bessel functions. The oscillator strength is calculated from the equation

$$f = \frac{2m_e}{\pi e^2 N_0} \int \sigma(\omega) d\omega = \frac{\omega_p^2 m_e \varepsilon_0}{N_0 e^2}$$

where the e is the electron charge and N_0 is the number of the electrons in the Co^{2+} ion of the unit cell. The oscillator strength was calculated as 0.102 and 0.155 due to the plasma frequency from the reflectivity and conductivity of $CoPc(AsF_6)_{0.5}$. By using the experimentally obtained value: E=0.5 eV, f=0.102 and 0.155, and d=3.148 Å, U and t were obtained as t=0.12 eV U=0.89 eV and t=0.16 eV U=1.00 eV, respectively. Therefore, the bandwidth of d-band is evaluated to be in the range of 0.5~0.6 eV. Since the optical transition between these split bands is polarized along the Co chain direction (c-axis), it is reasonable to assign the mid-infrared band at ~0.5 eV to this optical transition form the filled lower Hubbard band to vacant upper Hubbard band. The excitation energy of this transition is comparable with that of a half-filled quasi 1D π-electron system such as LiPc.[26] This small excitation energy is surprising, because the excitation energy or the gap between the split bands is associated with the on-site Coulomb energy. In the Co chain, the electrons in the $3d_{z^2}$ band are confined in a narrow space, whereas the electrons in the π-band are more extended in large Pc. Thus the on-site Coulomb energy in the $3d_{z^2}$ band seems to be much large than that in the π-band. For example, the on-site Coulomb energy is estimated as ~5 eV in the one-dimension Ni complexes.[27] The remarkable reduction of the on-site Coulomb energy in $CoPc(AsF_6)_{0.5}$ is probably caused by the strong polarization effect by the conjugated π-electron in the macrocycle surrounding the Co chain along the c-axis. The low excitation energy of the mid-infrared transition suggests that the 3d-band is located near the Fermi level of the ¾-filled π-band. In this system, the macrocycle (Pc) contributes to the intra- and inter-

molecular polarization effect. As the metallic π-electrons are highly polarizable, we consider that the inter-molecular polarization effect is dominant in this compound.

Let us briefly compare the reflectivity of $CoPc(AsF_6)_{0.5}$ with that of $CuPc(I_3)_{0.33}$. The reflectivity in the infrared region has not been reported in the latter compound. According to the reflectivity observed down to 3500 cm^{-1}, the plasma edge appears at ~4500 cm^{-1} with the plasma frequency of 6.7×10^3 cm^{-1}.[2] The plasma frequency is not close to that of $CoPc(AsF_6)_{0.5}$ but to $NiPc(AsF_6)_{0.5}$, although the $3d$ orbital of Cu^{2+} is singly occupied. This result suggests that the $3d$ orbital of Cu^{2+} does not contribute to the low-energy optical transition along the conducting axis. This suggestion is consistent with the extremely small orbital overlap between the nearest neighbor Cu-Cu. Therefore the resemblance between $CuPc(I_3)_{0.33}$ and $NiPc(AsF_6)_{0.5}$ is reasonable. This comparison also supports the interpretation that the $3d_{z^2}$ orbital contributes to the low-energy optical transition in $CoPc(AsF_6)_{0.5}$.

Figure 16 shows the reflection spectra of alloy $Ni_xCo_{1-x}Pc(AsF_6)_{0.5}$ polarized parallel to c-axis in infrared region. In the range of $0\leq x\leq0.45$, the spectral shapes are essentially the same, except that the plasma edge slightly moves to the high-frequency side. This means that the center energy of the π band of $NiPc(AsF_6)_{0.5}$ nearly coincides with that of $CoPc(AsF_6)_{0.5}$. The x dependence of the reflectivity is not a weighted average. The characteristic line shape of $CoPc(AsF_6)_{0.5}$ is observed only in the region of $0.87\leq x\leq1$, which is closer to $x=1$. The optical conductivity spectra of alloys are shown in Fig. 17, which were obtained by the Kramers-Kronig transformation of the parallel to c-axis reflectance spectra. Before the Kramers-Kronig transformation, the data below 600 cm^{-1} were extrapolated using the Hagen-Rubense method defined as following:

$$R = 1 - 2\sqrt{\frac{\nu}{\sigma}}$$

where R is the reflectance, ν is the frequency, σ is the conductivity. This spectral dependence is consistent with our interpretation that the optical transition in the mid-infrared region is assignable to the inter-molecular charge-transfer transition along the Co chain that requires the CoPc pair. The probability to find the pair does not increase linearly but proportionally to x^2.

4.2.5 Band model

Combining the results of ESR, reflectivity and polarized Raman spectra, the schematic energy diagram of $NiPc(AsF_6)_{0.5}$ and $CoPc(AsF_6)_{0.5}$ about the HOMO band of the Pc, $3d_{z^2}$ and $3d_{x^2-y^2}$ bands of the metal is shown in Fig. 18. The arrows denote the optical transitions polarized along the conducting axis found in this study. From the results of x dependence reflectivity polarized parallel to c-axis, the Fermi level of π bands is placed in the same energy level. We have performed the pressure dependence of the optical absorption of $NiPc(AsF_6)_{0.5}$ and $CoPc(AsF_6)_{0.5}$, and have clarified that the filled $3d_{z^2}$ band is closely located to the Fermi level.[10] The difference between $NiPc(AsF_6)_{0.5}$ and $CoPc(AsF_6)_{0.5}$ is the energy level of the $3d_{z^2}$ band, that is, the $3d_{z^2}$ band of $CoPc(AsF_6)_{0.5}$ is a little higher than that of $NiPc(AsF_6)_{0.5}$. Therefore the lower Hubbard band ($(3d_{z^2})^1$ band) is closely located to the Fermi level in $CoPc(AsF_6)_{0.5}$, whereas the upper Hubbard band ($(3d_{z^2})^2$ band) is close to the Fermi level in $NiPc(AsF_6)_{0.5}$. As a result, as shown by the arrows in Fig. 18, the $E//c$ spectrum consists of two optical transitions (two components) in $CoPc(AsF_6)_{0.5}$ and one optical transition

(single component) in $NiPc(AsF_6)_{0.5}$. The existence of a very weak band is deduced from the Raman spectrum of the alloy, $Co_xNi_{1-x}Pc(AsF_6)_{0.5}$. This inter-molecular charge-transfer transition is denoted by the long arrow. This energy diagram explains the nearly temperature-independent paramagnetic term in the magnetic susceptibility. The corresponding values for powdered samples are $(4–5)\times10^{-4}$ emu/mol for $CoPc(AsF_6)_{0.5}$ and $(0.5–1)\times10^{-4}$ emu/mol for $NiPc(AsF_6)_{0.5}$. The enhanced paramagnetic susceptibility in $CoPc(AsF_6)_{0.5}$ is ascribed to the highly correlated 1D $3d_{z^2}$ band.

4.3 Summary

In the ESR experiment, the orientation of doped CoPc and SOMO of CoPc were well characterized by the hyperfine structure of organic alloys $Co_xNi_{1-x}Pc(AsF_6)_{0.5}$ in the range of $0<x\leq0.09$. It was confirmed that the unpaired *d*-electron in Co occupies the $3d_{z^2}$ orbital. In the Raman spectra of alloys, we found new vibrational bands enhanced by a resonance effect, and pointed out the existence of a very weak optical transition polarized at ~2 eV along the *c*-axis. Based on the analysis of the low-energy reflectivity, we conclude that the $3d_{z^2}$ orbital forms a half-filled 1D band, which is split into filled lower band and vacant upper band, owing to the on-site Coulomb energy. The bandwidth of $CoPc(AsF_6)_{0.5}$ was estimated as 1.8~2.1 eV for the π-band and 0.5~0.6 eV for the *d*-band. The difference in optical property between $NiPc(AsF_6)_{0.5}$ and $CoPc(AsF_6)_{0.5}$ is attributed to the different energy level of the $3d_{z^2}$ orbital.

References

[1] M. Y. Ogawa, B. M. Hoffman, S. Lee, M. Yudkowski, and W. P. Halperin, *Phys. Rev. Lett.*, **57,** 1177 (1986).

[2] M. Y. Ogawa, J. Martinsen, S. M. Palmer, J. L. Stanton, J. Tanaka, R. L. Green, B. M. Hoffman, and J. A. Ibers, *J. Amer. Chem. Soc.*, **109,** 1115 (1987).

[3] G. Quirion, M. Poirier, K. K. Liou, M. Y. Ogawa, and M. Hoffman, *Phys. Rev.* B, **37,** 4272 (1988).

[4] G. Quirion, M. Poirier, K. K. Liou, and B. M. Hoffman, *J. Phys.* I France, **2**, 741 (1992).

[5] M. Y. Ogawa, S. M. Palmer, K. K. Liou, G. Quirion, J. A. Thomson, M. Poirer, and B. M. Hoffman, *Phys. Rev.* B, **39**, 10682 (1989).

[6] G. Quirion, M. Poirier, K. K. Liou, and B. M. Hoffman, *Phys. Rev.* B, **43**, 860 (1991).

[7] J. Thompson, K. Murata, R. Durcharne, M. Poirier, and B. M. Hoffman, *Phys. Rev.* B, **60**, 523 (1999).

[8] J. Martinsen, J. L. Stanton, R. L. Green, J. Tanaka, B. M. Hoffman, and J. A. Ibers, *J. Amer. Chem. Soc.*, **107**, 6915 (1994).

[9] H. Yamakado, T. Ida, A. Ugawa, K. Yakushi, K. Awaga, Y. Maruyama, K. Imaeda, and H. Inokuchi, *Synth. Met.*, **62**, 169 (1994).

[10] K. Yakushi, H. Yamakado, M. Yoshitake, N. Kosugi, H. Kuroda, T. Sugano, M. Kinoshita. A. Kawamoto, and J. Tanaka, *Bull. Chem. Soc. Jpn.*, **62**, 687 (1989).

[11] B. Bleany, *Philos. Mag.*, **42**, 441 (1951).

[12] J. M. Assour and W. K. Kahn, *J. Amer. Chem. Soc.*, **87**, 207 (1965).

[13] B. A. Goodman and J. B. Paynon, *Adv. Inorg. Chem. Radiochem.*, **13**, 135 (1972).

[14] Y. Nishida and S. Kida, *Inorg. Nucl. Chem. Letters,* **7**, 325 (1971).

[15] O. Drozdova, H. Yamochi, K. Yakushi, M. Uruichi, S. Horiuchi, and G. Saito, *J. Am. Chem. Soc.*, **112**, 4436 (2000).

[16] C. R. Bartholomew, A. A. McConnell, and W. E. Smith, *J. Raman Spectrosco.*, **20**, 595 (1989).

[17] The a_{2g} symmetry is inactive in normal Raman scattering. However, it is well known in prophyrin and phthalocyanine that the a_{2g} mode is allowed in the resonance region. T. G. Spiro and T. C. Strekas, *J. Am. Chem. Soc.*, **96**, 338 (1974).

[18] F. W. Kutzler and E. E. Ellis, *J. Chem. Phys.*, **84**, 1033 (1986).

[19] X.-Y. Li, R. S. Czernuszewicz, J. R. Kincsid, Y. O. Su, and T. G. Spiro, *J. Phys. Chem.*, **94**, 31 (1990).

[20] X.-Y. Li, R. S. Czernuszewicz, J. R. Kincsid, P. Stein, and T. G. Spiro, *J. Phys. Chem.*, **94**, 47 (1990).

[21] When we take the anisotropic unit cell into account, the corresponding function is given by $f(x)=(1-x^{1/3}(2a/c)^{2/3})x(1-x)$ in th erange of $0\leq x<0.2$. However, the difference from the function $f(x)=x(1-x)^2$ is negligible for the qualitative discussion.

[22] F. Wooten, *Optical properties of solids,* Academic, New York, 173 (1972).

[23] C. C. Homes, M. Reedyk, D. A. Cradles and T. Timusk, *Applied optics;* **32**, 2976 (1993).

[24] V. Vescoli, L. Degiorgi, W. Henderson, G. Gruner, K. P. Starkey, L. K. Montgomery, *Science*, **281**, 1181 (1998).

[25] D. Baeriswyl, J, Carmelo, and A. luther, *Phys. Rev.* **33**, 7247 (1986).

[26] K. Yakushi, T. Ida, A. Ugawa, H. Yamakado, H. Ishii, and H. Kuroda, *J. Phys.*

Chem., **95**, 7636 (1991).

[27] H. Okamoto, Y. Shimoda, Y. Oka, A. Chainani, T. Takahashi, H. Kitagawa, T. Mitani, K. Toriumi, K. Inoue, T. Manabe, and M. Yamashita, *phys. Rev.* B, **54**, 8434 (1996).

Table1 Correlation diagram in $CoPc(AsF_6)_{0.5}$

molecule D_{4h}	site C_{4h}	unit cell D_{4h} (Z=2)	selection rule
14 a_{1g} (in-plane) 13 a_{2g} (in-plane)	27 A_g	27 A_{1g} (in-phase) 27 A_{2g}(out-of-phase)	$\alpha_{xx}+\alpha_{yy},\alpha_{zz}$
14 b_{1g} (in-plane) 14 b_{2g} (in-plane)	28 B_g	28 B_{1g} (in-phase) 28 B_{2g} (out-of-phase)	$\alpha_{xx}-\alpha_{yy}$ α_{xy}
13 e_g (out-of-plane)	13 E_g	26 E_g	α_{xz},α_{yz}
6 a_{1u} (out-of-plane) 8 a_{2u} (out-of-plane)	14 A_{1u}	14 A_{1u} (in-phase) 14 A_{2u} (out-of-phase)	T_z
7 b_{1u} (out-of-plane) 7 b_{2u} (out-of-plane)	14 B_{1u}	14 B_{1u} (in-phase) 14 B_{2u} (out-of-phase)	
28 e_u (in-plane)	28 E_u	28 E_u	T_x, T_y

Table2. Correlation diagram in $NiPc(AsF_6)_{0.5}$

molecule D_{4h}	site C_1	unit cell C_{2v} (Z=4)	selection rule
14 a_{1g} (in-plane)	124 A_1	124 A_1	α_{xx}, α_{yy}, α_{zz}
13 a_{2g} (in-plane)			T_z
14 b_{1g} (in-plane)		124 A_2	α_{xy}
14 b_{2g} (in-plane)			
13 e_g (out-of-plane)		124 B_1	α_{xz}
6 a_{1u} (out-of-plane)			T_x
8 a_{2u} (out-of-plane)			
7 b_{1u} (out-of-plane)		124 B_2	α_{yz}
7 b_{2u} (out-of-plane)			T_y
28 e_u (in-plane)			

Table 3. Parameters of Drude and Lorentz functions for reflectivity

	ε_∞	ω_p ($10^3 cm^{-1}$)	γ ($10^3 cm^{-1}$)	Ω_p ($10^3 cm^{-1}$)	Ω_0 ($10^3 cm^{-1}$)	Γ ($10^3 cm^{-1}$)
$NiPc(AsF_6)_{0.5}$	2.38(5)	4.28(6)	0.17(1)	6.22(2)	0.74(1)	1.04(6)
$CoPc(AsF_6)_{0.5}$	2.07(2)	8.59(8)	0.78(5)	3.75(2)	3.90(2)	3.10(4)

Table 4. Parameters of Drude and Lorentz functions for conductivity

	ε_∞	ω_p ($10^3 cm^{-1}$)	γ ($10^3 cm^{-1}$)	Ω_p ($10^3 cm^{-1}$)	Ω_0 ($10^3 cm^{-1}$)	Γ ($10^3 cm^{-1}$)
$NiPc(AsF_6)_{0.5}$	2.38(9)	4.28(7)	0.16(5)	5.95(0)	0.62(0)	0.61(8)
$CoPc(AsF_6)_{0.5}$	2.4(0)	9.29(8)	1.11(4)	4.62(1)	3.9(0)	4.95(9)

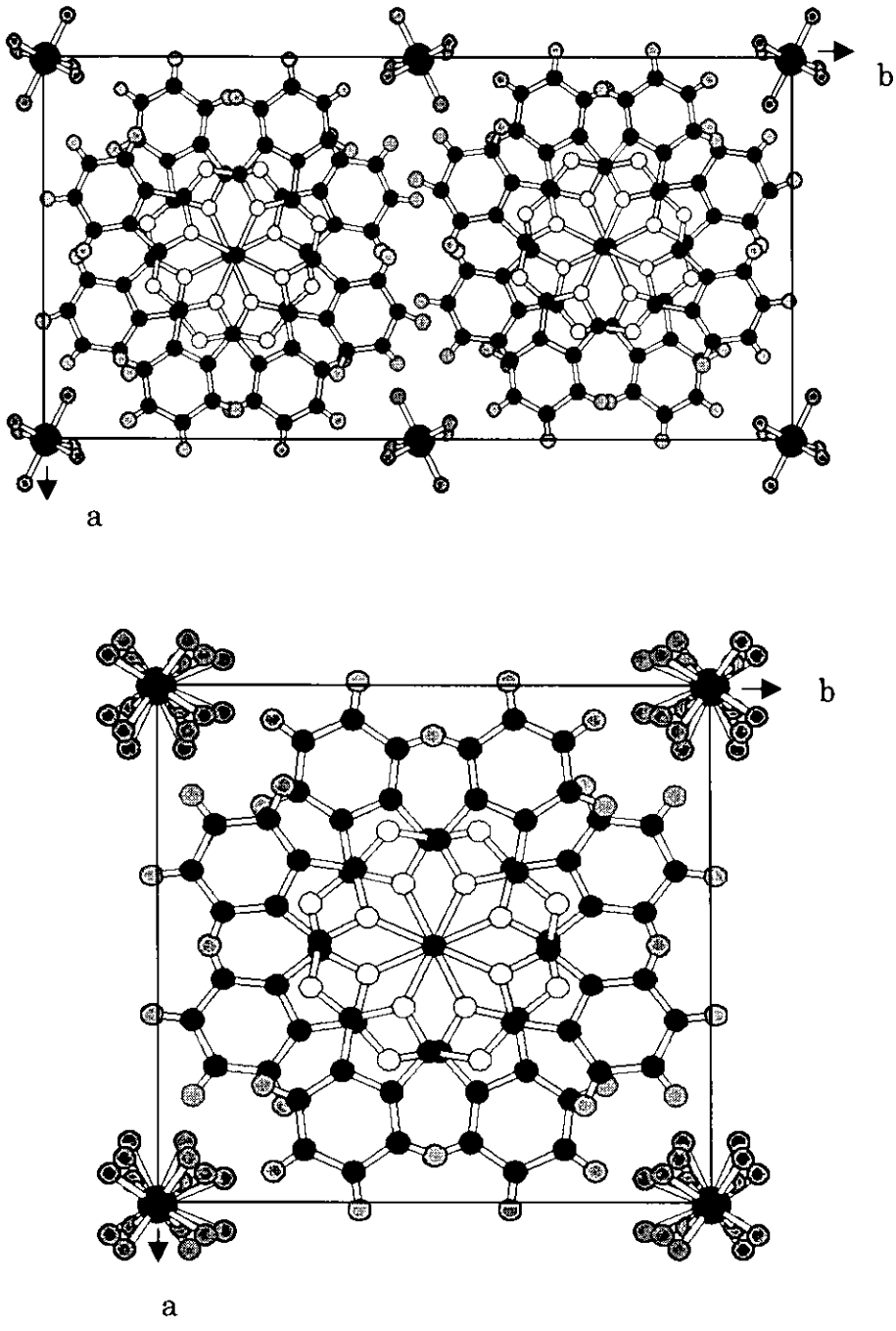

Fig.1 Crystal structure of $Co_{0.25}Ni_{0.75}Pc(AsF_6)_{0.5}$ (top) and $Co_{0.45}Ni_{0.55}Pc(AsF_6)_{0.5}$ (bottom) viewed along the stacking direction
(*cited from Y. Yonehara's thesis)

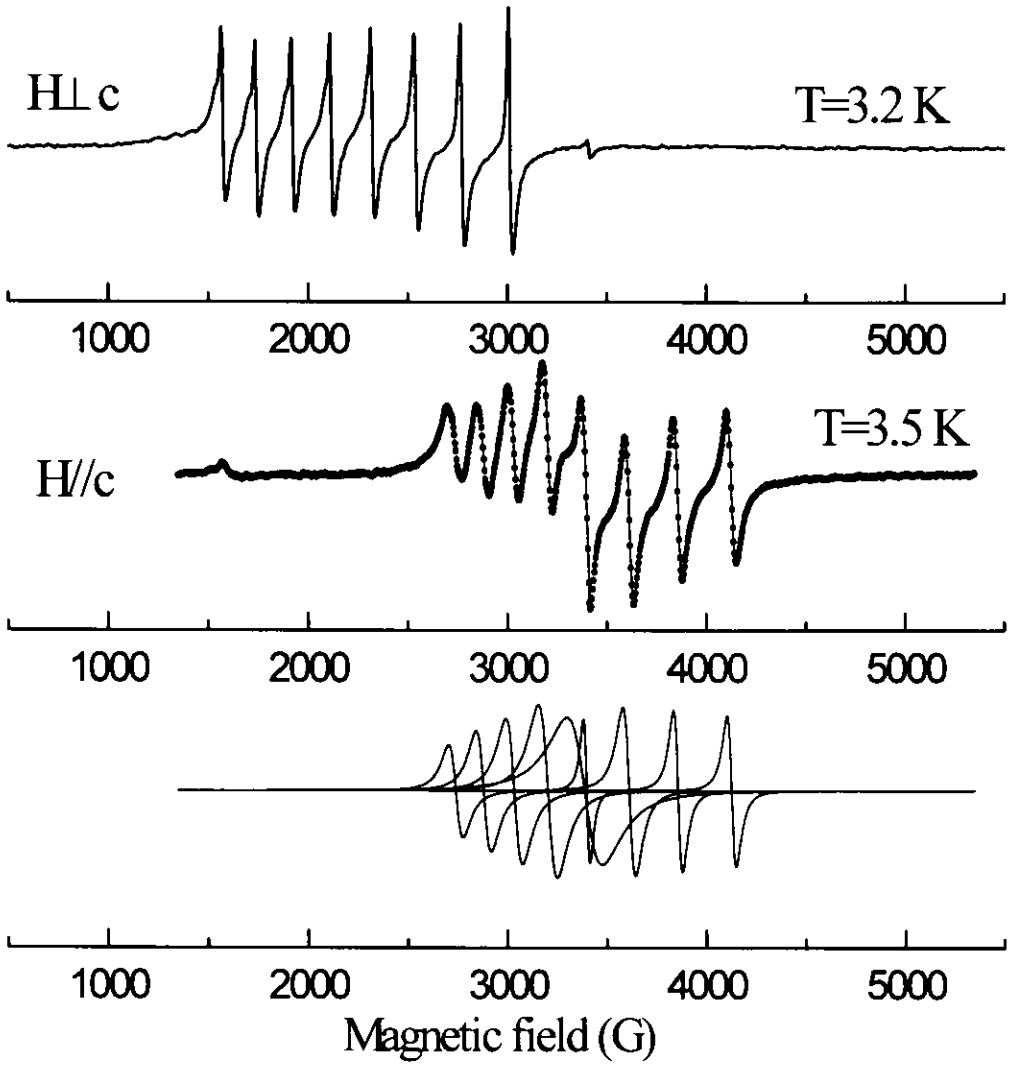

Fig.2 Anisotropic hyperfine structure of the oriented single crystals of $Co_{0.01}Ni_{0.99}Pc(AsF_6)_{0.5}$. The circles in the *H//c* spectrum represent the experimental data, and the solid line is the least-squares-fit curve composed of 8 sharp and 1 broad Lorentzians. Each Lorentzian is drawn at the bottom of this figure.

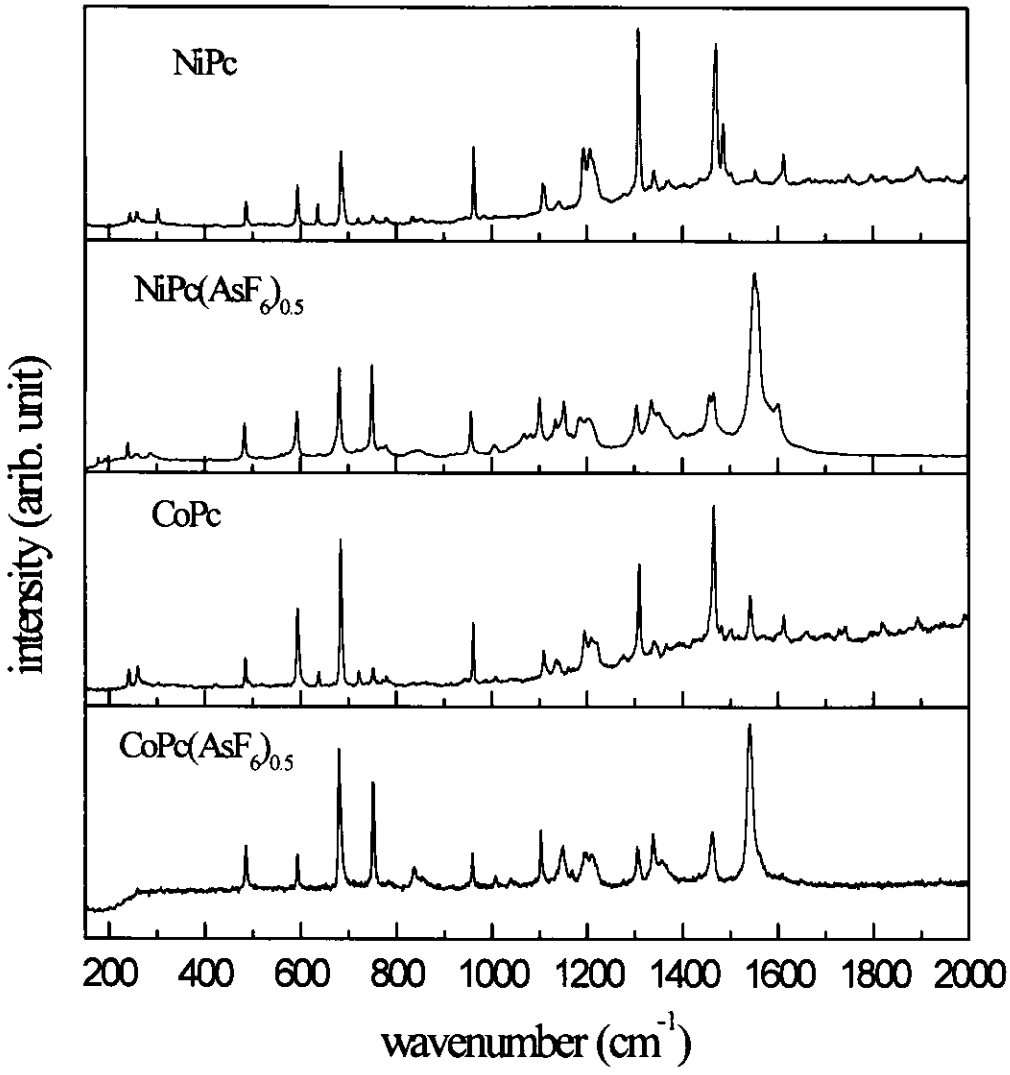

Fig. 3 He-Ne laser excited Raman spectra of neutral and charge-transfer compounds polarized along *c*-axis

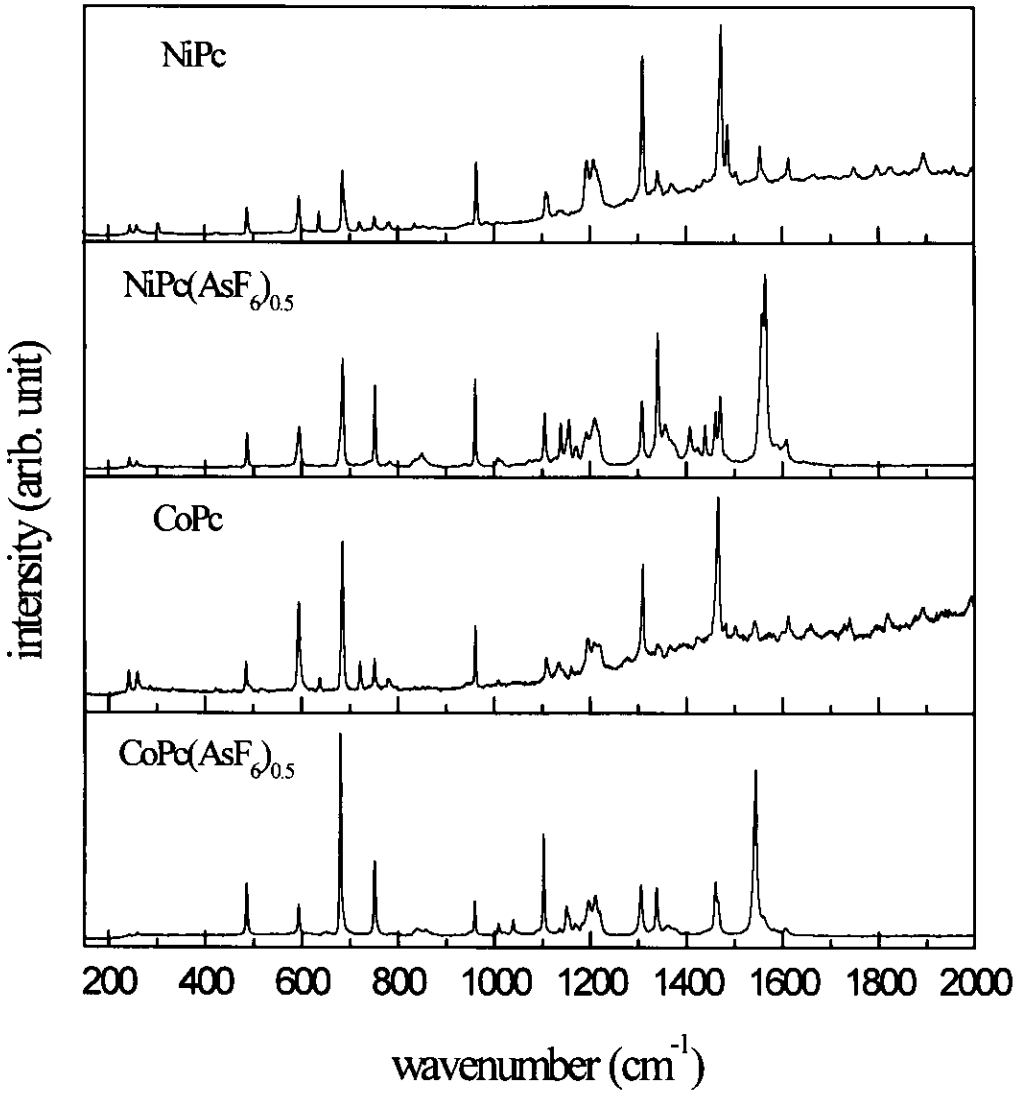

Fig. 4 He-Ne laser excited Raman spectra of neutral and charge-transfer compounds polarized perpendicular to *c*-axis

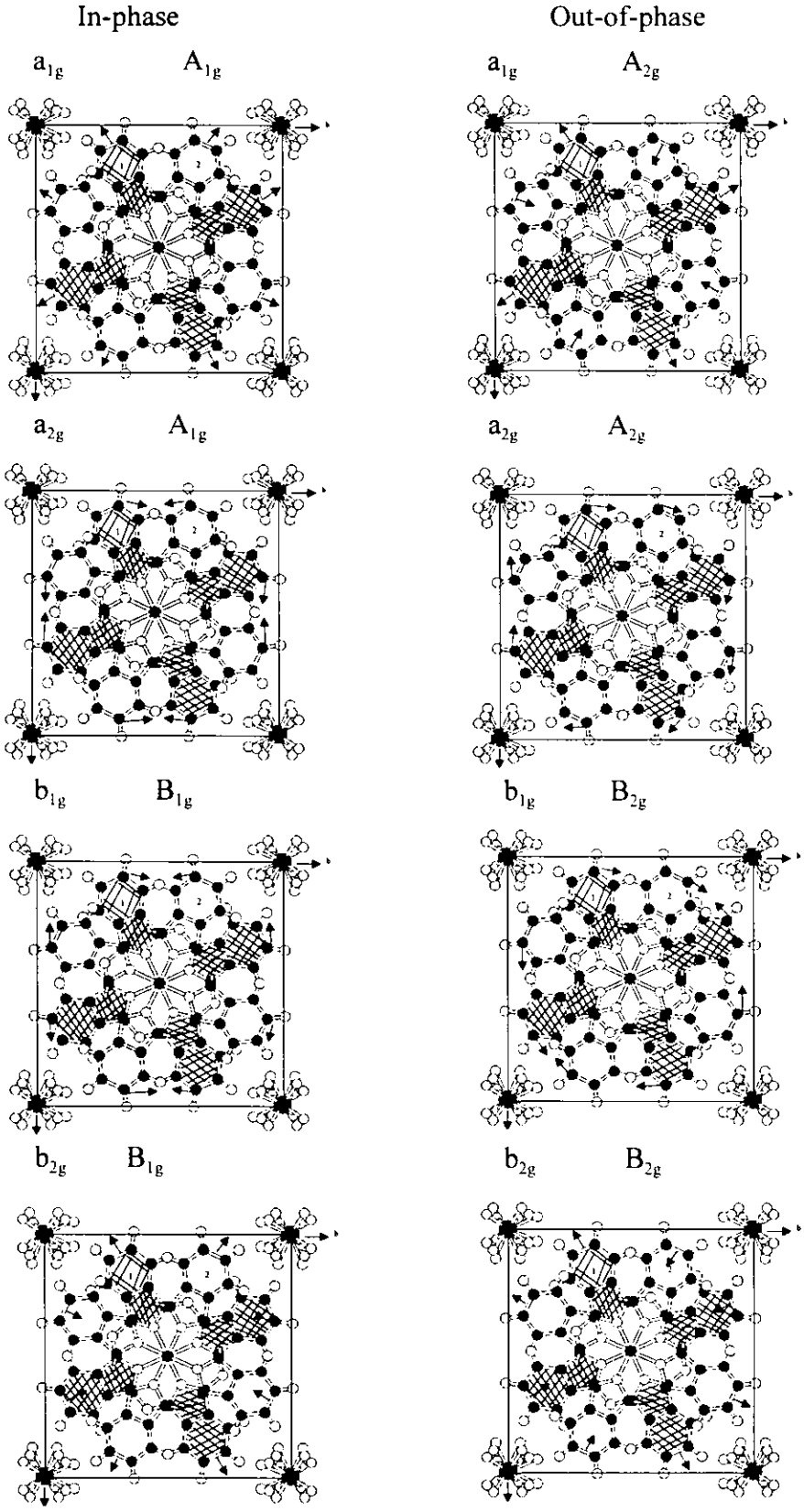

Fig. 5 The symmetry of in-phase and out-of-phase vibrations

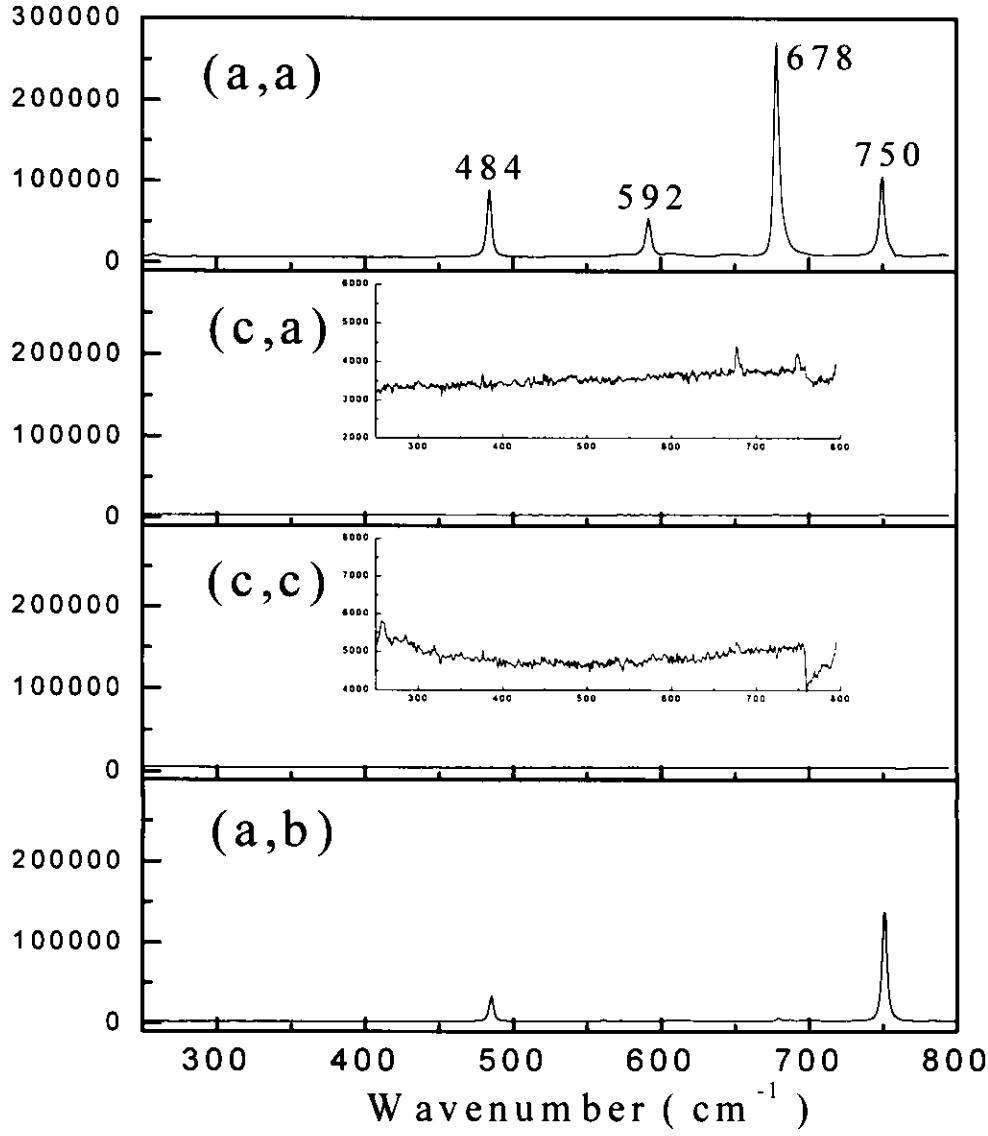

Fig.6 Polarized Raman spectra of $CoPc(AsF_6)_{0.5}$ excited by He-Ne laser

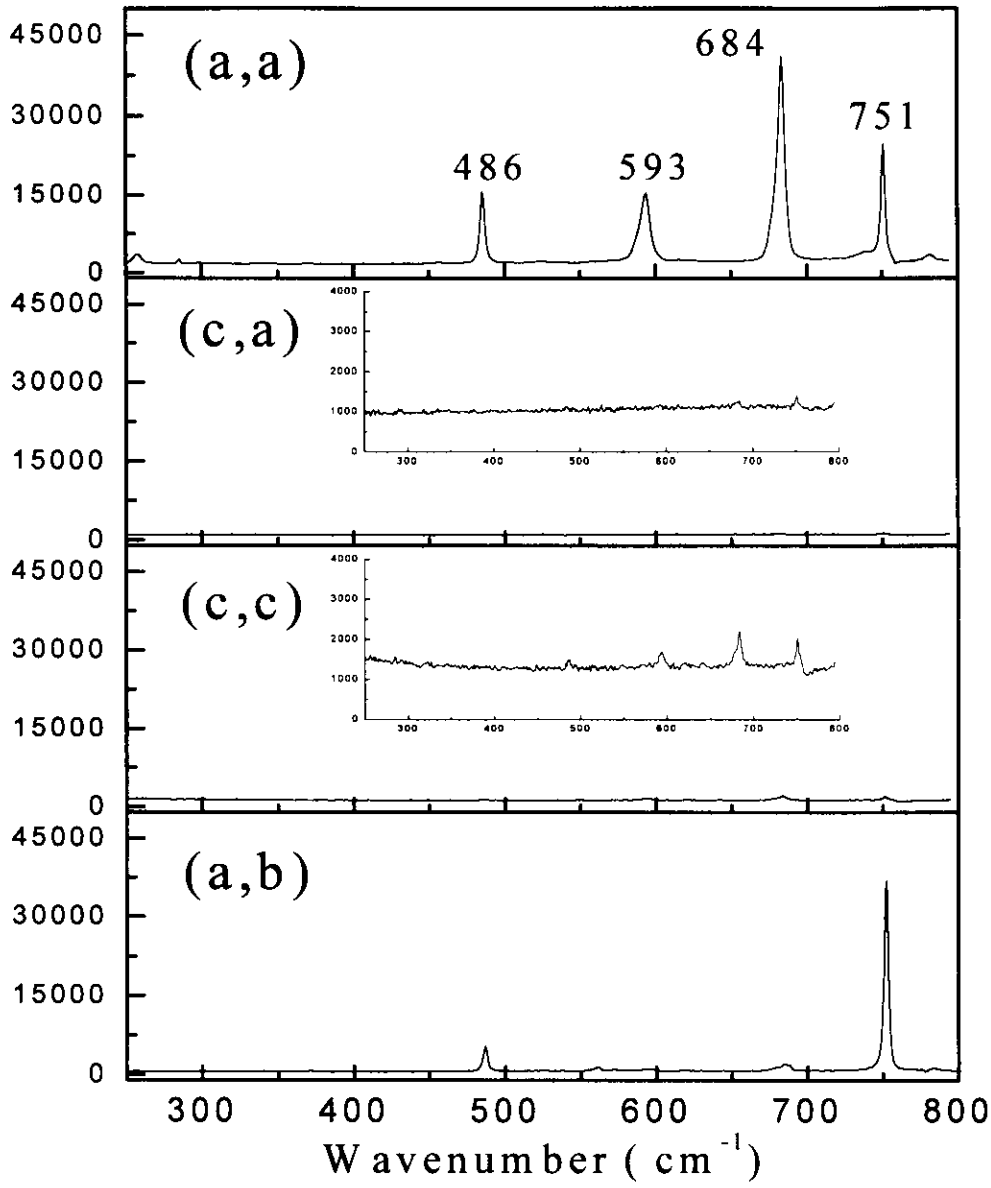

Fig.7 Polarized Raman spectra of $NiPc(AsF_6)_{0.5}$ excited by He-Ne laser

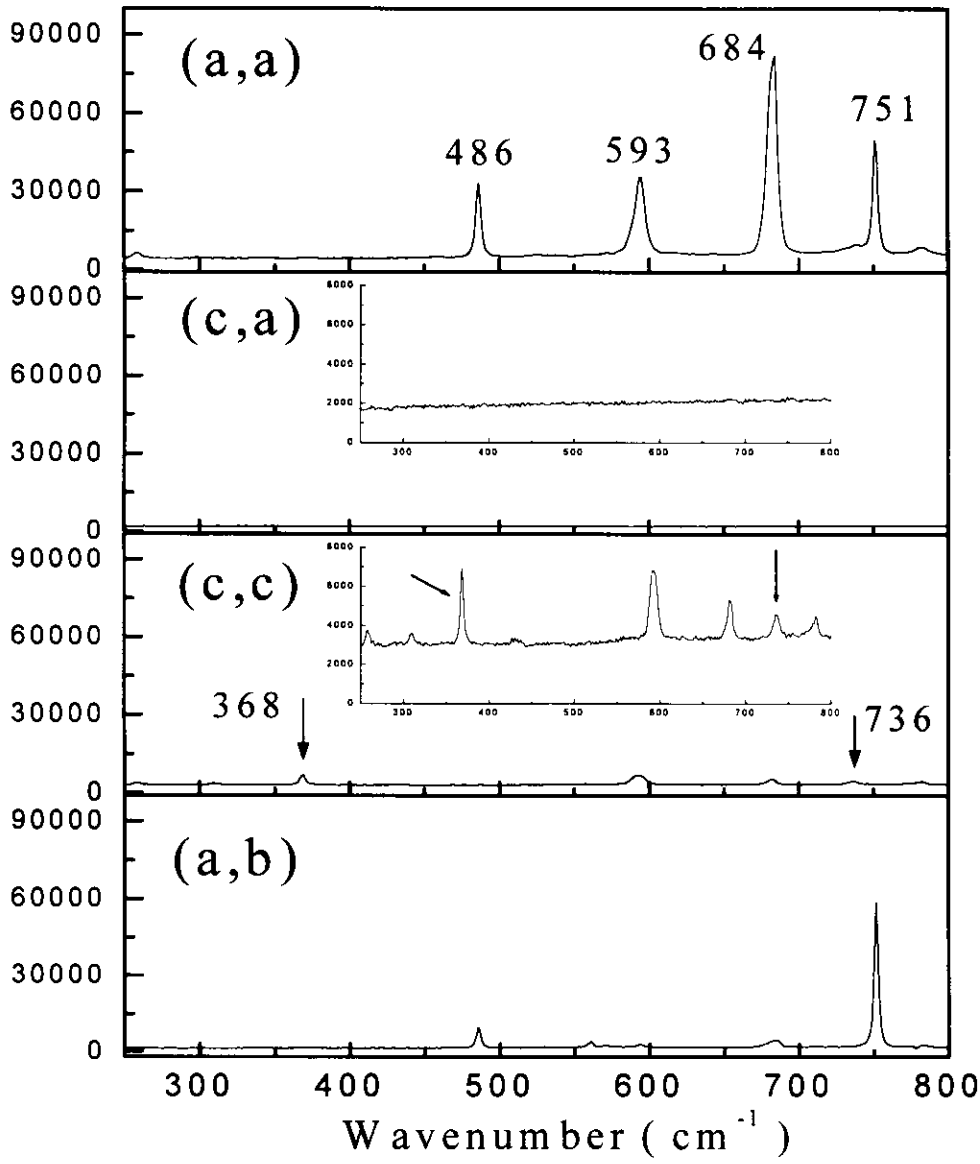

Fig. 8 Polarized Raman spectra of $Co_{0.25}Ni_{0.75}Pc(AsF_6)_{0.5}$ excited by He-Ne laser

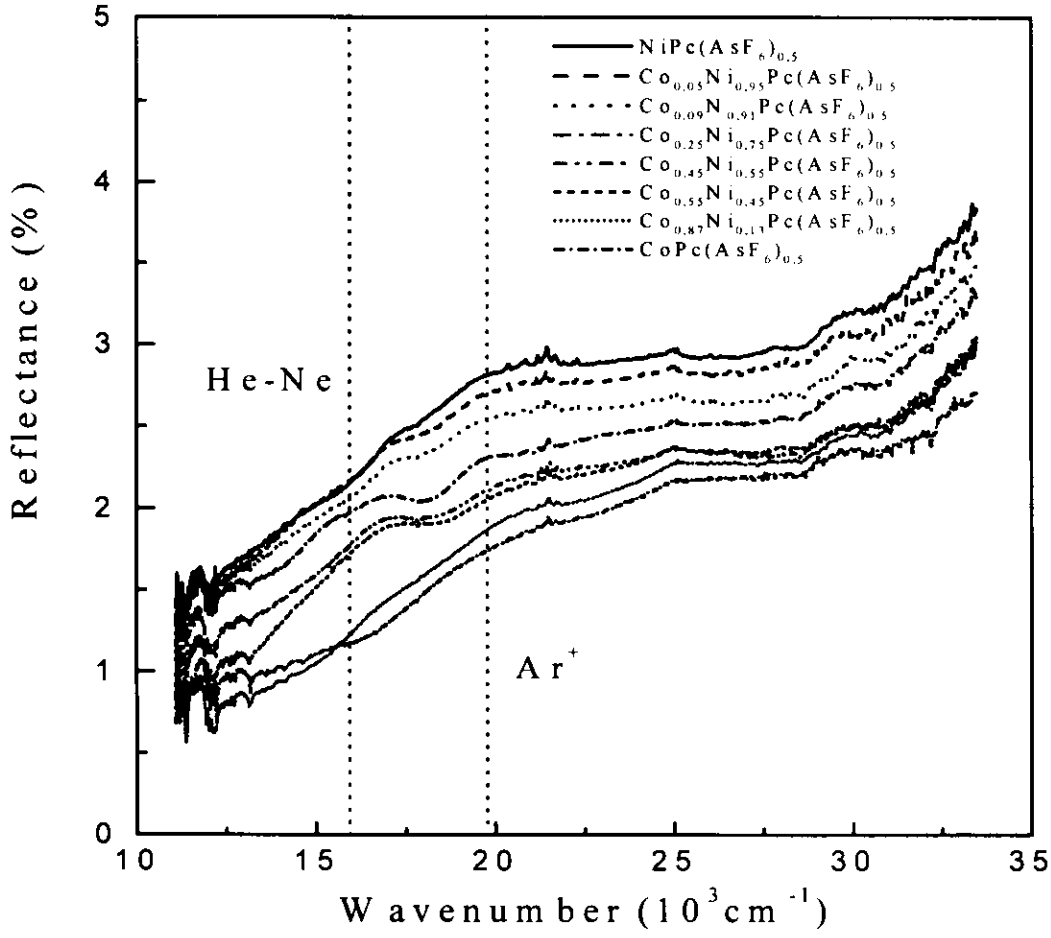

Fig. 9 Reflectivity of alloy $Co_xNi_{1-x}Pc(AsF_6)_{0.5}$ ($0 \le x \le 1$) parallel to *c*-axis in visible region

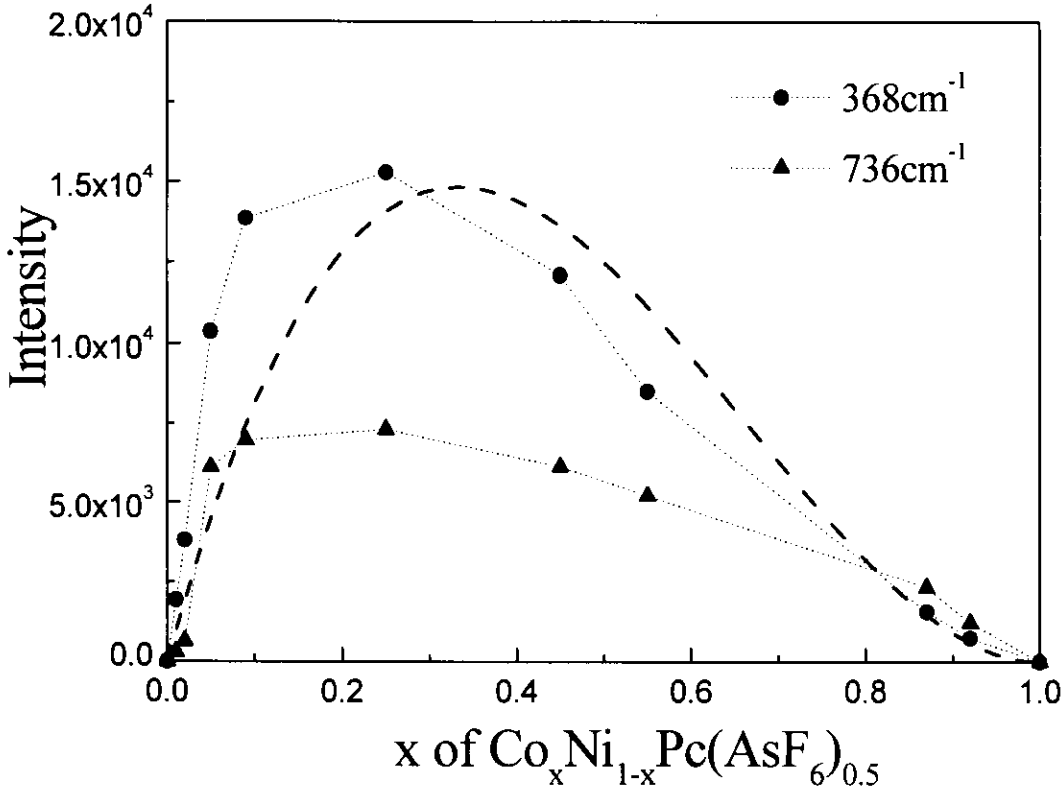

Fig. 10 Intensities of the new Raman band which appears only in mixed crystals. The dotted line is the function $x(1-x)^2$ (see text).

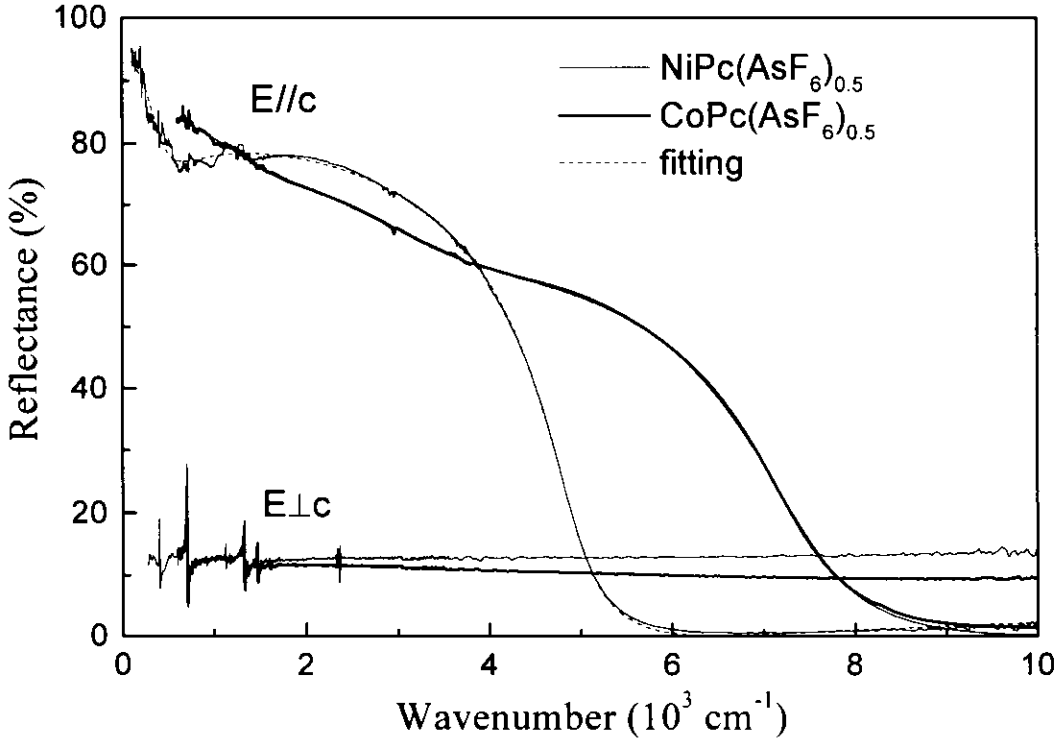

Fig. 11 Reflectivity of $NiPc(AsF_6)_{0.5}$ and $CoPc(AsF_6)_{0.5}$ polarized parallel and perpendicular to *c*-axis

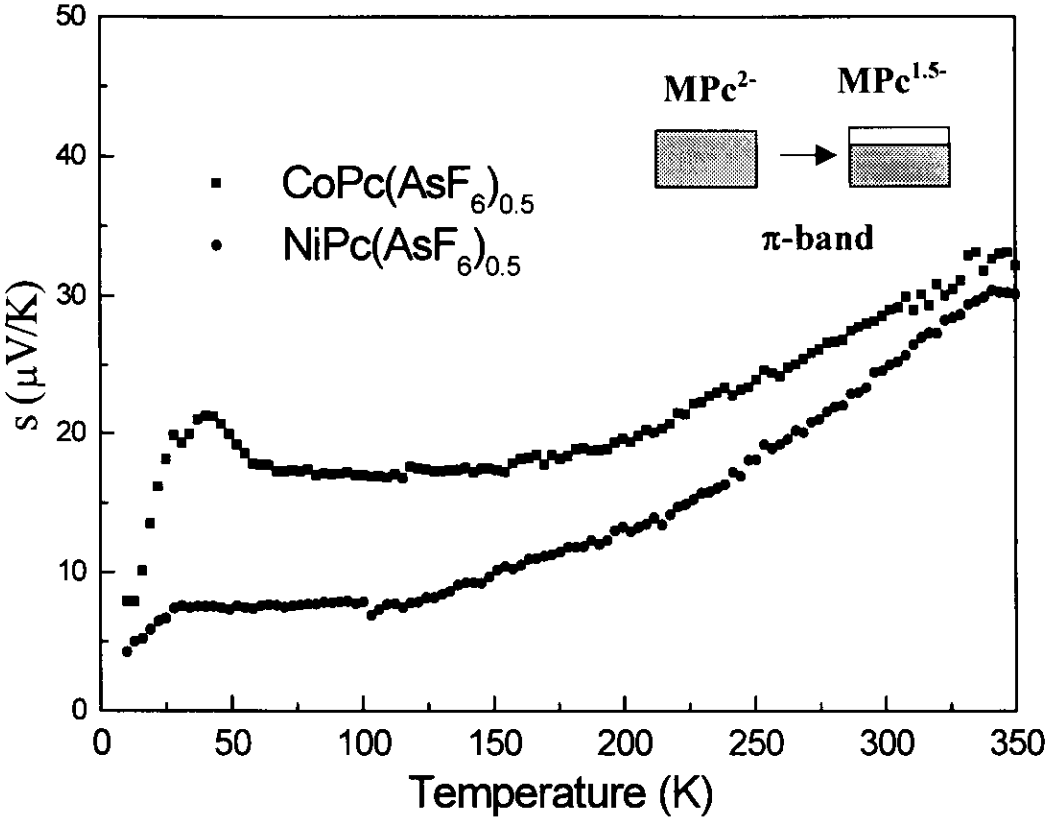

Fig.12 Thermopower of $NiPc(AsF_6)_{0.5}$ and $CoPc(AsF_6)_{0.5}$

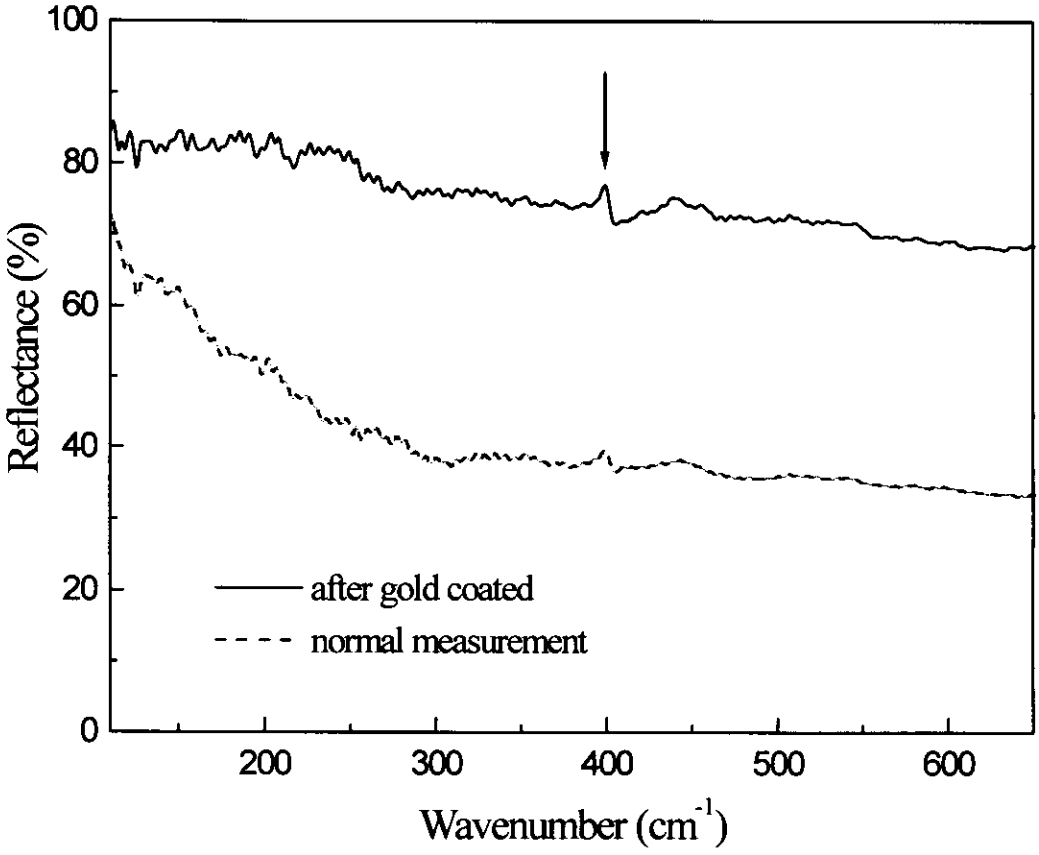

Fig. 13 Reflectivity of $NiPc(AsF_6)_{0.5}$ in far infrared region parallel to *c*-axis

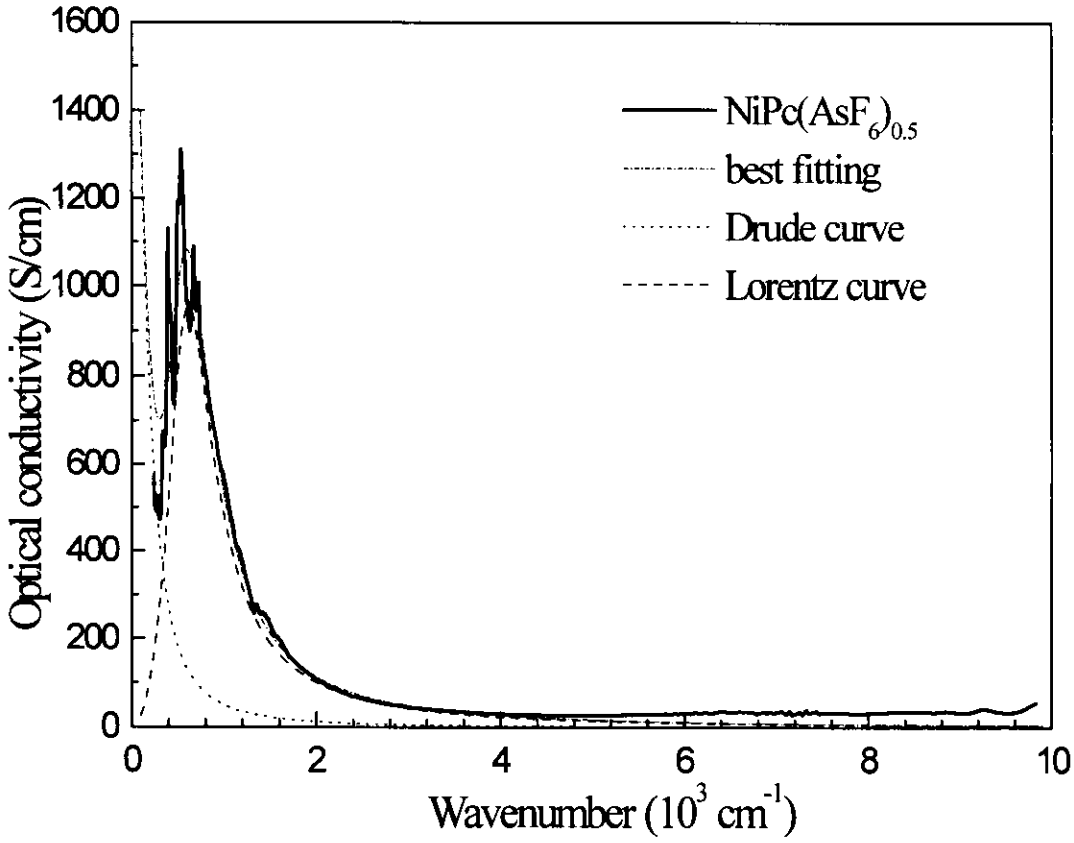

Fig. 14 Optical conductivity of $NiPc(AsF_6)_{0.5}$ along *c*-axis with the best-fitting curves

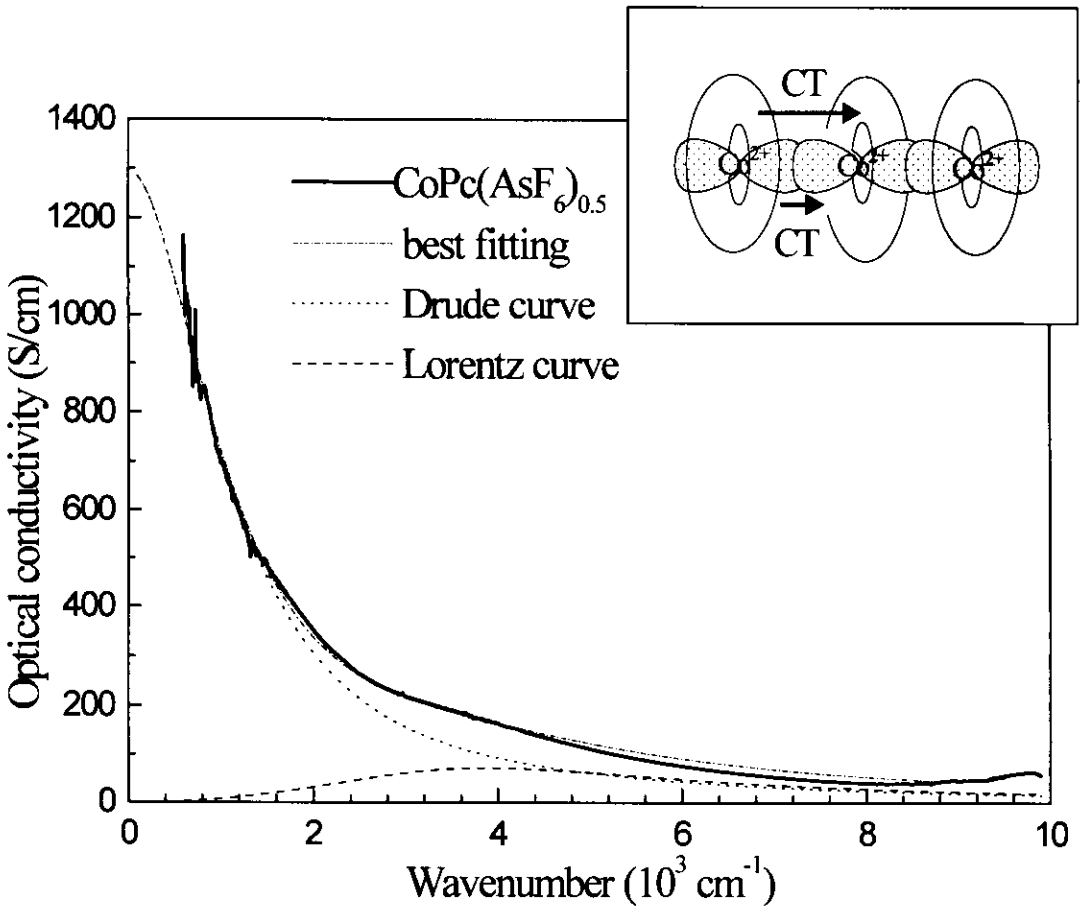

Fig. 15 Conductivity of $CoPc(AsF_6)_{0.5}$ along *c*-axis with the best-fitting curves

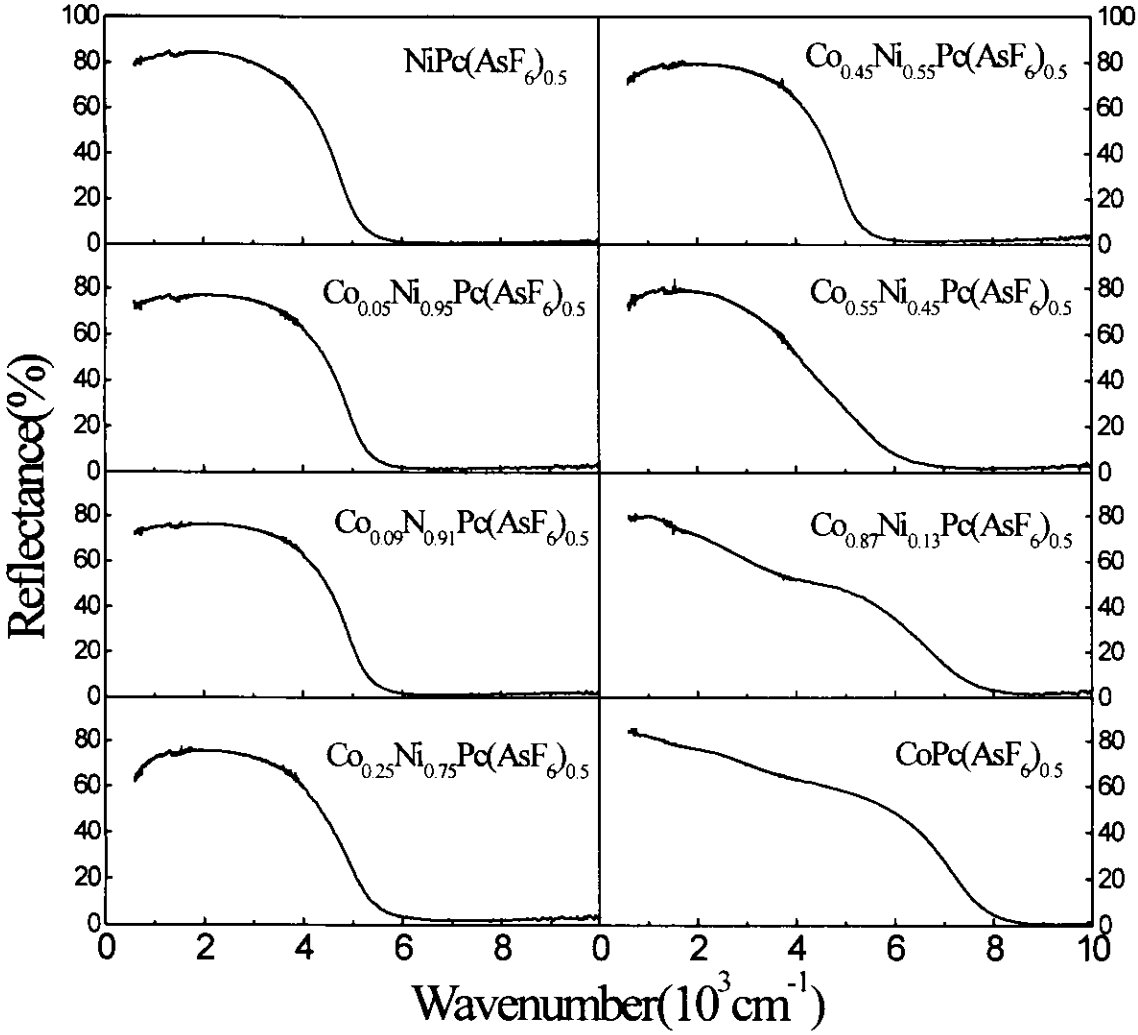

Fig.16 Reflection spectra of mixed crystal $Co_xNi_{1-x}Pc(AsF_6)_{0.5}$ parallel to *c*-axis in infrared region

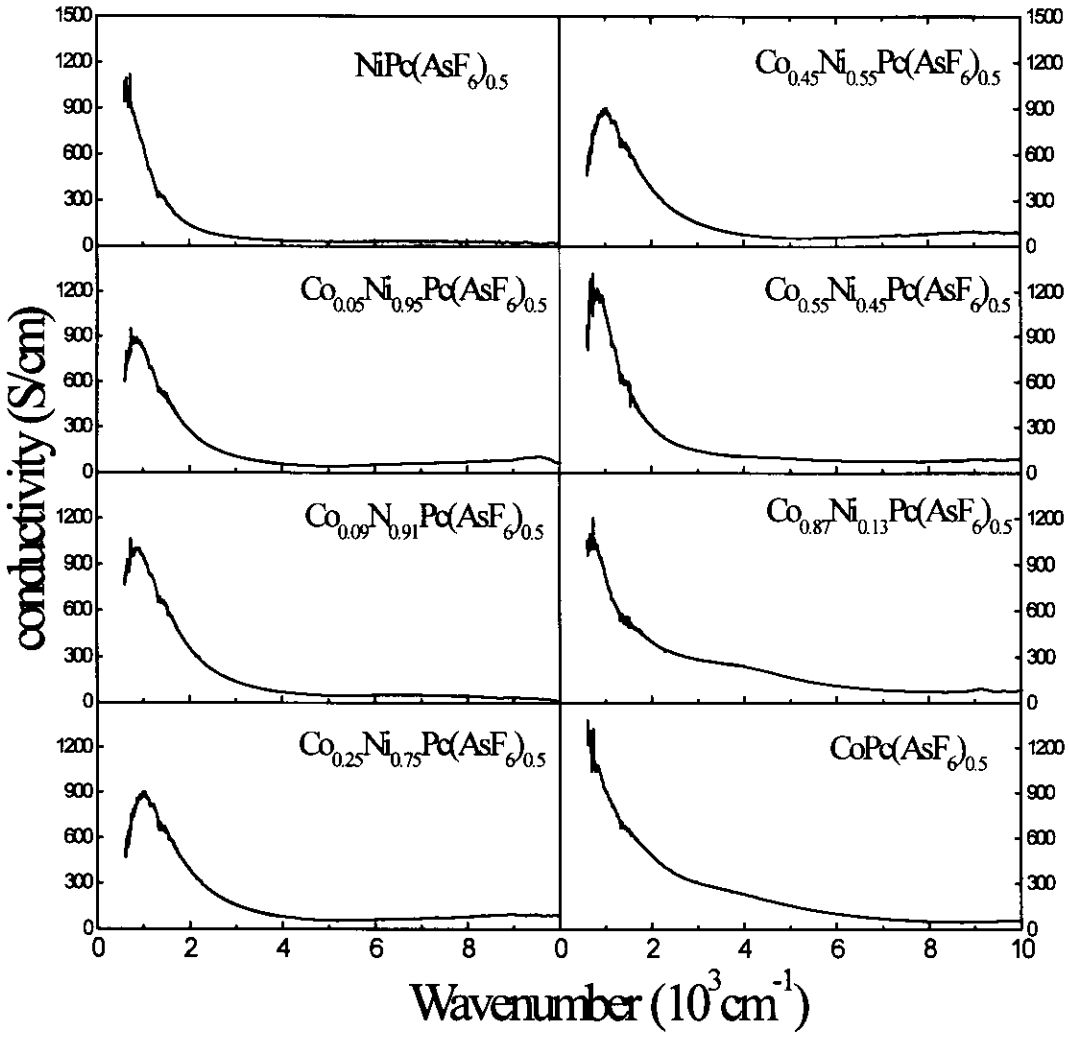

Fig.17 Conductivity spectra of $Co_xNi_{1-x}Pc(AsF_6)_{0.5}$ parallel to *c*-axis in infrared region

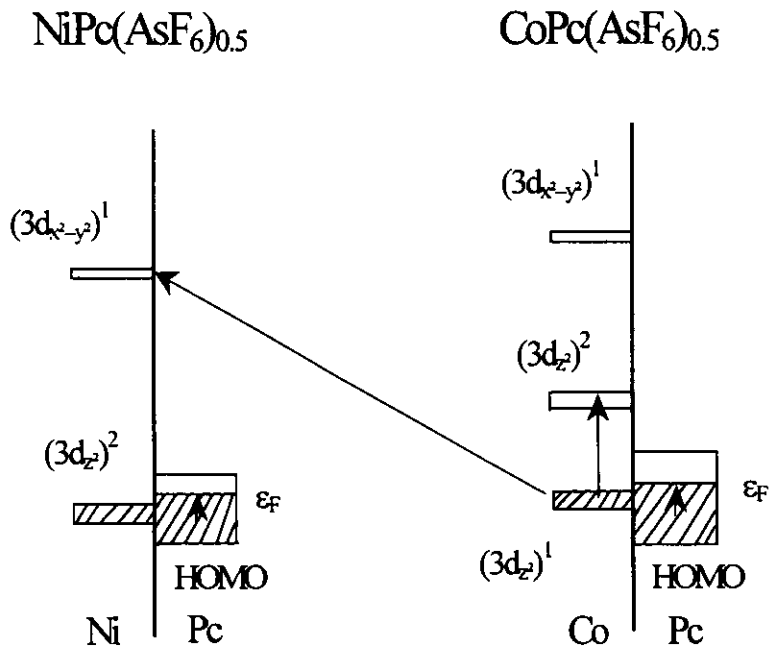

Fig. 18 Schematic energy diagrams of $NiPc(AsF_6)_{0.5}$ and $CoPc(AsF_6)_{0.5}$

Chapter 5

Magnetic properties of organic alloy $Co_xNi_{1-x}Pc(AsF_6)_{0.5}(0 \leq x \leq 1)$

M. Simonyan, Y. Yonehara, Y. Ding, and K. Yakushi

Hyperfine structure and exchange coupling with conduction electron in quasi-one-dimensional organic metal $Co_{0.01}Ni_{0.99}Pc(AsF_6)_{0.5}$

Phys. Rev., B, **63** (2001) 113103

5.1 Introduction

The quasi one-dimensional phthalocyanine conductors $M\text{Pc}(X)_y$ (M=H_2^{2+}, Co^{2+}, Ni^{2+}, Cu^{2+}, Pt^{2+}; Pc=$(C_{32}N_8H_{16})^{2-}$; y=0.5 for X=AsF_6^-, ClO_4^-, SbF_6^-, y=0.33 for I_3^-) constitute a unique system that involves magnetic metal ions near the conducting pathway. Both the paramagnetic (M=Co^{2+}, Cu^{2+}) and diamagnetic (M=H_2^{2+}, Ni^{2+}, Pt^{2+}) phthalocyanine yield nearly isostructure conductive crystals. Owing to this property, comparative study of the phthalocyanine-based conductors with paramagnetic and diamagnetic phthalocyanine ($M^{2+}Pc^{2-}$) and alloy systems has been studied in order to elucidate the influence of the localized spins on the conduction electrons. The first study was reported by Ogawa *et al.* on $CuPc(I_3)_{0.33}$, in which a magnetic order was suggested below 8 K by electron spin resonance (ESR), static susceptibility, and NMR measurements.[1] They suggested a strong coupling between the localized spin of Cu^{2+} (S=1/2) and the conduction electron of the Pc chain. Subsequently, they suggested the presence of the cross-relaxation process between the localized spin and itinerant electron through the analysis of the temperature-dependent linewidth of ESR.[2] The influence of the localized spin of Cu^{2+} on the conductivity was studied by Quirion *et al.* on $CuPc(I_3)_{0.33}$ and analogous compounds, which in the microwave resistivity experiment they found a huge negative magneto-resistance and proposed a spin-flip scattering process produced by Cu^{2+} local spin.[3,4] The essential idea was consistent with the findings of a study of the alloys, $Cu_xNi_{1-x}Pc(I_3)_{0.33}$[5,6] and $Cu_xH_{2(1-x)}Pc(I_3)_{0.33}$.[7] The concentration ($X$) dependence of the magnetization of $Cu_xNi_{1-x}Pc(I_3)_{0.33}$ was simulated by Monte Carlo methods using dipolar, direct, and Ruderman-Kittel-Kasuya-Yosida indirect (RKKY) exchange interaction.[8]

Martinsen *et al.* reported the phthalocyanine conductor of another paramagnetic ion, Co^{2+}(S=1/2), on $CoPc(I_3)_{0.33}$, in which the central metal spine was responsible for the conductivity.[9] The microwave conductivity of the alloy $Cu_xNi_{1-x}Pc(I_3)_{0.33}$ provided the same conclusion.[10,11] On the other hand, the Pc chain in the similar Co-containing phthalocyanine conductor $CoPc(AsF_6)_{0.5}$[12] played a part in the electronic conductivity in contrast to $CoPc(I_3)_{0.33}$, and thus the Co^{2+} ions were anticipated to play the same role as Cu^{2+} in $CuPc(I_3)_{0.33}$. However, the magnetic moment of Co^{2+} was suppressed by the direct Co-Co exchange interaction.[13] $CoPc(AsF_6)_{0.5}$ itself does not show ESR absorption, because the extremely fast relaxation time does not allow to get observable signal, whereas the nearly isostructural diamagnetic phthalocyanine conductor, $NiPc(AsF_6)_{0.5}$, shows a very narrow ESR signal originated from the Pc^- species in the crystal.[14] The role of the Co^{2+} spin in this compound remains unclear. An important factor in our understanding on the properties of $CoPc(AsF_6)_{0.5}$ is the exchange energy, $J_{\pi d}$, between the localized spin of Co^{2+} and itinerant spin of π holes. The purpose of the ESR properties of dilute $Co_xNi_{1-x}Pc(AsF_6)_{0.5}$ is to obtain the magnitude of the exchange interaction between the local moment of Co^{2+} ions and itinerant spins of Pc-ligand.

To reduce the direct Co-Co exchange interaction, we prepared the alloy $Co_xNi_{1-x}Pc(AsF_6)_{0.5}$.[15] We found an anisotropic hyperfine structure in the magnetically diluted alloy system, quasi one-dimensional organic conductor, $Co_xNi_{1-x}Pc(AsF_6)_{0.5}$ in the range $0<x\leq0.09$. The hyperfine signal was replaced by a broad Lorentzian signal at ~30 *K*. The broad signal shifted and narrowed with increasing temperature. We interpreted the temperature-dependent g value and linewidth using a molecular filed approximation, which has been used to interpret the ESR line shape of a dilute alloy.

We also carried out a numerical simulation for the temperature dependence of the g value and line shape of dilute magnetic alloy $Co_{0.01}Ni_{0.99}Pc(AsF_6)_{0.5}$ based on Hasegawa's phenomenological theory. The density of state at Fermi level and the exchange energy between the local spin of Co^{2+} and itinerant π-spin of the Pc chain were obtained. In this chapter, the ESR results of ESR sample and static spin susceptibility study of 1D organic conductors $Co_xNi_{1-x}Pc(AsF_6)_{0.5}$ are presented and interpreted in term of the exchange interaction between conductive and local spins.

5.2 Results and discussion

5.2.1 Hyperfine structure

We have determined the crystal structure of $Co_xNi_{1-x}Pc(AsF_6)_{0.5}$ with x=0, 0.25, 0.45, and 1. The crystals of x=0.25 and 0.45 belong to orthorhombic and tetragonal systems respectively, which are isostructural to $NiPc(AsF_6)_{0.5}$ (x=0)[14] and $CoPc(AsF_6)_{0.5}$ (x=1).[13] The boundary of the tetragonal and orthorhombic systems is between x=0.25 and 0.45 in this alloy system. Therefore we consider $Co_xNi_{1-x}Pc(AsF_6)_{0.5}$ (x=0.005, 0.01, 0.014, 0.02, 0.05, and 0.1), which will be called "ESR sample" in this Chapter for convenience, are isostructural to $NiPc(AsF_6)_{0.5}$. Thus all ESR samples have crystal structure close to $NiPc(AsF_6)_{0.5}$. The unit cell of $NiPc(AsF_6)_{0.5}$ involves two conducting columns with a metal-over-metal stack, half of the unit cell being almost same as the unit cell of $CoPc(AsF_6)_{0.5}$. Based on this crystal structure, we will discuss the mean separation of the magnetic dopant CoPc along the stacking axis in $Co_{0.01}Ni_{0.99}Pc(AsF_6)_{0.5}$. In $Co_{0.01}Ni_{0.99}Pc(AsF_6)_{0.5}$, one CoPc molecule is involved in 100 NiPc molecules, the average number of molecules (N) between the nearest neighbor

CoPc molecules is $\sqrt[3]{100}$ =4.6. Since CoPc has an anisotropic shape like a disk, N is also anisotropic. The unit size of the molecule including the counter ion AsF_6^- is estimated as $a=b$=14.234 *Å*, $c/2$=3.148 *Å* from the lattice parameters of tetragonal $CoPc(AsF_6)_{0.5}$, therefore the average numbers along the stacking c-axis and a- and b-axes are $N_c=\sqrt[3]{100} \times a/(c/2)$=21 and $N_a=N_b=\sqrt[3]{100} \times a/a$=4.6. Accordingly, we find one CoPc molecule per 21 NiPc molecules in a one-dimensional conducting column. Therefore, the mean separation between the magnetic dopants along the stacking axis in $Co_{0.01}Ni_{0.99}Pc(AsF_6)_{0.5}$ is estimated to be 66 *Å*. $Co_{0.01}Ni_{0.99}Pc(AsF_6)_{0.5}$ shows metallic conductivity near the room temperature at least down to 200 *K*. At present, however, we have not determined the complete conductivity temperature dependence, since the crystals are too fragile to withstand temperature change.

It has been demonstrated by Assour and Kahn that the magnetically diluted (1:1000-10000) single crystal of β-CoPc shows an axially symmetric ESR signal with clearly resolved Co hyperfine features at 77 *K*.[16] This system $Co_{0.01}Ni_{0.99}Pc$ does not show clear Co hyperfine features before electrochemical oxidation. However, in the conducting system $Co_{0.01}Ni_{0.99}Pc(AsF_6)_{0.5}$ involving the same concentration of magnetic ions, the well-resolved hyperfine structure of Co^{2+} (I=7/2) is observed at 3.5 *K* ($H//c$) and 3.2 *K* ($H\perp c$) as shown in Fig. 1 and 2. This hyperfine structure is very anisotropic. The spectrum is spread over 1500 *G* in both directions of magnetic field. No super-hyperfine structure is found from the neighboring four nitrogen atoms (I=1). The individual hyperfine resonance line has a derivative peak-to-peak linewidth of $\Delta H_{//}$=60 *G* and $\Delta H_{\perp}$=23 *G*, where $\perp$ and // represent the magnetic field perpendicular and parallel to c-axis. The separation between hyperfine lines significantly increases toward higher

field. The g value is determined at the mid-field between M_I=±1/2 lines. Around 3410 G, we find a weak signal with g=1.987 and ΔH=20 G at low temperature. The same signal is perfectly separated from the main lines, when the magnetic field is perpendicular to the c-axis. The intensity of this signal depends upon the sample and it is 10^3 times smaller than that of the basic signal in this sample. This signal seems to be attributed to a crystals defect.[17] Such a signal often arises even in the multiply sublimed diamagnetic phthalocyanine solids.[18] On increasing temperature, the hyperfine structure of $Co_{0.01}Ni_{0.99}Pc(AsF_6)_{0.5}$ weakens each line without increasing its linewidth, finally being replaced by the broad signal above 30 K as shown in Fig. 1 and Fig. 2. Above 30 K, the broad signal narrows the linewidth with increasing temperature, and the $H\perp c$ signal in particular shows a significant g shift. At room temperature, the signal becomes a single Lorentizan with $\Delta H_\perp$=130 G, $g_\perp$=2.078 and $\Delta H_{//}$=81 G, $g_{//}$=1.98.

Hyperfine structure of $Co_{0.01}Ni_{0.99}Pc(AsF_6)_{0.5}$ is interpreted based on the Hamiltonian involving the electron and nuclear spins in the field of axial symmetry,[19] which is used to analyze the ESR signal of the magnetically diluted CoPc in β-NiPc and α-ZnPc crystals.[16] The spin Hamiltonian is given as

$$H=\mu_B\{g_{//}H_zS_z + g_\perp(H_xS_x+H_yS_y)\} + AS_zI_z + B(S_xI_x + S_yI_y) + Q\{I_z^2 - 1/3I(I+1), \quad (1)$$

where μ_B is the Bohr magneton, H the applied magnetic filed, $g_{//}$ and $g_\perp$ principal g values, A and B the anisotropic hyperfine coupling constant between the unpaired electron and the cobalt nuclear spin, S and I the electron and nuclear spin operators. The term in Q comes from the interaction of the nuclear electric quadrupole moment with the gradient of the electric field at the nucleus. Since the magnitude of the quadrupole parameter Q is much smaller than A and B, we neglect this term in the analysis. Bleaney

has considered the second-order interaction between electron and nuclear spins to account for the unequal spacing of the resonance lines in the axially symmetric paramagnetic salts.[19] The resonance condition is given as

$$H_{//} = \frac{H_0}{g_{//}} - \frac{AM_I}{g_{//}} - B^2 \frac{I(I+1) - M_I^2}{2g_{//}H_0} \qquad (2)$$

for $\theta = 0°$ and

$$H_{\perp} = \frac{H_0}{g_{\perp}} - \frac{BM_I}{g_{\perp}} - \left(A^2 - B^2\right)\frac{I(I+1) - M_I^2}{4g_{\perp}H_0} \qquad (3)$$

for $\theta = 90°$, where H_0 is the static magnetic field, M_I the nuclear spin quantum number ($M_I = \pm 1/2, \ldots \pm 7/2$). In the first approximation, the interaction with nuclear spin splits each electronic spin state into $2I+1$ equally spaced levels with the separation of A or B. Second-order terms in M_I^2 cause a linear change in the separation between the hyperfine lines. For θ=0° and θ=90°, the separation always increases toward higher fields. The hyperfine constants A and B are determined by the least-squares calculation to produce the 16 lines in equation (2) and (3).

Table 1 presents the g values and hyperfine parameters in $Co_{0.01}Ni_{0.99}Pc(AsF_6)_{0.5}$ along with those of CoPc diluted in the insulating β-NiPc and α-ZnPc crystals. The hyperfine constants of Co^{2+} ion in $Co_{0.01}Ni_{0.99}Pc(AsF_6)_{0.5}$ resemble those in β-$Co_{0.01}Ni_{0.99}Pc$ rather than α-$Co_{0.01}Zn_{0.99}Pc$. This is ascribed to the local environment around the nuclear spin in Co^{2+} ion. As shown in Fig. 3, the α- and β-modifications of MPc take different overlap patterns,[20] so the Co^{2+} ion feels a different environment when it is doped in the α-ZnPc and in β-NiPc host crystals. In the α-ZnPc crystals [see Fig.3*b*], the Co^{2+} ion is not directly coordinated from the axial direction, whereas in the

β-NiPc crystals [see Fig.3*c*] it is coordinated at the axial position by the two N atoms of the neighbor molecules. As shown in Fig. 3*a*, the local environment of the Co^{2+} ion doped in $NiPc(AsF_6)_{0.5}$ resembles that in β-NiPc rather than in α-ZnPc.[21] This seems to be the reason for the similar hyperfine constant between $Co_{0.01}Ni_{0.99}Pc(AsF_6)_{0.5}$ and β-$Co_{0.001}Ni_{0.999}Pc$. As shown in Fig. 1 and 2, no super-hyperfine structure from the nearest four nitrogen atoms (I=1) is observed in $Co_{0.01}Ni_{0.99}Pc(AsF_6)_{0.5}$ as well as in magnetically diluted CoPc in α-ZnPc and β-NiPc. This result indicates that the unpaired d-electron occupies the $3d_{z^2}$ orbital of Co^{2+}, and this orbital is not extended to the nitrogen atoms.[22] The very anisotropic g value also supports the $3d_{z^2}$ orbital for the location of the unpaired electron in CoPc.[23] The large anisotropy comes from the contribution of the orbital moment due to the large spin-orbital interaction in Co^{2+}. Nishida *et al.* have calculated the g values of CoPc based on the configuration of the $3d$-holes as $(d_{x^2-y^2})^2(d_{z^2})^1$,[23] and have given the following equations for the anisotropic g value,

$$g_{//}=2 \text{ and } g_{\perp}= 2-\frac{6\lambda k^2}{\Delta}, \qquad (4)$$

where Δ is the separation between the ground and lowest excited states with E_g symmetry. Incidentally, they estimate λ as -515 cm^{-1} and orbital reduction factor k^2 as 0.8. It is interesting to notice that the anisotropic g value also resemble the CoPc diluted in β-NiPc. The resemblance of the anisotropic g value as well as the anisotropic hyperfine constant to the magnetically diluted CoPc in β-NiPc indicates that the hyperfine signal of this compound is coming from $CoPc^0$ substituted in the molecular column of $NiPc^{0.5+}$. This result means that all the doped CoPc exists as a neutral

molecule, since the ESR signal of $CoPc^+$ is very different from that of $CoPc^0$ due to the dipole-dipole interaction between $3d_{z^2}$ spin and π spin on the same molecule. It should be noted that the magnetic impurity in this alloy is well characterized by the analysis of the hyperfine structure.

As described in the section of the introduction, $CoPc(AsF_6)_{0.5}$ does not show ESR signal because the extremely fast relaxation time. In the alloy system, the ESR signal becomes visible already in the compound of $Co_{0.09}Ni_{0.91}Pc(AsF_6)_{0.5}$ below 140 *K*. This phenomenon indicates that the ESR signal of $Co_xNi_{1-x}Pc(AsF_6)_{0.5}$ is very sensitive to concentration of Co^{2+} ion, because of the strong sensitivity of the resonance *g*-value, linewidth and hyperfine splitting to small change in concentration of Co^{2+} ion. In ESR samples, the hyperfine structure is observed at low temperature, which is replaced by a single Lorentzian line above 30 *K* except $Co_{0.09}Ni_{0.91}Pc(AsF_6)_{0.5}$ as shown in Fig. 4 and 5 for crystal $Co_{0.05}Ni_{0.95}Pc(AsF_6)_{0.5}$ in both magnetic field parallel and perpendicular to *c*-direction. In low temperature range the temperature behavior of ESR signal of crystals except $Co_{0.09}Ni_{0.91}Pc(AsF_6)_{0.5}$ was analogous to the behavior of $Co_{0.01}Ni_{0.99}Pc(AsF_6)_{0.5}$. The parameters of hyperfine splitting as well as the parameters of individual lines were very close to those for $Co_{0.01}Ni_{0.99}Pc(AsF_6)_{0.5}$. The evaluation of hyperfine structure with decreasing *x* is shown in Fig. 6 and 7 in both directions at 3.2 *K*, respectively. ESR samples within experimental errors show similar hyperfine splitting with approximate the same parameters. The same analysis shows that the parameters of hyperfine splitting A=0.019 cm^{-1}, B=0.029 cm^{-1} obtained for $Co_{0.01}Ni_{0.99}Pc(AsF_6)_{0.5}$ reproduced the resonance fields for all ESR samples.

ESR samples show more or less expressed signal with g=1.995. While this signal is very weak in x=0.01, 0.05 or 0.1, it was observed rather well in x=0.005 or 0.02. This line shows no tendency for systematic behavior and appears unpredictably. The g-value as well as linewidth did not show any essential change with the change of the temperature. With decreasing temperature the integral intensity of this signal has Curie-like behavior and at 3.2 K is 100 times large than at room temperature. It seems that this signal comes from impurity or a crystal defect. Such signal always arises in pure phthalocyanine compounds with metals in diamagnetic state and is originated from a crystal defect.[18,24]

5.2.2 Temperature dependence of g value and linewidth

Figure 8 shows the temperature dependence of the g values and linewidths of $Co_{0.01}Ni_{0.99}Pc(AsF_6)_{0.5}$, which suggests that the exchange interaction between the localized 3d-spin and itinerant π-hole is involved in the relaxation process. If an itinerant π-hole strongly interacts with a localizd 3d-electron, the ESR lines of itinerant π- and localized 3d-spins merge into a single line. In fact, the high-temperature ESR signal suggests this case. This situation corresponds to the so-called "bottleneck regime" in dilute magnetic alloys.[25] In this regime, the cross-relaxation rates between itinerant and local spins are much faster than the spin-lattice relaxation rates of the local and itinerant spins, and the effective g value is given by the following equation,[25]

$$g_{eff}^{\perp,//} = \frac{g_\pi \chi_\pi + g_d^{\perp,//} \chi_d^{\perp,//}}{\chi_\pi + \chi_d^{\perp,//}} \qquad (5)$$

where $g_d^{\perp,//}$ is the g value of Co^{2+} ions, g_π the isotropic g value of π-holes [g_π=2.0023 for $NiPc(AsF_6)_{0.5}$]. If we take the molecular field approximation, χ_d and χ_π are given by the following equations,[25]

$$\chi_d = \frac{\chi_d^0(1+\lambda\chi_\pi^0)}{1-\lambda^2\chi_d^0\chi_\pi^0} \text{ and } \chi_\pi = \frac{\chi_\pi^0(1+\lambda\chi_d^0)}{1-\lambda^2\chi_d^0\chi_\pi^0}, \tag{6}$$

where χ_d^0 is the magnetic susceptibility by the bare local moment on Co^{2+}, χ_π^0 the susceptibility of the Pauli paramagnetism in $NiPc(AsF_6)_{0.5}$), and λ the molecular field coefficient. They are given by the following equations.

$$\chi_\pi^0 = \frac{N_A}{2}(g_\pi\mu_B)^2 D_F \tag{7}$$

$$\chi_d^0 = \frac{N_A c_0 (g_d\mu_B)^2 S(S+1)}{3k_B T} \tag{8}$$

$$\lambda = \frac{2J_{\pi d}}{N_A g_\pi g_d \mu_B^2}, \tag{9}$$

where D_F is the density of state per hole and per spin at the Fermi level, c_0 the concentration of the magnetic ion, N_A Avogadro number, $J_{\pi d}$ the exchange energy between the local and itinerant spins. The temperature dependence of the effective g value is expressed by the two independence parameters, D_F and $J_{\pi d}$. The equation (5) reproduces the observed $g_\perp(T)$ curve for the broad signal ($20K<T<300K$) very closely, if we use D_F=3.8±0.2 eV^{-1} and $J_{\pi d}$=–0.001±0.03 eV. The calculated $g_\perp(T)$ curve is illustrated by solid line in the top panel of Fig. 8. The density of state is calculated as D_F=1.5 eV^{-1} when we take the ¾-filled one-dimensional tight-binding band with the transfer integral of t=0.3 eV.[14] Organic metals have a strong correlation effect, which

enhances the density of state. Taking this correlation effect into account, the agreement is satisfactory. Because of the small $J_{\pi d}$, the molecular field coefficient is small, so that the correction term $\lambda\chi_d^0$ and $\lambda\chi_\pi^0$ is negligible in the equation (6) in all temperature region. So the effective g value are approximately expressed by the susceptibility weighted average of the local and itinerant moments. Owing to the relation $g_{d//} \approx g_\pi$, the effective $g_{//}$ value is expected to be close to temperature independent g_π. In fact, the $g_{//}$ value is nearly temperature independent as shown in the top panel of Fig.8. The standard deviation for D_F is small enough, but $J_{\pi d}$ is insensitive to $g_\perp(T)$.

5.2.3 Numerical simulation of the ESR signal

To estimate $J_{\pi d}$ more precisely for $Co_{0.01}Ni_{0.99}Pc(AsF_6)_{0.5}$, we conducted a numerical calculation of the ESR line shape based on Hasegawa's phenomenological theory for a dilute random alloy, which was solved by Barnes *et al* including a hyperfine structure.[26] Equations (6)-(9) derived from the molecular field approximation are used in this model. The Korringa relaxation rate is introduced as $1/T_{d\pi}=4\pi(D_F J)^2 K_B T/h$ to describe the relaxation rate of the local spin *via* the interaction with the itinerant π spin. The spin-lattice relaxation rate is assumed to be temperature independent. $1/T_{dL,\perp}=23$ G and $1/T_{dL,//}=61$ G are taken from the ESR linewidth of the individual hyperfine line, and $1/T_{\pi L,\perp}=100$ G and $1/T_{\pi L,//}=70$ G are taken so as to adjust the room-temperature linewidth. The resonance magnetic fields of the hyperfine lines are taken from the experimentally observed values. In this model, the line broadening at low temperature is ascribed to the hyperfine interaction. With the density of state $D_F=3.8$ eV^{-1}, we simulated the line shape by changing the exchange energy $J_{\pi d}$. For example, $|J_{\pi d}|=0.001$

eV is too small to explain the observed broad signal because in this case a narrow signal of π spins appears separately from hyperfine signals of $3d$ spins in the whole temperature range. The simulation with $|J_{\pi d}|$=0.02 eV, on the other hand, reproduces the g shift but does not reproduce the line broadening upon cooling. In this case, the linewidth is already narrowed above 20 K. The open squares and circles in Fig. 8 show the g value (top) and linewidth (bottom) obtained from the line shape calculated with $|J_{\pi d}|$=0.013 eV. As shown in Fig. 9, this simulation with $|J_{\pi d}|$=0.013 eV properly explains both the temperature-dependent g shift and line narrowing above 30-40 K. Below this temperature, the observed ESR line shape is very different from the calculation. In the temperature range of 10 $K<T<30$ K, the hyperfine signal coexists with the broad line, and the replacement by the broad line appears to be continuous. Below 10 K, the hyperfine structure increases the line intensity according to Curie law. The weak broad line disappears in the strong hyperfine signals. The above model with $|J_{\pi d}|$=0.013 eV cannot reproduce the well-resolved hyperfine structure. This means that some part of Co^{2+} spins are decoupled with π holes below 30 K. Furthermore, the hyperfine signal decreases more strongly than predicted by the Curie law above 30 K. We thus speculate that the π holes may be weakly localized in this alloy below 30 K.

Ogawa *et al.* estimate the dynamical exchange term between local and mobile spins in $Cu_xNi_{1-x}Pc(I_3)_{0.33}$, and presented the coefficient of T as 0.055.[5] If we interpret this coefficient as $4\pi(D_F J)^2$ in the Korringa relaxation rate, the exchange energy is estimated as $|J| \leq 0.017$ eV, since D_F in the 5/6-filled band is larger than that of the ¾-filled band.[27] This $|J_{\pi d}|$ value is comparable to that in $Co_{0.01}Ni_{0.99}Pc(AsF_6)_{0.5}$. The exchange parameter in the phthalocyanine conductor is much smaller than that in

inorganic alloy, the corresponding value being ≈1 eV for $3d$ ions and ≈0.05 eV for $4f$ ions.[25] Using the parameters, D_F and $|J_{\pi d}|$, the Kondo effect and RKKY temperatures are roughly estimated as $T_K \approx W\exp(-1/D_F|J_{\pi d}|)=2\times10^{-5}$ K and $T_{RKKY}\approx|J_{\pi d}|^2 D_F=7$ K, where W is the bandwidth (=1.2 eV) of $NiPc(AsF_6)_{0.5}$.[14] This estimation is consistent with the Curie-Weiss behavior of the low-temperature magnetic susceptibility as shown in Fig. 10. $J_{\pi d}$ involves on-molecule exchange term J_{mo} and covalent mixing term J_{cm}, thereby $J_{\pi d}=J_{mo}+J_{cm}$. J_{mo} is estimated from the following Coulomb energy $\iint \phi_\pi(r_2)\varphi_d(r_1)\frac{e^2}{r_{12}}\phi_\pi(r_1)\varphi_d(r_2)dr_1dr_2$, where ϕ_π and φ_d are the HOMO of Pc^{2-} and $3d_{z^2}$ orbital of Co^{2+}, respectively. According to the molecular orbital calculation of NiPc, HOMO has nodes at Ni and N sites, and the $3d_{z^2}$ orbital is also localized near the Ni site.[28] They mutually occupy separate sites in the phthalocyanine molecule, so the differential overlap $\phi_\pi(r)\varphi_d(r)$ seems to be very small in every site in the molecule. If the molecular orbital of CoPc resembles NiPc, the above Coulomb energy seems to be very small. Covalent mixing comes from the hybridization of the Co $3d_{z^2}$ orbital and Pc HOMO of the neighbor molecule. J_{cm} is proportional to $S_{\pi d}$, which is given be the following equation:

$$S_{\pi d} = \iint \phi_\pi(r)\varphi_d(r)dr$$

The small value of J_{cm} suggests the small hybridization. This suggestion is consistent with the characteristic feature of HOMO and $3d_{z^2}$ orbital.

5.2.4 Magnetic susceptibility

Figure 10 shows the static magnetic susceptibility of $Co_{0.01}Ni_{0.99}Pc(AsF_6)_{0.5}$. As shown in this figure, the susceptibility consists of Curie-Weiss and temperature-independent terms. The observed susceptibility is fitted very well by the equation, $\chi_{\perp,//}(T)=C_{\perp,//}/(T-\theta_{\perp,//})+\chi_{0\perp,//}$ down to 2 *K*, where $\perp$ and // represent the magnetic field perpendicular and parallel to *c*-axis, *C* is the Curie constant, θ is the Weiss temperature, χ_0 is the temperature independent Pauli term. The Curie constant and Weiss temperature in $Co_{0.01}Ni_{0.99}Pc(AsF_6)_{0.5}$ are determined as $C_\perp$=0.0075 emuK/mol, $\theta_\perp$=–0.25 *K*, $C_{//}$=0.0038 emuK/mol, and $\theta_{//}$=–0.28 *K*. The ratio of the Curie constant $C_\perp/C_{//}$ is a little smaller than $(g_\perp/g_{//})^2$. This is ascribed to a paramagnetic defect or impurity with an isotropic *g* value of 2.0023 in $NiPc(AsF_6)_{0.5}$. Taking the contribution of isotropic species into account, we determined the concentration of the paramagnetic species as 0.77% for doped CoPc and 0.21% for a defect. The concentration of CoPc agrees well with the dopant concentration (1%) in the starting material. Therefore both the sharp and broad signals contribute to the Curie constant, and thus the distance between the close CoPc molecules is long enough to avoid the direct exchange interaction.

The static magnetic susceptibility of all alloys shows Curie-like behavior and can be fitted very well as a sum of the temperature dependence Curie term associated with the Co spins, and the temperature independence Pauli term associated with the conduction electrons on the macrocycle of phthalocyanine rings. When the concentration of CoPc is increased, the Curie constant linearly increases in the range of $0.005 \le x \le 0.009$, and reaches a maximum around $x \approx 0.25$, and then decreases in the range of $0.05 \le x \le 1$. The *x* dependence of the Curie constant (*C*) and Weiss temperature (θ) are show in Fig. 11 together with the average distance (*L*) along the *c*-axis. The average

distance measured by the unit of inter-molecular distant along the stack ($c/2$) is estimated from the equation, $(2a/c)^{2/3}x^{-1/3}$ for $0 \leq x < 0.2$ and x^{-1} for $0.2 < x \leq 1$ taking the disk-like molecular shape into account. The Curie constant linearly increases when the average distance is less than 6 molecules along the stack ($0 \leq x < 0.1$). The straight lines (a) and (b) represent $(N_A g_\perp{}^2 \mu_B{}^2 S(S+1)/3k_B)x$ ($g_\perp$=3.045) and $(N_A g_{//}{}^2 \mu_B{}^2 S(S+1)/3k_B)x$ ($g_{//}$=2.056), in which N_A is Avogadro's number, μ_B is the Bohr magneton, K_B is Boltzmann's constant, respectively. In this range, all the doped CoPc contributes to the Curie term in magnetic susceptibility, and thereby the magnetic moments of CoPc molecules are nearly free from each other. The strength of the antiferromagnetic interaction between the magnetic moments is reflected in θ.[29] In the range of $0 \leq x < 0.1$, θ increases with x below 0.75 K. Therefore the indirect Co-Co interaction *via* the conduction electrons in the Pc chain seems to be very weak.[30] When x is increased, the Curie constant reaches a maximum around x=0.25 and decreases toward zero. This behavior is different from the cases of $Cu_xNi_{1-x}Pc(I_3)_{0.33}$ and $Cu_xNi_{2(1-x)}Pc(I_3)_{0.33}$[30], in which the Curie constants linearly increase in the whole range of $0 \leq x \leq 1$. The different x dependence of Curie constant is attributed to the different single occupied molecular orbital (SOMO), which is $3d_{z^2}$ in CoPc and is $3d_{x^2-y^2}$ in CuPc. The former is extended to the neighbor Co^{2+} in CoPc, whereas the latter is elongated to the four nitrogen atoms in the Pc plane. With increasing x, the average distance between CoPc in the stacking direction becomes short. When x=0.25, for example, L is about 2. As a result, there exists a considerable number of CoPc pairs in the same stack, which form a spin singlet. Therefore, the decrease of the Curie term in $x \geq 0.25$ is caused by the direct antiferromagnetic interaction, since the probability to find the CoPc in neighbor position

along the stack becomes higher. In $CoPc(AsF_6)_{0.5}$ (x=1), the Curie term is almost completely suppressed except for the small Curie component coming from a small amount of crystal defect. This result means that the 3*d*-orbital overlap between the neighbor molecules is extremely small in $CuPc(I_3)_{0.33}$ but significantly large in $CoPc(AsF_6)_{0.5}$.

Finally, it is necessary to emphasize that the change in Curie constant and Weiss temperature is similar to the behavior of spin glasses with the increase of antiferromagnetic correlations.[31] This fact supports that the observed an antiferromagnetic indirect coupling in $Co_xNi_{1-x}Pc(AsF_6)_{0.5}$ in low content of x, which is transformed to the direct antiferromagnetic interaction between Co^{2+} ions in $CoPc(AsF_6)_{0.5}$.

5.3 Summary

An anisotropic hyperfine structure was found at 3.2 *K* in the alloy system of $Co_xNi_{1-x}Pc(AsF_6)_{0.5}$ in the range of $0<x\leq0.09$. This hyperfine structure was identified as coming from the doped $CoPc^0$ molecule in $NiPc(AsF_6)_{0.5}$. This hyperfine signal was replaced by a broad signal at about 30 *K*, which narrows upon further increases of temperature. The exchange energy between the *d*- and π-spins and the density of state at the Fermi level were obtained as $|J_{\pi d}|$=0.013±0.002 eV and D_F=3.8±0.2 eV^{-1} based on the numerical simulation of the temperature dependence of *g*-value and line shape of the ESR signals of $Co_{0.01}Ni_{0.99}Pc(AsF_6)_{0.5}$. This means that the exchange interaction between *d*- and π-spins are extremely small. Using these parameters, the Kondo and RKKY temperatures were estimated as T_K =2×10^{-5} *K* and T_{RKKY}=7 *K*, respectively. This

result is consistent with the magnetic susceptibility of the alloy system which conforms to the Curie-Weiss law down to 2 *K*. The small exchange energy between *d*- and π-spins suggests a small hybridization between the Co $3d_{z^2}$ orbital and Pc HOMO. The enhancement of the Co concentration increases the CoPc pair, and then the direct antiferromagnetic interaction between the pairs suppresses the Curie constants. This feature is consistent with the formation of the half-filled 1D band.

References

[1] M. Y. Ogawa, B. M. Hoffman, S. Lee, M. Yudkowski, and W. P. Halperin, *phys. Rev.Lett.*, **57**,1177 (1986).

[2] M. Y. Ogawa, J. Martinsen, S. M. Palmer, J. L. Stanton, J. Tanaka, R. L. Green, B. M. Hoffman, and J. A. Ibers, *J. Amer. Chem. Soc.*, **109**, 1115 (1987).

[3] G. Quirion, M. Poirier, K. K. Liou, M. Y. Ogawa, B. M. Hoffman, *J. Phys. Rev. B*, **37**, 4272 (1988-I).

[4] G. Quirion, M. Poirier, C. Ayache, K. K. Liou, B. M. Hoffman, *J. phys. I France* **2**, 741 (1992).

[5] M. Y. Ogawa, S. M. Palmer, K. K. Liou, G. Quirion, J. A. Thompson, M. Poirier, B. M. Hoffman, *Phys. Rev. B*, **39**, 10682 (1989-I).

[6] G. Quirion, M. Poirier, K. K. Liou, B. M. Hoffman, *Phys. Rev. B*, **43**, 860 (1991).

[7] J. Thompson, K. Murata, R. Durcharne, M. Poirier, and B. M. Hoffman, *Phys. Rev.* B **60**, 523(1999).

[8] Q. Shen, D. E. Ellis, Y. Lee, W. P. Halperin, J. A. Thompson, b. M. Hoffman, *J. Mag. And Mag. Mater.*, **152**, 139 (1996).

[9] J. Martinsen, J. L. Stanton, R. L. green, J. Tanaka, B. M. Hoffman, J. A. Ibers, *J. Amer. Chem. Soc.*, **107**, 6915 (1985).

[10] G. Quirion, M. poirier, M. castonguay, K. K. Liou, B. M. Hoffman, *Phys. Rev. B*, **42**, 2831 (1990-I).

[11] K. K. Liou, C. S. Jacobsen, B. M. Hoffman, *J. Aner. Chem. Soc.*, **111**, 6616 (1991).

[12] K. Yakushi, H. Yamakado, T. Ida, A. Ugawa, *Solid State Commun.*, **78**, 919 (1991).

[13] H. Yamakado, T. Ida, A. Ugawa, K. Yakushi, K. Awaga, Y. maruyama, K. Imaeda, H.

Inokuchi, *Synth. Met.*, **62**, 169 (1994).

[14] K. Yakushi, H. Yamakado, M. Yoshitake, N. Kosugi, H. Kuroda, T. Sugano, M. Kinoshita, A. Kawamoto, J. Tanaka, *Bull. Chem. Soc. Jpn.*, **62**, 687 (1989).

[13] Y. Ding, M. Simonyan, Y. Yonehara, M. Uruichi, and K. Yakushi, *J. Mater. Chem.*, **11**, 1469 (2001); Y. Yonehara and K. Yakushi, *Synth. Met.* **103**, 2214(1999).

[16] J. M. Assour, W. K. Kahn, *J. Amer. Chem. Soc.* **87**, 207 (1965).

[17] The much strong signal is observed at the same field in more highly concentration mixed crystal $Co_{0.02}Ni_{0.98}Pc(AsF_6)_{0.5}$. It shows up even at room temperature for $H\perp c$, and the intensity followings the Curie law. Therefore the origin of this narrow signal is attributed to the impurity or crystal defects.

[18] J. M. Assour, S. E. Harrison, J. *Phys. Chem.*, **68**, 872 (1964).

[19] B. Bleany, *Philos. Mag.*, **42**, 441 (1951).

[20] F. H. Moser, A. L. Thomas, "The phthalocyanines" vol. 1, p22 (CRC press, Boca Raton, FL, 1983).

[21] As shown in Fig. 3a, the ion is coordinated at the nearly axial positions by the two Ni^{2+} ions instead of N atoms in $Co_{0.01}Ni_{0.99}Pc(AsF_6)_{0.5}$.

[22] B. A. Good man and J. B. Paynin, Advan. *Inorg. Chem. Radiochem.*, **13**, 135 (1972).

[23] Y. Nishida, S. kida, *Inorg. Nucl. Chem. Letters*, **7**, 325(1971).

[24] Y. Yonehara, K. Yakyshi, *Synth. Met.*, **94**, 149 (1998).

[25] S. E. Barnes, *Adv. Phys*, **30**,801 (1981).

[26] S. E. Barnes, J. Dupraz, and R. Orbach, *J. Appl. Phys.*, **42**, 1659(1971).

[27] The density of state is given as $D_F=(\pi t sin(ck_F))^{-1}$ in the one-dimensional tight-binding model. Since the band-filling factor of $CuPc(I_3)_{0.33}$ is large, k_F so that D_F is larger than

those of $NiPc(AsF_6)_{0.5}$.

[28] F. W. Kutzler and D. E. ELLIS, *J. Chem. Phys.*, **84**, 1033(1986).

[29] I. Martin and P. Phillips, *Phys. Rev.*, B, **60**, 530 (1999).

[30] J. A. Thompson, K. Murata, R. Durcharne, M. Poirier, and B. M. Hoffman, *Phys. Rev., B*, **60**, 523 (1999).

[31] S. E. Barnes, *Phys. Rev.*, B30, **7**, 3944 (1984).

Table 1. Anisotropic g values and hyperfine constants

material	temperature (K)	$g_{//}$	$g_{\perp}$	A (cm^{-1})	B (cm^{-1})
$Co_{0.01}Ni_{0.99}Pc(AsF_6)_{0.5}$	3.2, 3.5	2.056(4)	3.045(4)	0.019(1)	0.029(1)
β-$Co_{0.001}Ni_{0.999}Pc$[a)]	77, 27	1.89(1)	2.94(1)	0.015(1)	0.028(1)
α-$Co_{0.001}Zn_{0.999}Pc$[a)]	300, 77, 27	2.007(3)	2.422(3)	0.0116(3)	0.0066(3)

[a)] These data are taken from Ref. 16.

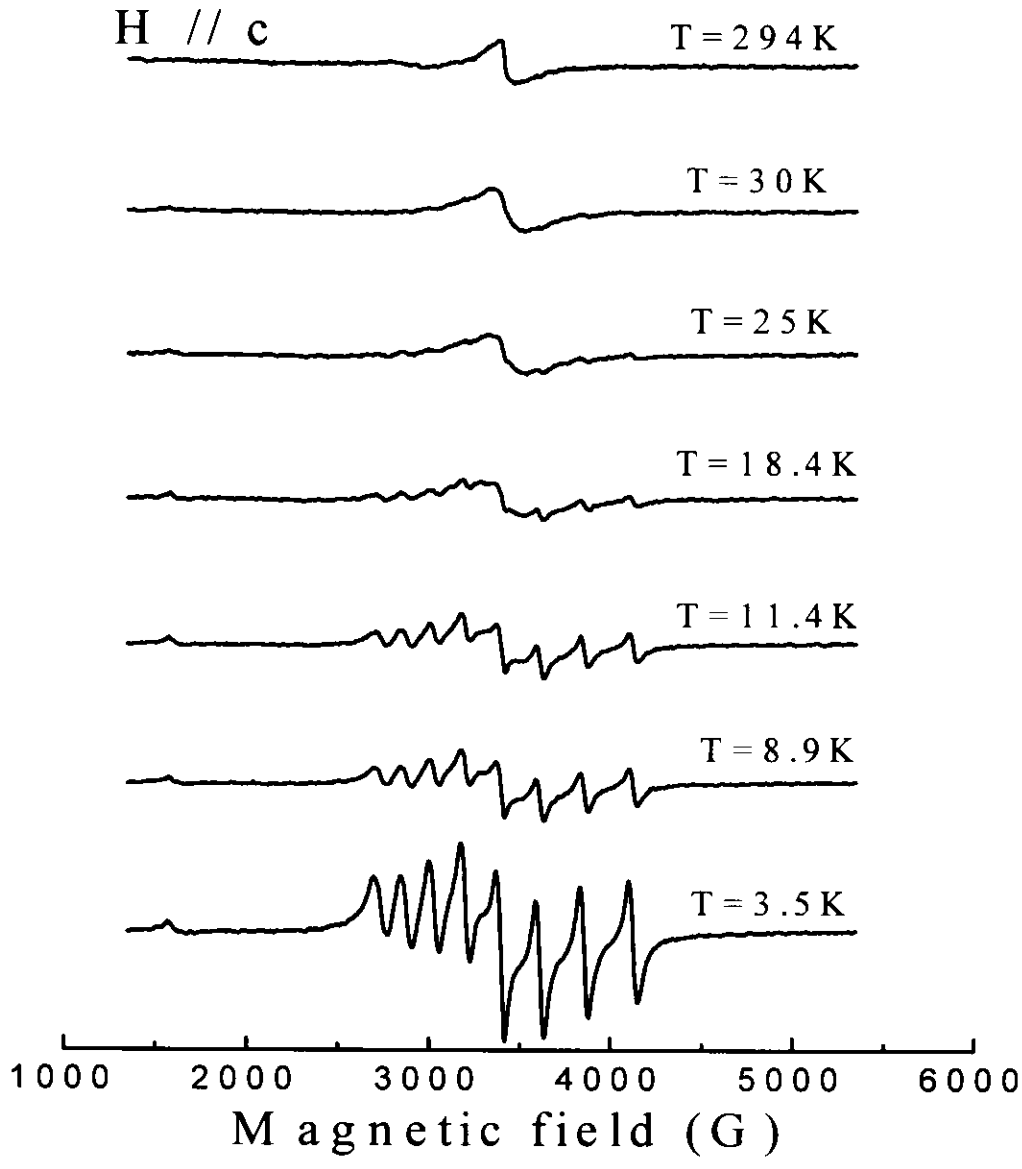

Fig.1 Temperature dependence of ESR signal of $Co_{0.01}Ni_{0.99}Pc(AsF_6)_{0.5}$ *H//c*

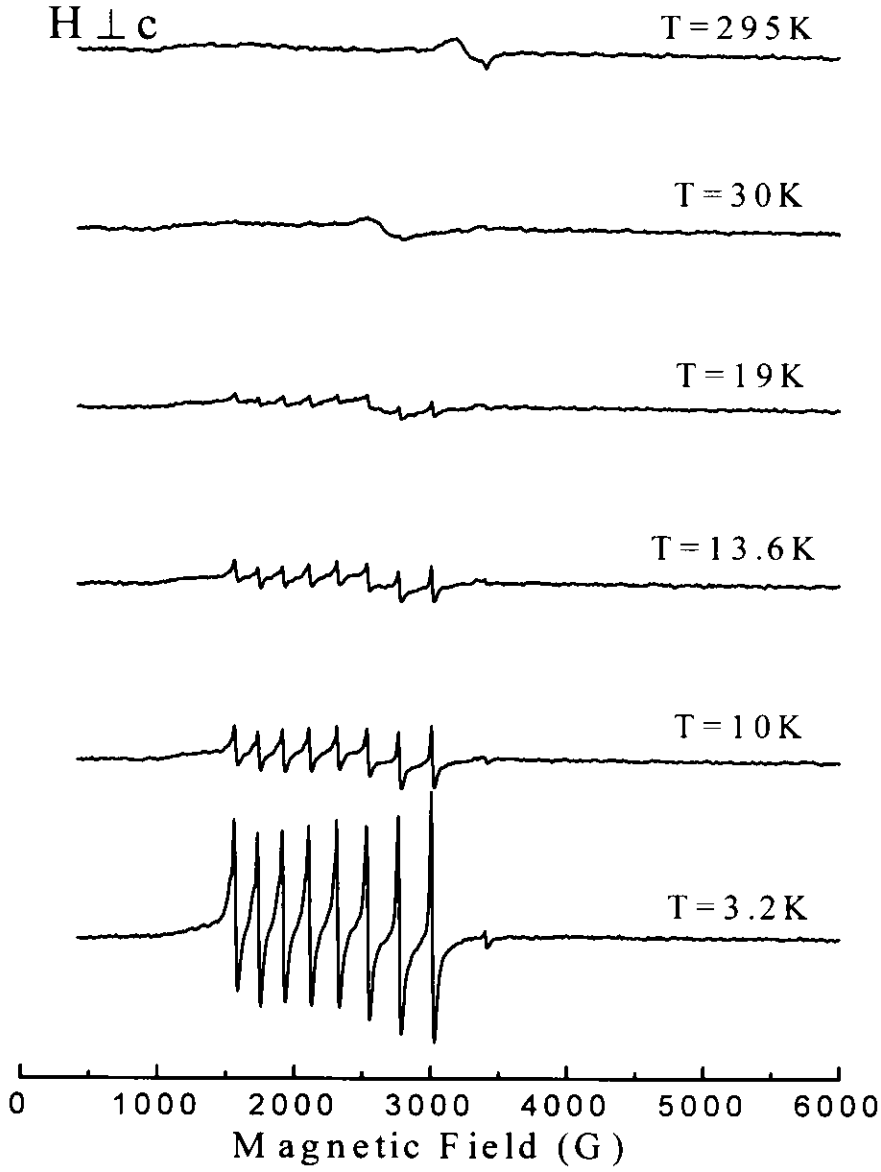

Fig.2 Temperature dependence of ESR signal of $Co_{0.01}Ni_{0.99}Pc(AsF_6)_{0.5}$ $H \perp c$

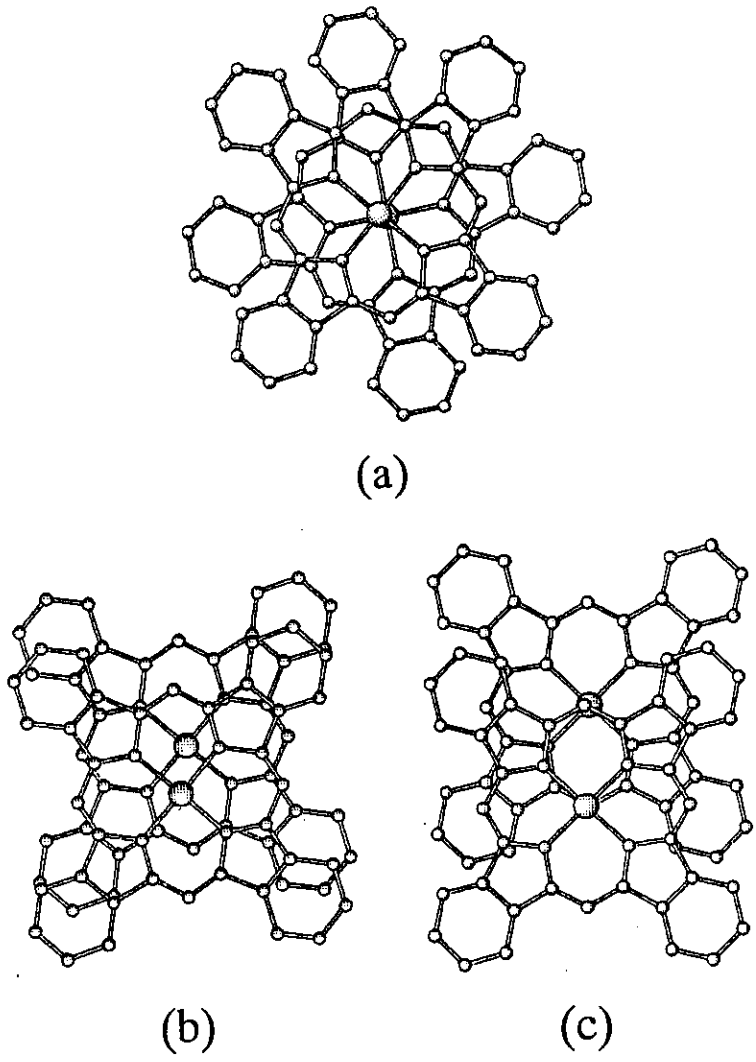

Fig. 3 Overlap patters of phthalocyanine molecules in (a) $NiPc(AsF_6)_{0.5}$, (b) α-type *M*Pc, and (c) β-type *M*Pc

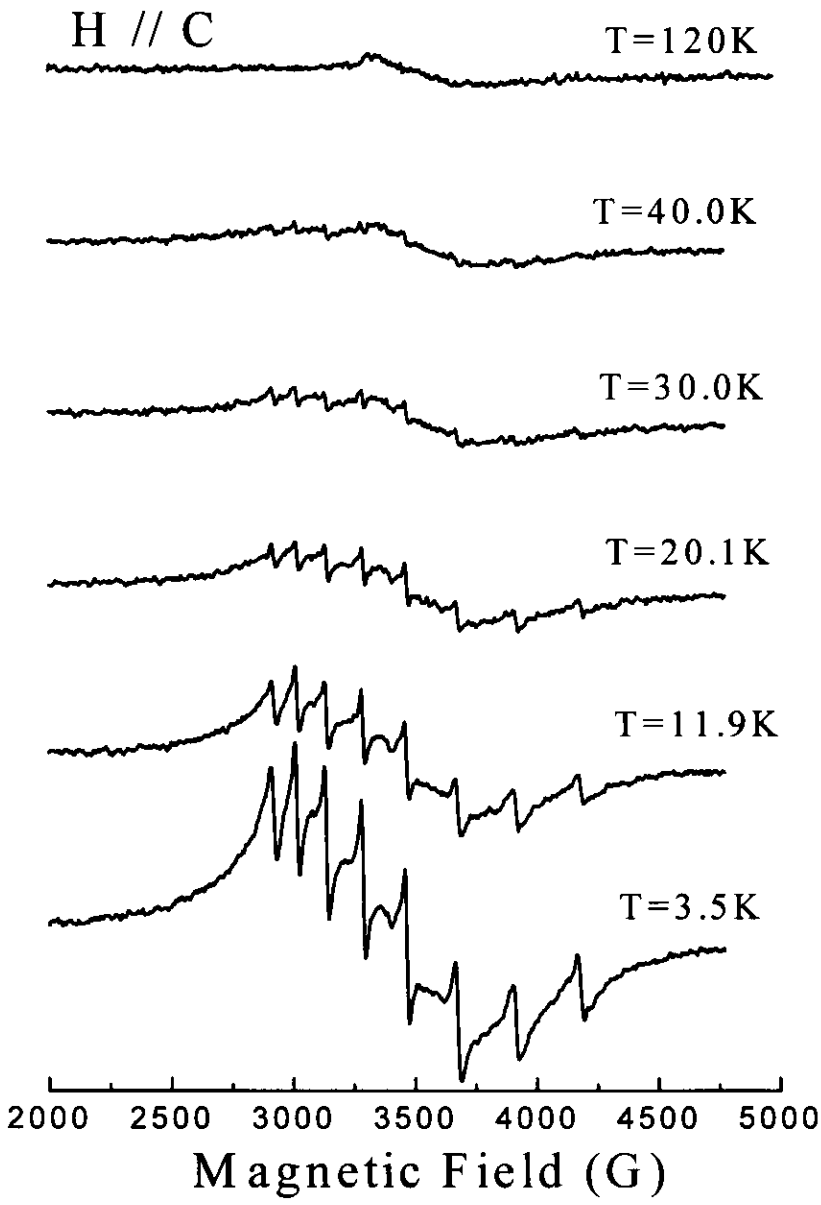

Fig. 4 Temperature dependence of ESR signal of $Co_{0.05}Ni_{0.95}Pc(AsF_6)_{0.5}$ *H//c*

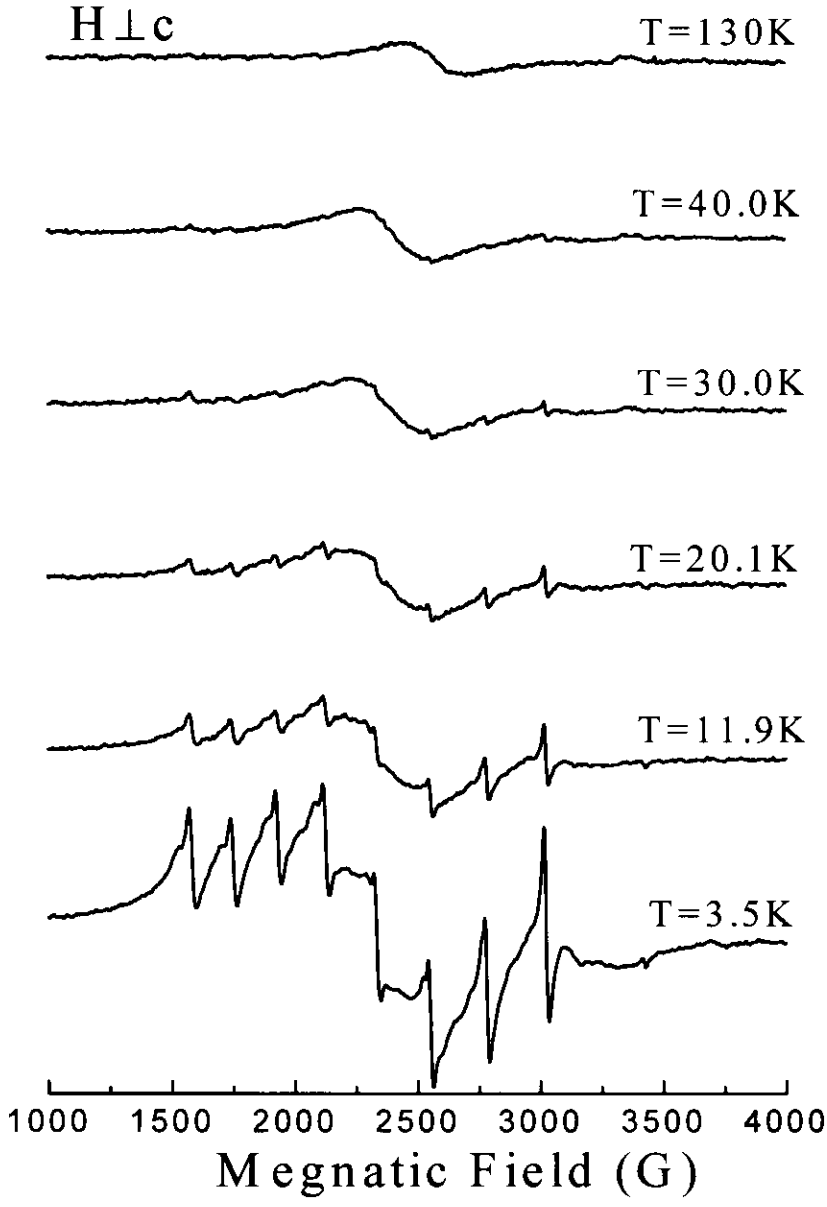

Fig.5 Temperature dependence of ESR signal of $Co_{0.05}Ni_{0.95}Pc(AsF_6)_{0.5}$ $H \perp c$

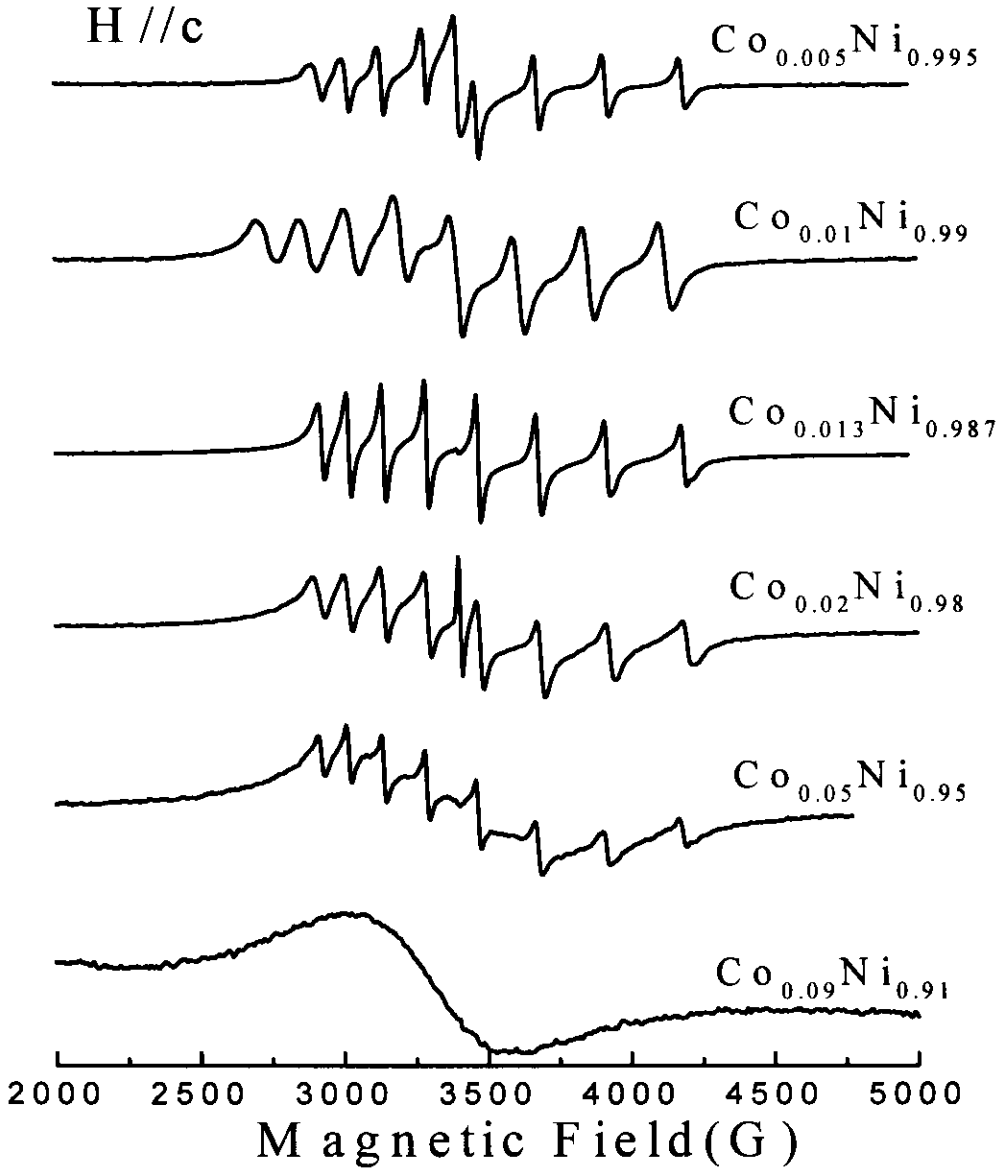

Fig.6 The concentration behavior of hyperfine structure of $Co_xNi_{1-x}Pc(AsF_6)_{0.5}$ *H//c*

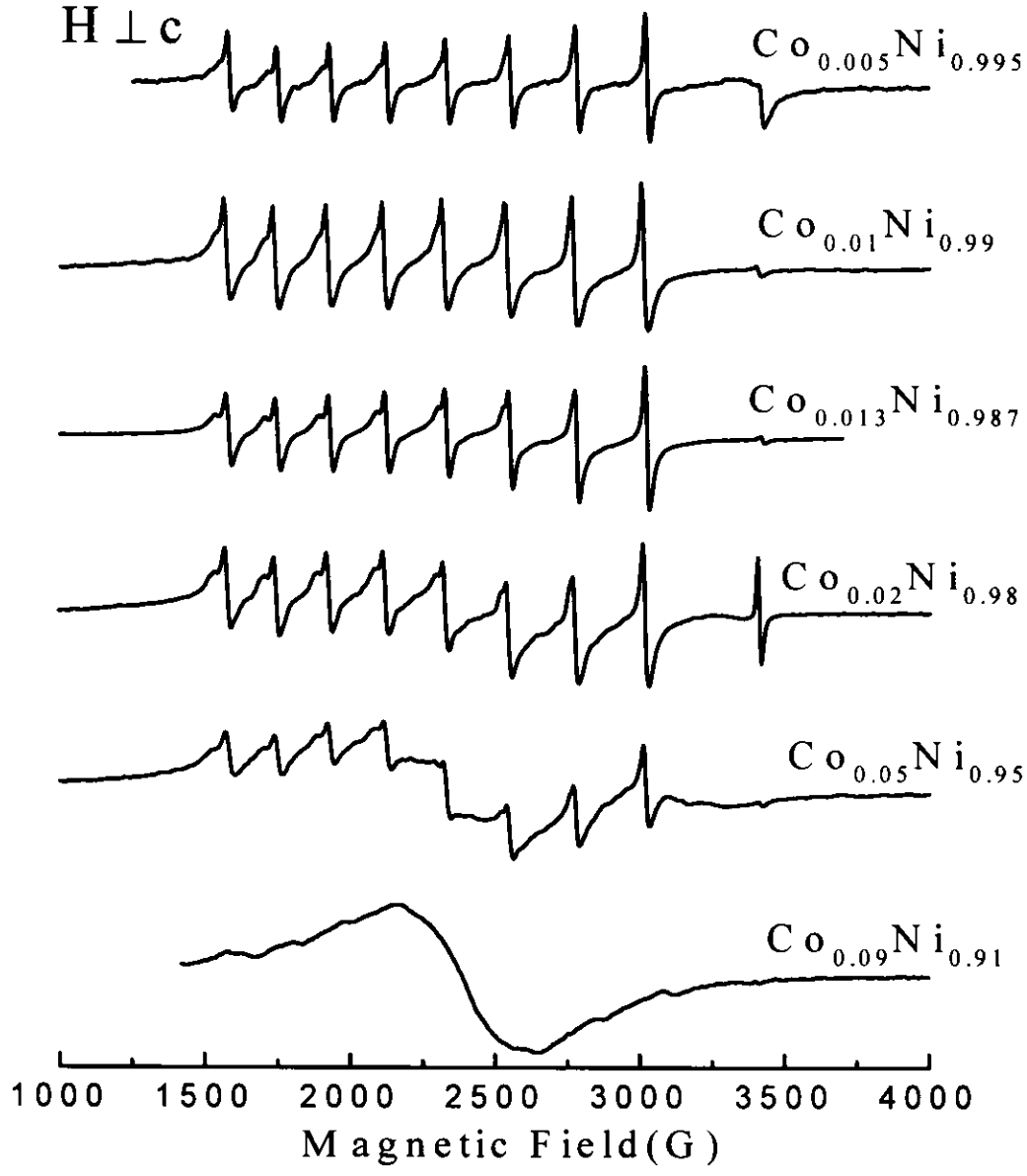

Fig. 7 The concentration behavior of hyperfine structure of $Co_xNi_{1-x}Pc(AsF_6)_{0.5}$ $H \perp c$

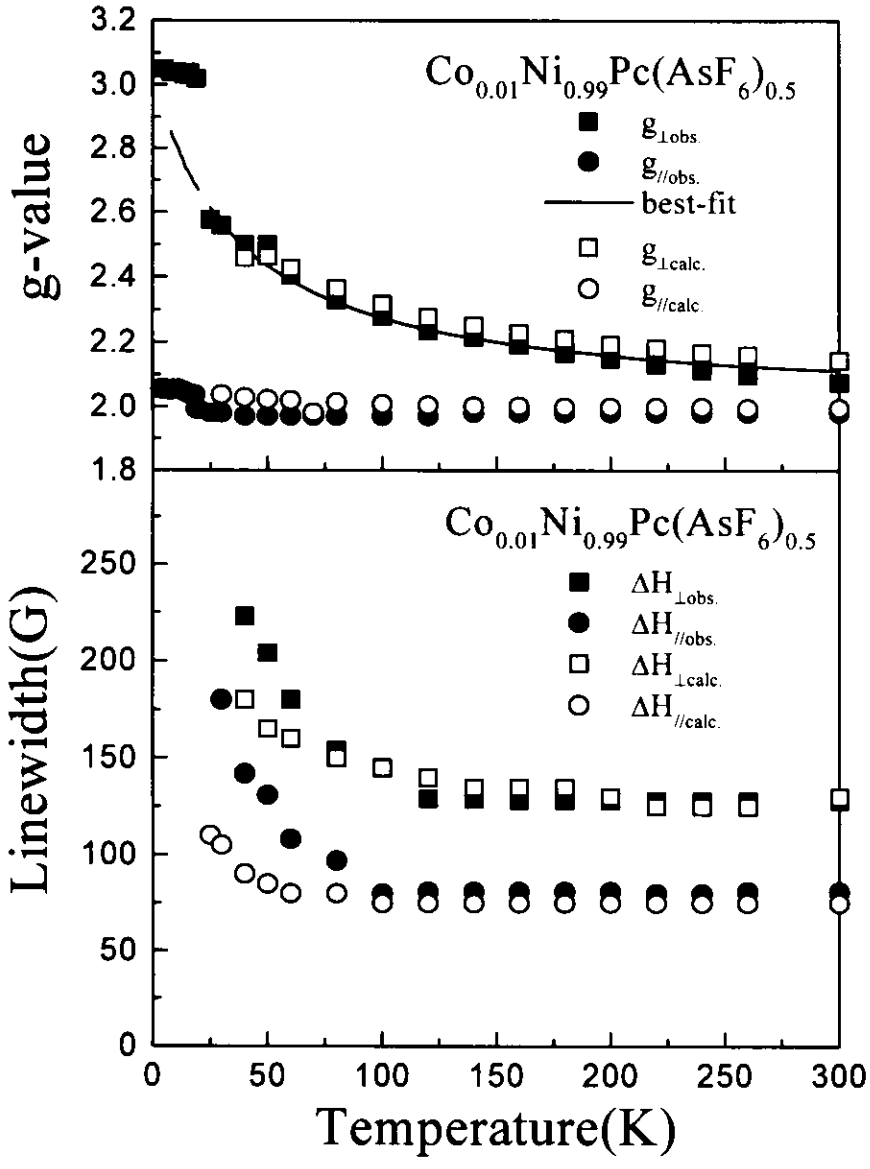

Fig. 8 Temperature dependence of g values (top) and the linewidths of the broad signals (bottom) of $Co_{0.01}Ni_{0.99}Pc(AsF_6)_{0.5}$.

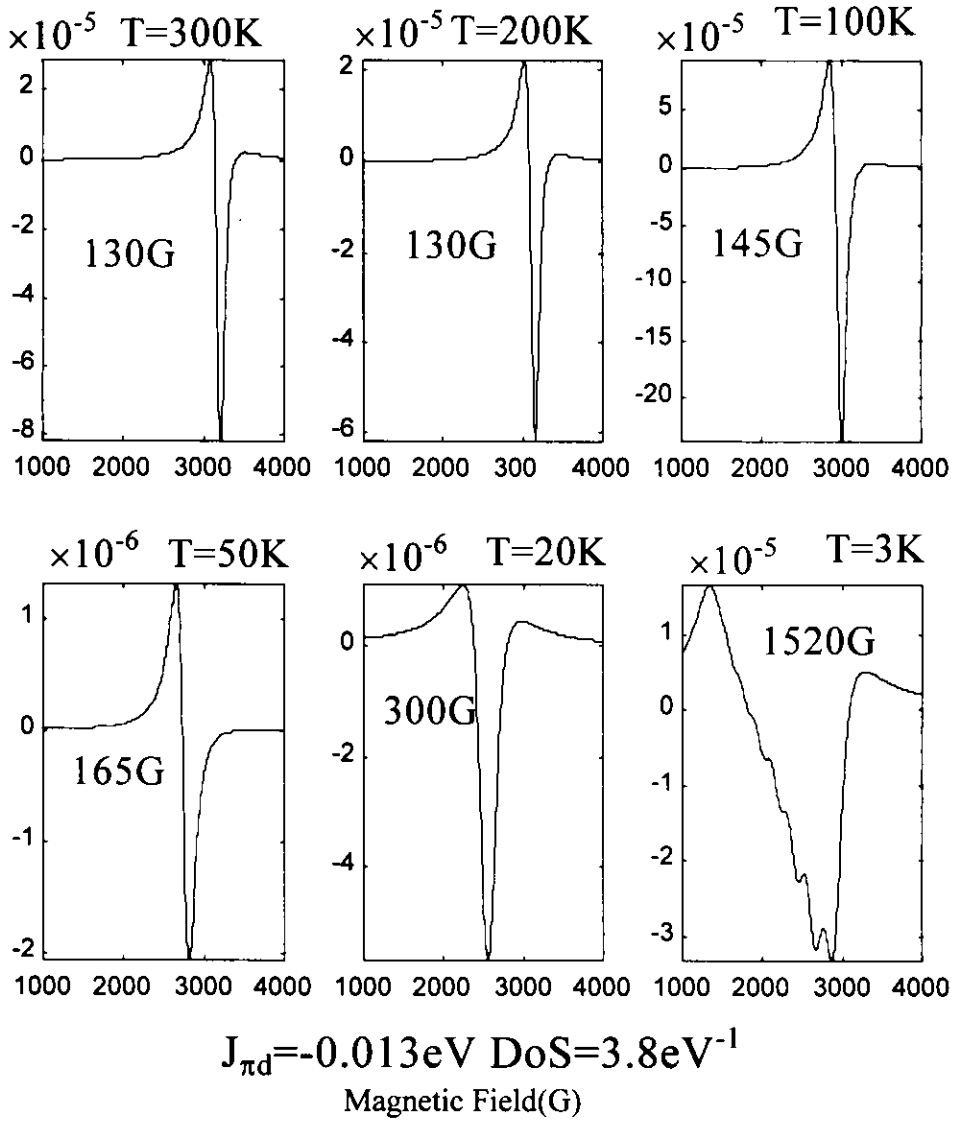

Fig.9 Simulation of the ESR signal based on the molecular-field model for a dilute magnetic alloy using the parameters $|J_{\pi d}|$ =0.013 eV and D_F=3.8 eV^{-1}. The numerical values in the figures denote the derived peak-to-peak linewidth.

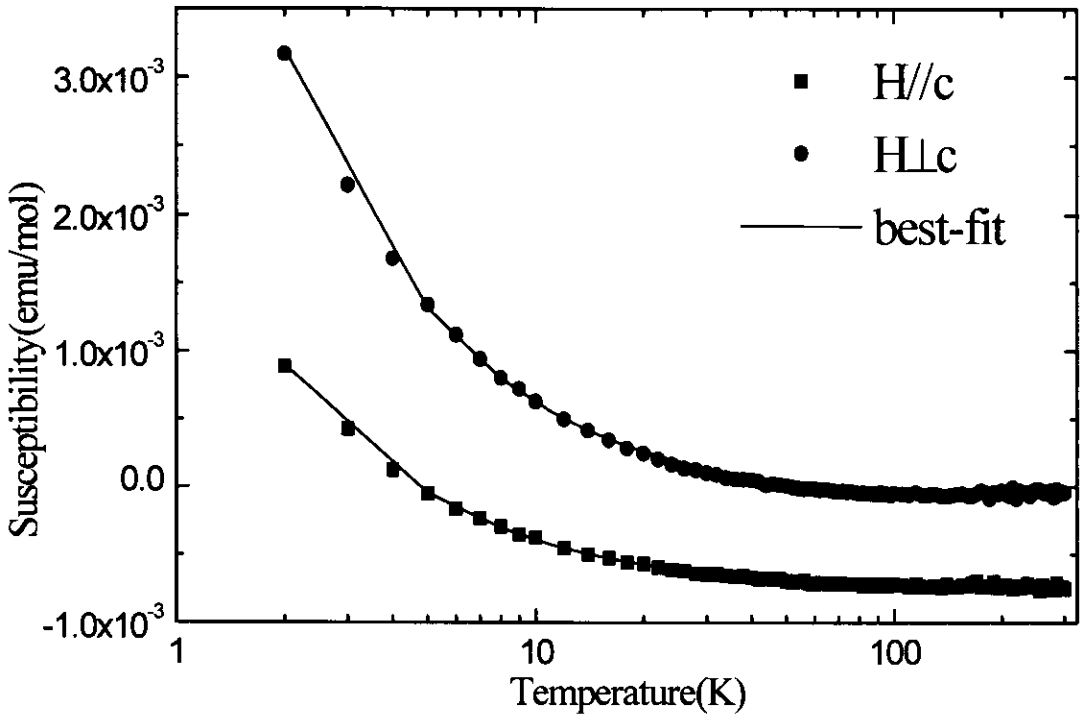

Fig.10 Static magnetic susceptibility of the oriented crystals of $Co_{0.01}Ni_{0.99}Pc(AsF_6)_{0.5}$. The diamagnetic part is not corrected. Solid lines are the best-fit curves of a Curie-Weiss model.

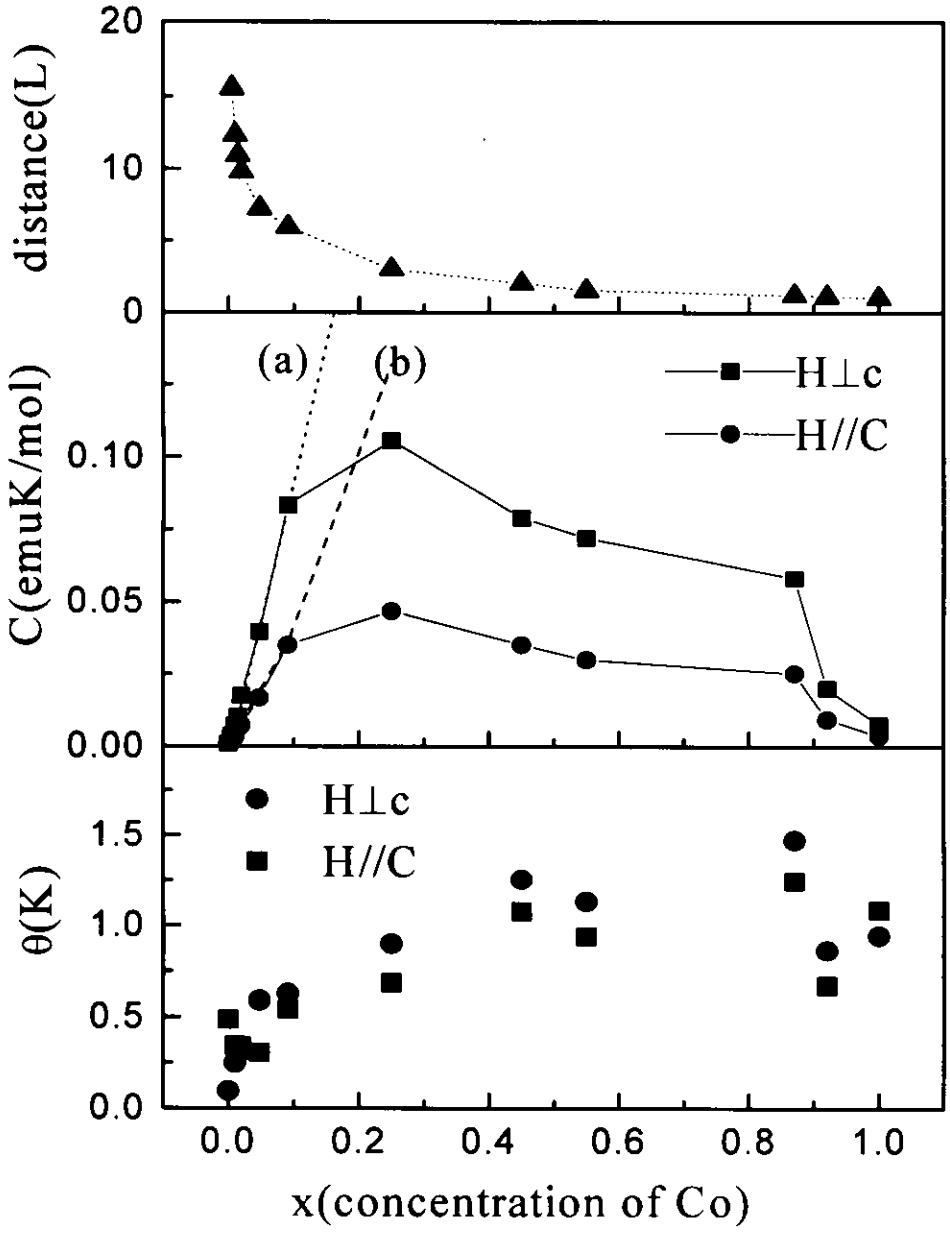

Fig. 11 Concentration (x) dependence of Curie and Weiss constants together with the average distances between the doped CoPc molecules within the same molecular stack of $Co_xNi_{1-x}Pc(AsF_6)_{0.5}$.

Chapter 6

General conclusion

The results of this study on the organic charge-transfer alloy system of $Co_xNi_{1-x}Pc(AsF_6)_{0.5}$ are summarized at the present stage described as follows.

(1) The appearance of the new Raman bands in alloys

The appearance of the new Raman bands at 368 cm^{-1} and 736 cm^{-1} in the alloys is interpreted as a resonance effect. This finding indicates that a new excited state is formed in the mixed crystals. The optical transition to this new excited state is polarized along the *c*-axis. Therefore the excited state is associated with the inter-molecular charge-transfer state between the 3*d* orbitals of neighboring CoPc and NiPc. The Co concentration dependence of the Raman intensity of the new peaks presents an asymmetric tendency with respect to Co concentration of x, and is qualitatively reproduced by the function of $x(1-x)^2$. This implies that the band at 368 cm^{-1} is assigned to the a_{1g} mode of NiPc. According to the molecular orbital calculation, the energy difference between $3d_{z^2}$ and $3d_{x^2-y^2}$ orbitals is close to the excitation energy of the new optical transition. Therefore, the new optical transition is assigned to the inter-molecular charge-transfer transition from the $3d_{z^2}$ orbital of Co to the $3d_{x^2-y^2}$ orbital of Ni. This means that the introduction of the electron into the $3d_{x^2-y^2}$ orbital induces the geometrical change to the inner macrocycle.

(2) 1D Hubbard band of $CoPc(AsF_6)_{0.5}$

Based on the analysis of the well-resolved hyperfine structure in the very dilute alloy, the unpaired *d*-electron in Co was confirmed to occupy the $3d_{z^2}$ orbital, which is extended perpendicular to the molecular plane. As the $3d_{z^2}$ orbital is doubly occupied in

NiPc and singly occupied in CoPc, a repulsive force works between the neighboring Ni atoms in $NiPc(AsF_6)_{0.5}$, whereas an attractive force works between the Co atoms in $CoPc(AsF_6)_{0.5}$. This result explains the systematic change of the *c* parameters of the mixed crystal. Comparing with the spectrum of $NiPc(AsF_6)_{0.5}$, the reflectivity of $CoPc(AsF_6)_{0.5}$ in the mid-infrared region shows an additional optical transition. Therefore, we analyzed the reflection and conductivity spectra using Drude and Lorentz models. The much larger total plasma frequency of the $CoPc(AsF_6)_{0.5}$ strongly suggests that the 3*d* orbital also contributes to the optical transition of $CoPc(AsF_6)_{0.5}$ in the mid-infrared region. The Drude and Lorentz terms are associated with the ¾-filled π-band and ½-filled *d*-band. Assuming the 1D tight-binding model for the π-band and 1D Hubbard band model for the *d*-band, the bandwidth of $CoPc(AsF_6)_{0.5}$ was estimated as 1.8~2.1 eV for the π-band and 0.5~0.6 eV for the *d*-band. Therefore, the inter-band transition between the two Hubbard bands contributes the enhancement of the plasma frequency for $CoPc(AsF_6)_{0.5}$ as well as the additional band in the mid-infrared region. The low excitation energy of the mid-infrared transition suggests that the 3*d*-band is located near the Fermi level of the ¾-filled π-band. The formation of the 1D 3*d* band explains the observed characteristic line shape of $CoPc(AsF_6)_{0.5}$ in the polarized parallel to the *c*-axis reflection spectra in the high Co concentration.

(3) Magnetic property

It was proved that the hyperfine structure of the very dilute alloys comes from the $CoPc^0$ because the very resemblance of the splitting constant to the magnetically diluted CoPc in β-NiPc. Using a molecular field approximation, we analyzed the temperature

dependence of the g value and linewidth in the high temperature regime, in which the hyperfine signal was replaced by a single Lorentzian line. The broad single line comes from the coupling between the d- and π-spins through the exchange interaction. Based on the numerical simulation of the g value and line shape of the ESR signals of $Co_{0.01}Ni_{0.99}Pc(AsF_6)_{0.5}$, the exchange interaction between d- and π-spins and the density of state at Fermi level were obtained as $|J_{\pi d}|$=0.013±0.002 eV and D_F=3.8±0.2 eV^{-1}, respectively. Using these parameters, the Kondo and RKKY temperatures were estimated as 2×10^{-5} K and 7 K. This result is consistent with the magnetic susceptibility of the alloy system which conforms to the Curie-Weiss law down to 2 K. The small exchange energy between the d- and π-spins suggests a small hybridization between the Co $3d_{z^2}$ orbital and Pc HOMO. The enhancement of the Co concentration increases the CoPc pair, and then the direct antiferromagnetic interaction between the pairs suppresses the Curie constants in the high Co concentration. This feature is consistent with the formation of the half-filled 1D band.

In conclusion, the formation of the $3d_{z^2}$ band was verified by the optical spectrum and the magnetic properties of $Co_xNi_{1-x}Pc(AsF_6)_{0.5}$. Both results are consistent with each other.